Lecture 13

Hydraulic Fracturing for Unconventional Resources

비전통 자원개발을 위한 수압파쇄

Ki-Bok Min, PhD

Professor
Department of Energy Resources Engineering
Seoul National University

SEOUL NATIONAL UNIVERSITY

Disclaimer

SEOUL NATIONAL UNIVERSITY

- All the figures in the slides are taken from "Zoback MD, Kohli AH, 2019, Unconventional Geomechanics, Cambridge Univ press" & "Zoback MD, 2007, Reservoir Geomechanics, Cambridge Univ press" unless otherwise stated.
- Materials in these slides cannot be used without the written consent from the instructor

Hydraulic Fracturing for unconventional resources
Importance

SEOUL NATIONAL UNIVERSITY

- Unconventional hydrocarbon development
  - Shale gas/Tight oil production
  - Coalbed methane
  - Gas hydrates
- Unconventional Geothermal Energy
  - Enhanced Geothermal Systems

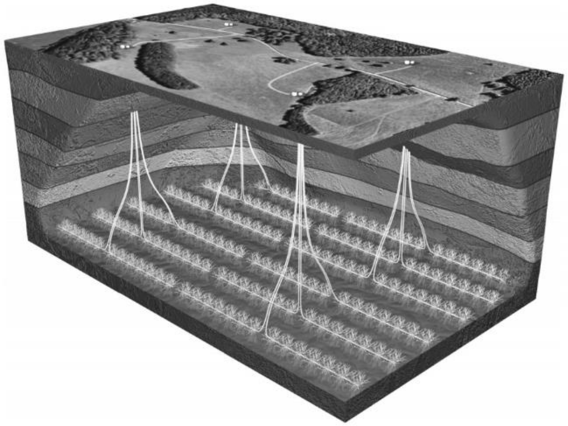

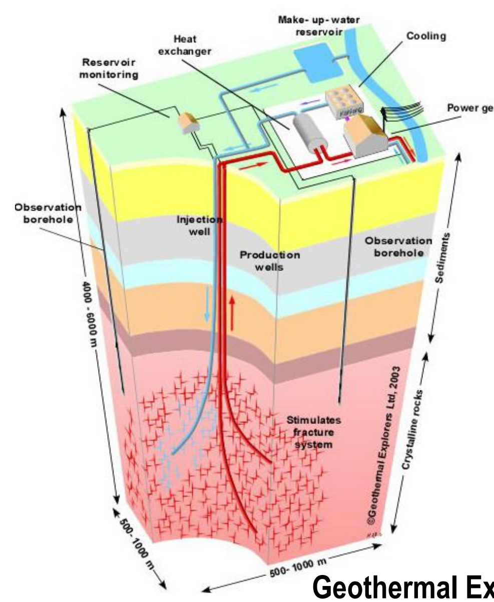

Geothermal Explorer, 2010

unconventional resources: oil and gas bearing formations with very low permeabilities (often requires hydraulic fracturing)

Hydraulic Fracturing for unconventional resources
Topic

SEOUL NATIONAL UNIVERSITY

- Introduction to unconventional geomechanics
  - Development of Unconventional oil and gas
  - Permeability
  - Horizontal Drilling and Multi-Stage Hydraulic Fracturing
- Horizontal Drilling and Multi-Stage Hydraulic Fracturing
  - Hydraulic fracturing
    - confinement
    - Initiation and propagation
    - Models of hydraulic fracturing – PKN, KGD and radial models
    - Effect of leakoff
    - Stress shadow effect
    - SNU Geomechanics Toolbox
  - Induced shear slip during hydraulic fracturing
- Deep Geothermal Energy (Enhanced Geothermal Systems)

Energy Mix
Climate Change - Paris Agreement

SEOUL NATIONAL UNIVERSITY

- The Paris Agreement (파리협약, 12 Dec 2015)
  - 195 countries agreed
  - …. pursuing efforts to limit the temperature increase to 1.5 °C above pre-industrial levels.
  - Check the target every five years.
  - Prepare 100 billion USD/year for developing countries

United Nations FCCC/CP/2015/L.9/Rev.1

Framework Convention on Climate Change

Distr.: Limited
12 December 2015

Original: English

Conference of the Parties
Twenty-first session
Paris, 30 November to 11 December 2015

Agenda item 4(b)
Durban Platform for Enhanced Action (decision 1/CP.17)
Adoption of a protocol, another legal instrument, or an agreed outcome with legal force under the Convention applicable to all Parties

ADOPTION OF THE PARIS AGREEMENT

Proposal by the President

Draft decision -/CP.21

The *Conference of the Parties*,

Recalling decision 1/CP.17 on the establishment of the Ad Hoc Working Group on the Durban Platform for Enhanced Action,

Also recalling Articles 2, 3 and 4 of the Convention,

Further recalling relevant decisions of the Conference of the Parties, including decisions 1/CP.16, 2/CP.18, 1/CP.19 and 1/CP.20,

Welcoming the adoption of United Nations General Assembly resolution A/RES/70/1, "Transforming our world: the 2030 Agenda for Sustainable Development", in particular its goal 13, and the adoption of the Addis Ababa Action Agenda of the third International Conference on Financing for Development and the adoption of the Sendai Framework for Disaster Risk Reduction,

Recognizing that climate change represents an urgent and potentially irreversible threat to human societies and the planet and thus requires the widest possible cooperation by all countries, and their participation in an effective and appropriate international response, with a view to accelerating the reduction of global greenhouse gas emissions,

Also recognizing that deep reductions in global emissions will be required in order to achieve the ultimate objective of the Convention and emphasizing the need for urgency in addressing climate change,

Acknowledging that climate change is a common concern of humankind, Parties should, when taking action to address climate change, respect, promote and consider their

as defined in Article 2;

54. *Also decides* that, in accordance with Article 9, paragraph 3, of the Agreement, developed countries intend to continue their existing collective mobilization goal through 2025 in the context of meaningful mitigation actions and transparency on implementation; prior to 2025 the Conference of the Parties serving as the meeting of the Parties to the Paris Agreement shall set a new collective quantified goal from a floor of USD 100 billion per year, taking into account the needs and priorities of developing countries;

55. *Recognizes* the importance of adequate and predictable financial resources, including for results-based payments, as appropriate, for the implementation of policy approaches and positive incentives for reducing emissions from deforestation and forest

Energy Mix
Climate Change - CO2 emission

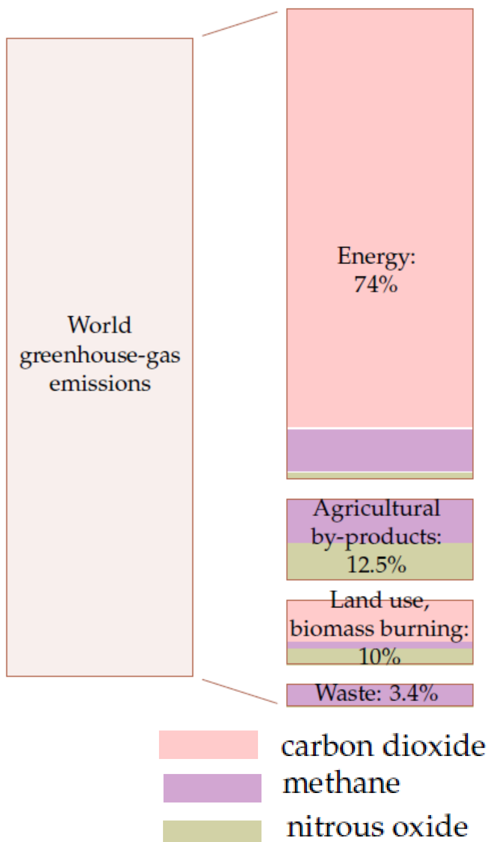

MacKay DJC, 2009, Sustainable energy without the hot air, UIT (based on 2000 data)

- Energy sector: ~74%
  - Power stations, industrial processes, transport fossil fuel processing, energy-use in buildings
- Climate change is essentially an energy issue

Energy mix
Energy Outlook

SEOUL NATIONAL UNIVERSITY

- Key technologies for reducing CO2 emissions under the BLUE Map scenario*

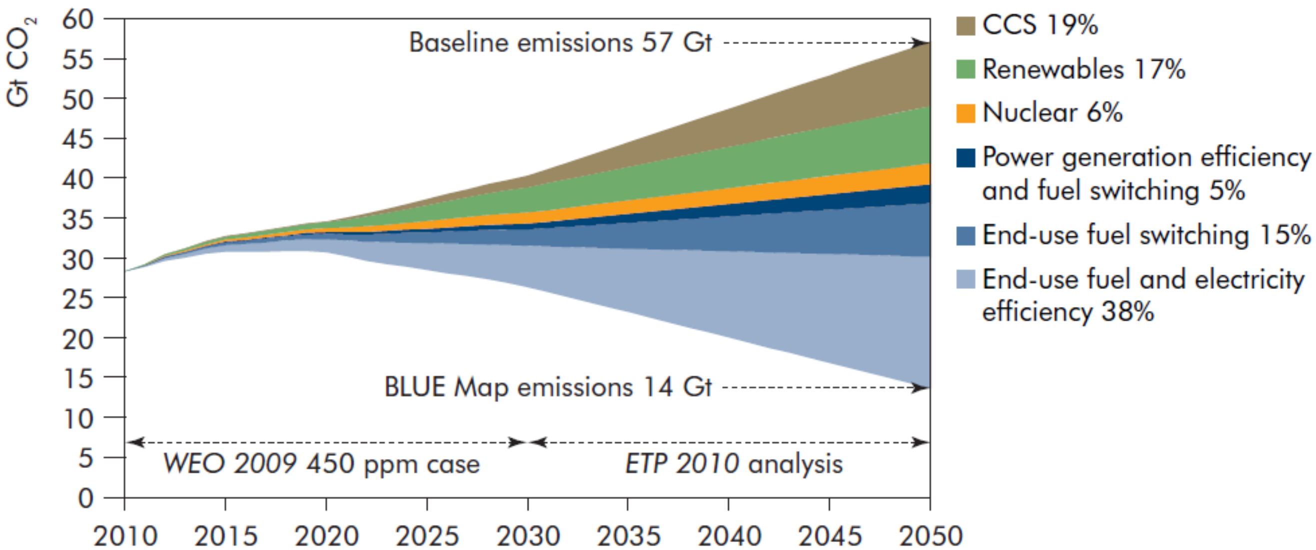

IEA, 2010, Energy Technology Perspective

*** BLUE Map scenario: CO2 emission reduced to half**

Energy mix
Energy Outlook

- Energy mix (Primary Energy) change due to climate change
  - Dramatic increase of renewables
  - Increase of gas

Primary energy consumption by fuel

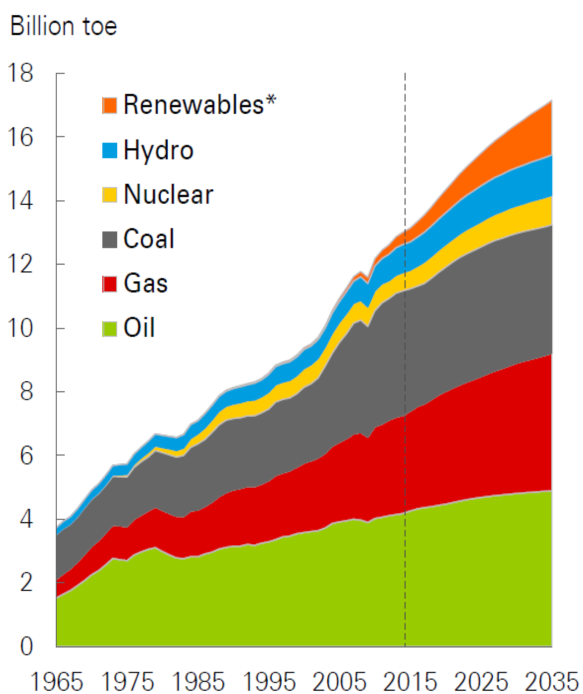

Shares of primary energy

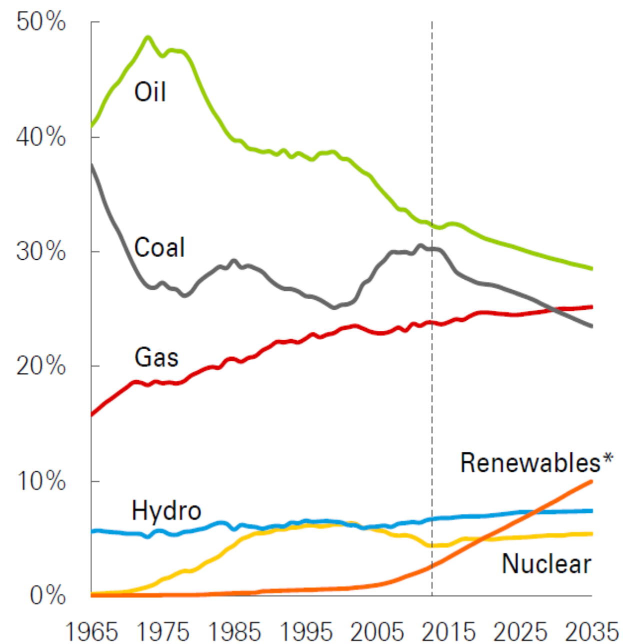

*Renewables includes wind, solar, geothermal, biomass, and biofuels

BP Energy Outlook, 2017

Energy mix
Energy Outlook - CCS

SEOUL NATIONAL UNIVERSITY

- Carbon Capture and Storage (CCS)
  - A bridge technology

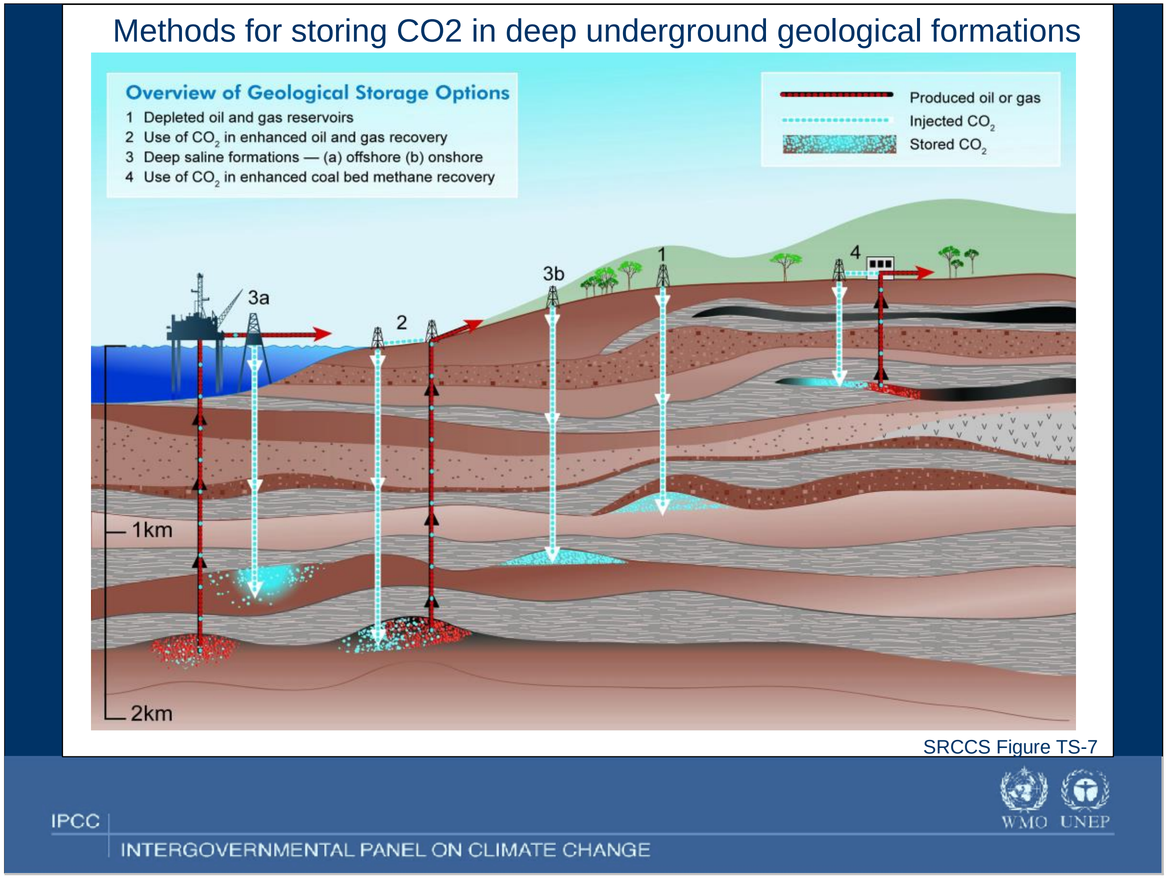

Energy mix
Energy Outlook - CCS

- Key Geomechanical issues for CCS technology

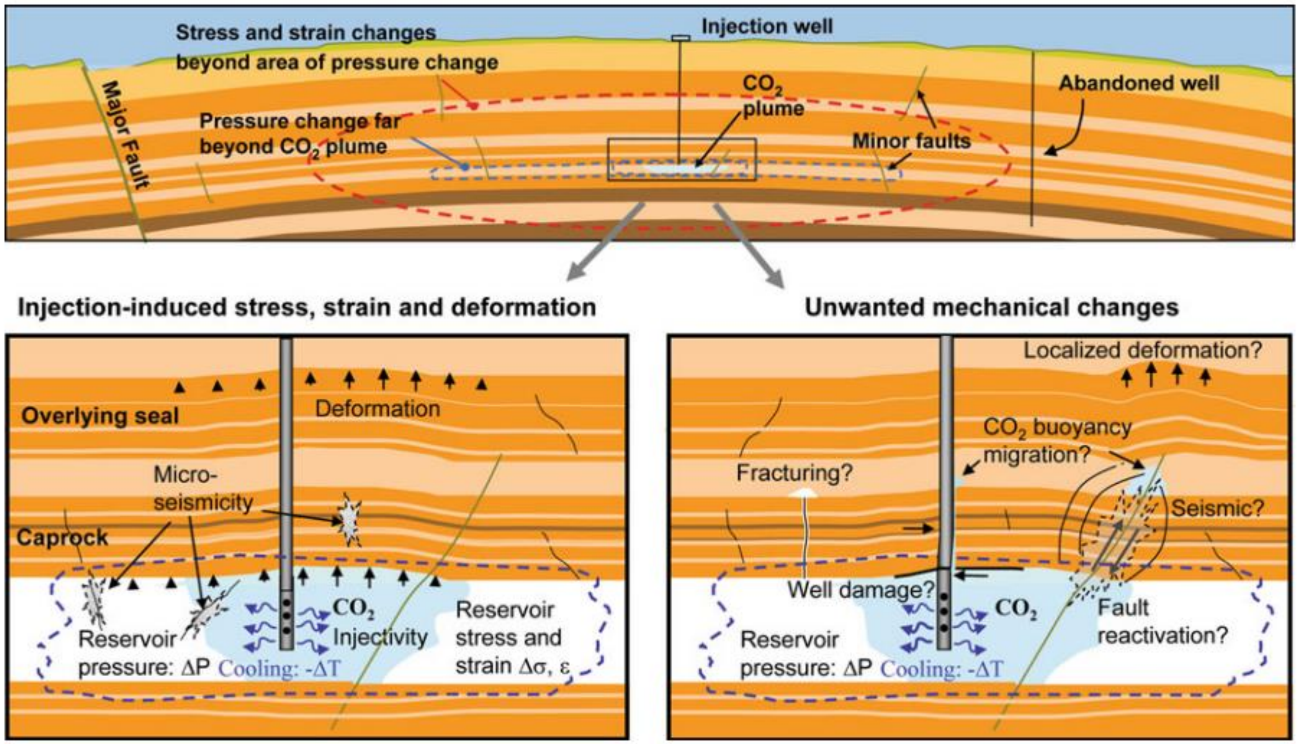

Fig. 1 Geomechanical processes and key technical issues associated with GCS in deep sedimentary formations. *Top* the different regions of influence for a CO_2 plume, reservoir pressure changes, and geomechanical changes in a multilayered system with minor and major faults. *Bottom left* injection-induced stress, strain, deformations and potential microseismic events as a result of changes in reservoir pressure and temperature, and *bottom right* unwanted inelastic changes that might reduce sequestration efficiency and cause concerns in the local community

Rutqvist J, 2012, The Geomechanics of CO2 Storage in Deep Sedimentary Formations, Geotech Geol Eng, 30:525-551

Energy mix
Energy Outlook - CCS

SEOUL NATIONAL UNIVERSITY

- Because even small- to moderate-sized earthquakes threaten the seal integrity of CO2 repositories, in this context, large-scale CCS is a risky, and likely unsuccessful, strategy for significantly reducing greenhouse gas emissions

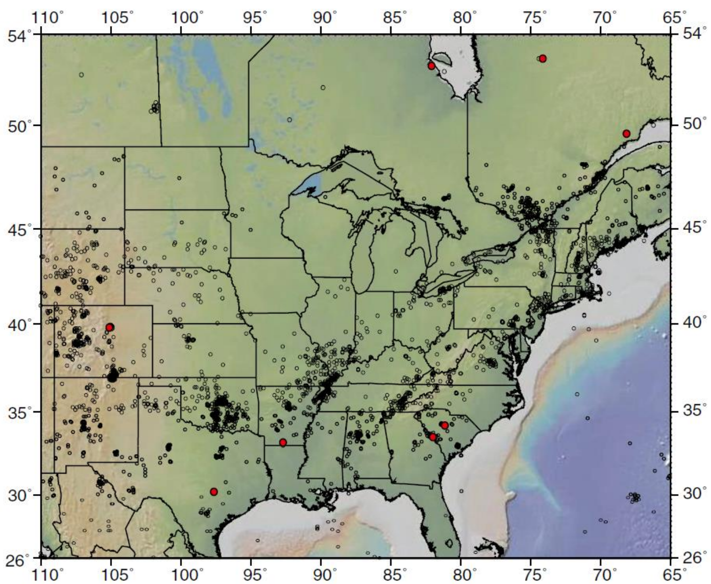

Earthquake >3 in the US (• : induced EQ M4-5)

PNAS

PERSPECTIVE

Earthquake triggering and large-scale geologic storage of carbon dioxide

Mark D. Zoback[a,1] and Steven M. Gorelick[b]

Departments of [a]Geophysics and [b]Environmental Earth System Science, Stanford University, Stanford, CA 94305

Edited by Pamela A. Matson, Stanford University, Stanford, CA, and approved May 4, 2012 (received for review March 27, 2012)

Despite its enormous cost, large-scale carbon capture and storage (CCS) is considered a viable strategy for significantly reducing CO_2 emissions associated with coal-based electrical power generation and other industrial sources of CO_2 [Intergovernmental Panel on Climate Change (2005) IPCC Special Report on Carbon Dioxide Capture and Storage. Prepared by Working Group III of the Intergovernmental Panel on Climate Change, eds Metz B, et al. (Cambridge Univ Press, Cambridge, UK); Szulczewski ML, et al. (2012) *Proc Natl Acad Sci USA* 109:5185–5189]. We argue here that there is a high probability that earthquakes will be triggered by injection of large volumes of CO_2 into the brittle rocks commonly found in continental interiors. Because even small- to moderate-sized earthquakes threaten the seal integrity of CO_2 repositories, in this context, large-scale CCS is a risky, and likely unsuccessful, strategy for significantly reducing greenhouse gas emissions.

carbon sequestration | climate change | triggered earthquakes

The combustion of coal for electrical power generation in the United States generates approximately 2.1 billion metric tons of CO_2 per year, ~36% of all US emissions. In 2011, China generated more than three times that much CO_2 by burning coal for electricity, which accounted for ~80% of its total emissions. (According to the Energy Information Agency of the US Department of Energy, total CO_2 emissions in China were 8.38 billion metric tonnes in 2011, with 6.95 billion tons from coal burning, nearly all of which is used electrical power generation.) From a global perspective, if large-scale carbon capture and storage (CCS) is to significantly contribute to reducing the accumulation of greenhouse gases, it must operate at a massive scale, on the order of 3.5 billion tons (1) of CO_2 per year, a volume roughly equivalent (2) to the ~27 billion barrels of oil currently produced annually around the world. (Under reservoir conditions, one billion tons of CO_2 occupies a volume of ~1.3 billion cubic meters, equivalent to 8.18 billion barrels. Thus, 3.5 billion tons of carbon dioxide would correspond to a volume of approximately 28.6 billion barrels. There are currently ~850,000 wells producing oil around the world.) Moreover, a leak rate from underground CO_2 storage reservoirs of less than 1% per thousand years is required for CCS to achieve the same climate benefits as renewable energy sources (3).

Before embarking on projects to inject enormous volumes of CO_2 at numerous sites around the world, it is important to note that over time periods of just a few decades, modern seismic networks have shown that earthquakes occur nearly everywhere in continental interiors. Fig. 1, *Upper* shows instrumentally recorded earthquakes in the central and eastern United States and southeastern Canada. Fig. 1, *Lower* shows instrumentally recorded intraplate earthquakes in south and east Asia (4). The seismicity catalogs are complete to magnitude (M) 3. The occurrence of these earthquakes means that nearly everywhere in continental interiors a subset of the preexisting faults in the crust is potentially active in the current stress field (5, 6). This is sometimes referred to as the *critically stressed* nature of the brittle crust (7). It should also be noted that despite the overall low rate of earthquake occurrence in continental interiors, some of the most devastating earthquakes in history occurred in these regions. In eastern China, the M 7.8, 1976 Tangshan earthquake, approximately 200 km east of Beijing, killed several hundred thousand people. In the central United States, three M 7+ earthquakes in 1811 and 1812 occurred in the New Madrid seismic zone in southeast Missouri.

Because of the critically stressed nature of the crust, fluid injection in deep wells can trigger earthquakes when the injection increases pore pressure in the vicinity of preexisting potentially active faults. The increased pore pressure reduces the frictional resistance to fault slip, allowing elastic energy already stored in the surrounding rocks to be released in earthquakes that would occur someday as the result of natural geologic processes (8). This effect was first documented in the 1960s in Denver, Colorado when injection into a 3-km-deep well at the nearby Rocky Mountain Arsenal triggered earthquakes (9). Soon thereafter it was shown experimentally (10) at the Rangely oil field in western Colorado that earthquakes could be turned on and off by varying the rate at which water was injected and thus modulating reservoir pressure. In 2011 alone, a number of small to moderate earthquakes in the United States seem to have been triggered by injection of wastewater (11). These include earthquakes near Guy, Arkansas that occurred in February and March, where the largest earthquake was M 4.7. In the Trinidad/Raton area near the border of Colorado and New Mexico, injection of produced water associated with coalbed methane production seems to have triggered a number of earthquakes, the largest being a M 5.3 event that occurred in August. Earthquakes seem to have been triggered by wastewater injection near Youngstown, Ohio on Christmas Eve and New Year's Eve, the largest of which was M 4.0. Although the risks associated with wastewater injection are minimal and can be reduced even further with proper planning (11), the situation would be far more problematic if similar-sized earthquakes were triggered in formations intended to sequester CO_2 for hundreds to thousands of years.

Deep borehole stress measurements confirm the critically stressed nature of the crust in continental interiors (12), in some cases at sites directly relevant to the feasibility of large-scale CCS. For example, deep borehole stress measurements at the Mountaineer coal-burning power plant on the Ohio River in West Virginia indicate a severe limitation on the rate at which CO_2 could be injected without the resulting pressure build-up initiating slip on preexisting faults (13). Because of the low permeability of the formations at depth, pore pressure increases would be expected to trigger slip on preexisting faults if CO_2 injection rates exceed approximately 1% of the 7 million tons of CO_2 emitted by the Mountaineer plant each year. Similarly, stress measurements at Teapot Dome, Wyoming, the US government-owned oil field where pilot CO_2

Author contributions: M.D.Z. and S.M.G. wrote the paper.

The authors declare no conflict of interest.

This article is a PNAS Direct Submission.

[1]To whom correspondence should be addressed. E-mail: zoback@stanford.edu.

www.pnas.org/cgi/doi/10.1073/pnas.1202473109

Zoback MD & Gorelick SM, Earthquake triggering and large-scale geologic storage of carbon dioxide, Proc National Academy of Science of the USA (PNAS), June 2012, www.pnas.org/cgi/doi/10.1073/pnas.1202473109

Energy mix
Energy Outlook – Enhanced Geothermal Systems

SEOUL NATIONAL UNIVERSITY

Hydrothermal

EGS

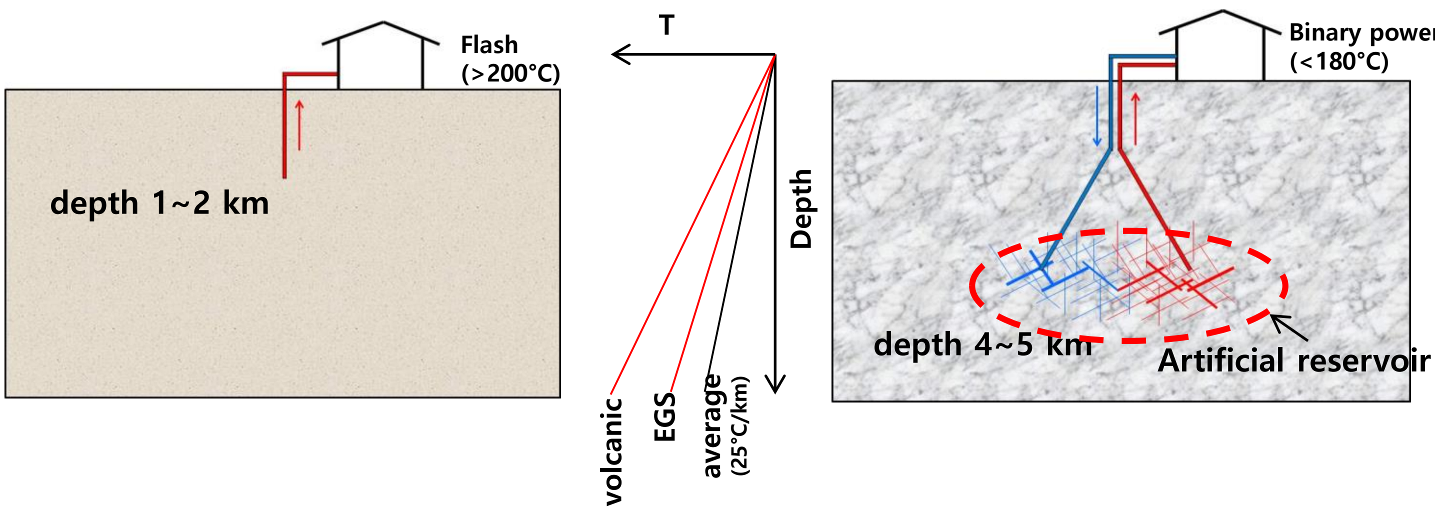

- Best geothermal gradient > 50°C/km)
  → shallow (1~2 km), drilling cost↓
- High permeability(> 10^{-15} m^2)
  → Hydraulic Stimulation x
- Optional injection hole
- Hydrotheral power generation

- Above average gradient (30~40°C/km)
  → deep (4~5 km), drilling cost ↑
- Low permeability (< 10^{-18} m^2)
  → Hydraulic stimulation key
- Compulsory injection hole
- Binary power generation

Various Views on Geothermal and EGS

A modest investment of $300-400 million over 15 years would demonstrate EGS technology at a commercial scale at several US field sites to reduce risks for private investment and enable the development of 100 GW.

JW Tester, Prof Cornell Univ, then MIT, 2007 – The future of geothermal energy

EGS is a clean, reliable base load energy…. Effectively unlimited supply of energy….you can bank on it.

Steve Chou, Nobel Laureate, LBNL, 2011 – Google.org

Geothermal will remain a globally marginal, although nationally and locally important, source of electricity. ~ 5% even if we were to develop the prospective potential of 138 GW.

Vaclav Smil, 2003 – energy at crossroads

…to treat geothermal heat the same way we currently treat fossil fuels: as a resource to be mined rather than collected sustainably. …Sadly for Britain, geothermal will only ever play a tiny part.

DJC MacKay, Prof Univ Cambridge, 2009 – Sustainable energy without hot air

Optimistic ⟷ **Pessimistic**

Unconventional Resources
Natural Gas production

- Natural Gas Production in the USA

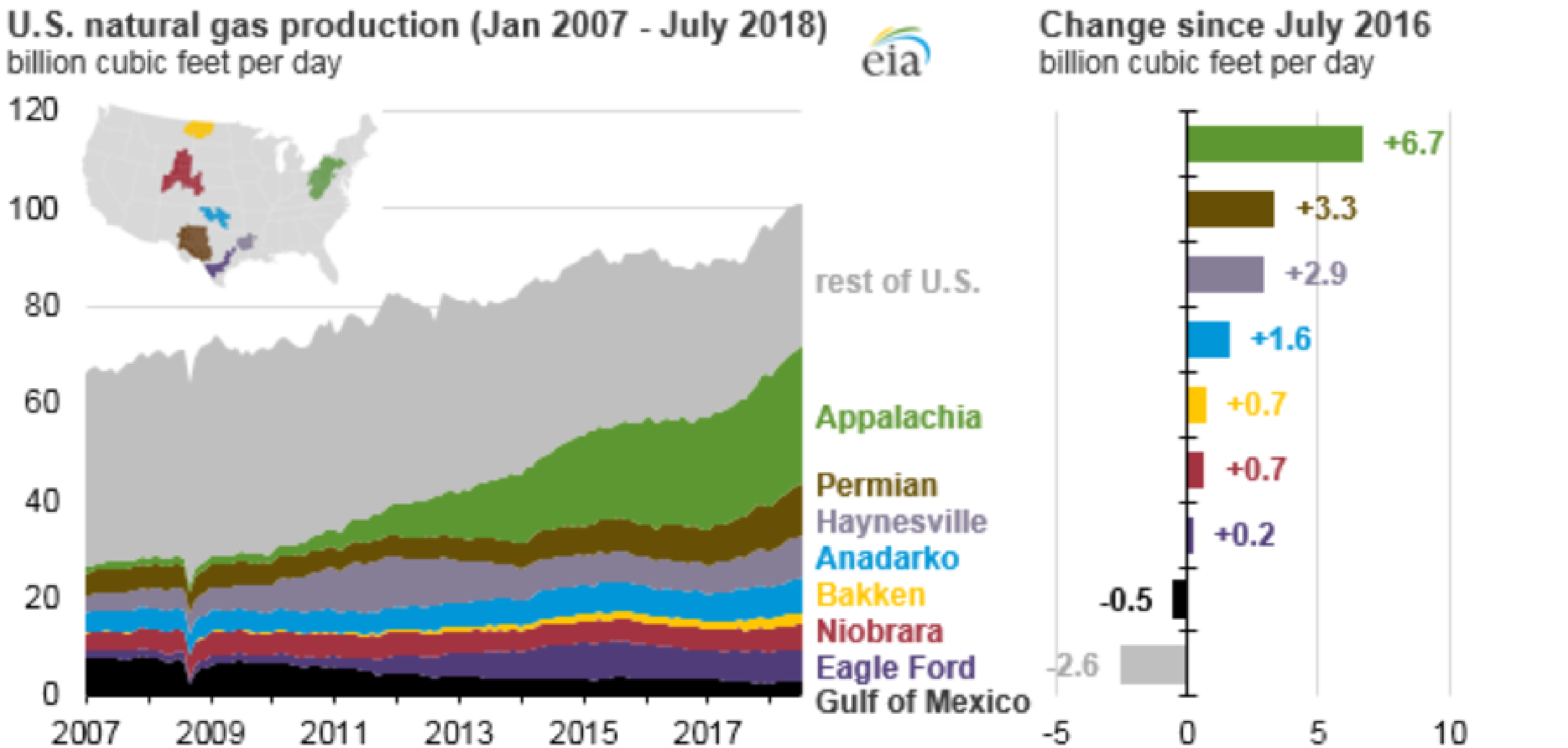

Source: U.S. Energy Information Administration, *Drilling Productivity Report*, *Natural Gas Monthly*, and *Short-Term Energy Outlook*

Unconventional Resources
Natural Gas production

- Horizontal wells:
  - Drilled vs. To be drilled

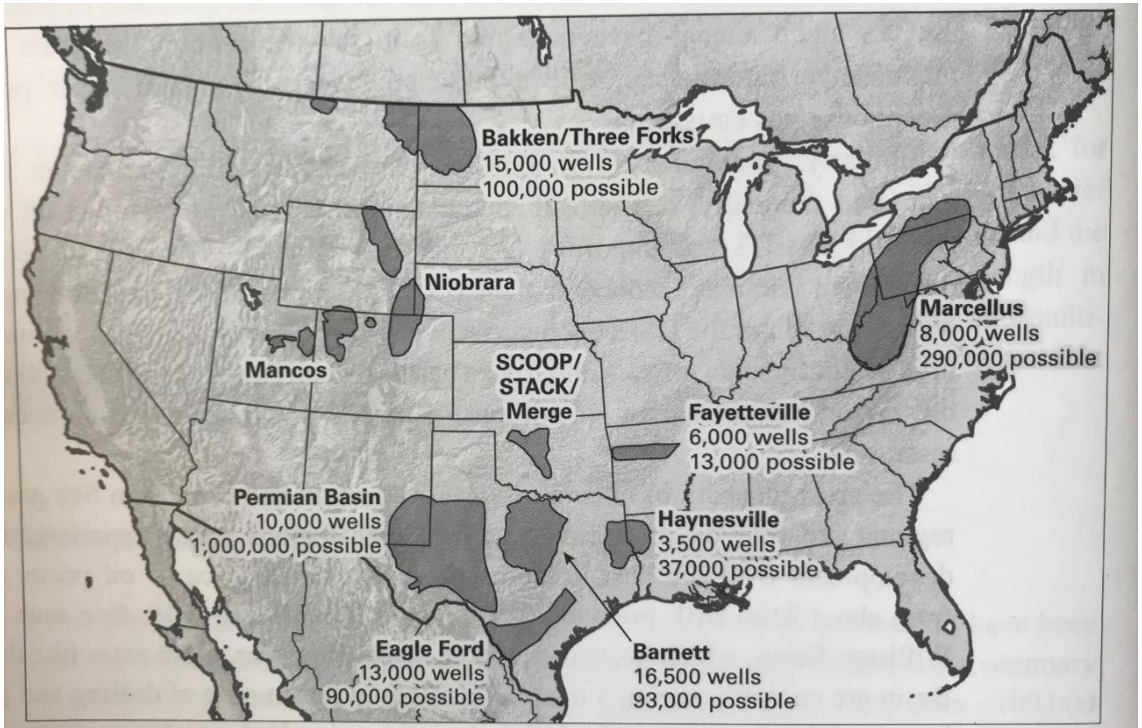

Figure 1.3 Horizontal wells drilled in major unconventional plays in the US as of 2017 and the numbers of wells that could be drilled in the future based on technically recoverable reserves. From Svetlana Ikonnikova, Bureau of Economic Geology, 2017.

Zoback MD, Kohli AH, 2019, Unconventional Geomechanics, Cambridge Univ

Unconventional Resources
Natural Gas production

SEOUL NATIONAL UNIVERSITY

- Locations of unconventional oil and gas plays & estimates of recoverable reserves

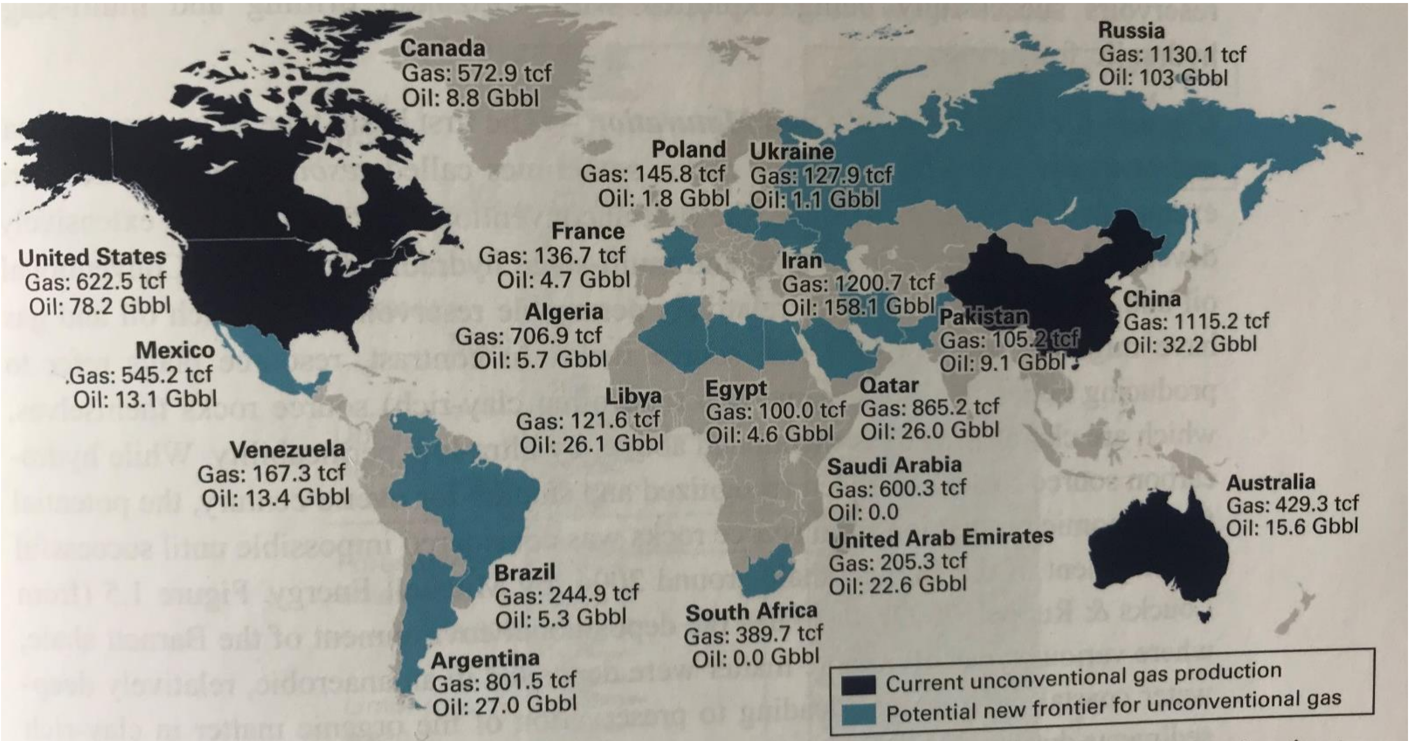

Figure 1.4 Locations of unconventional oil and gas plays throughout the world and estimates of technically recoverable reserves. World Energy Council, 2016; US Energy Information Agency.

Consumption of natural gas in the US in 2018: ~ 30 tcf

Zoback MD, Kohli AH, 2019, Unconventional Geomechanics, Cambridge Univ

Unconventional Resources
Permeability

- Ranges of permeability values for conventional and unconventional reservoir

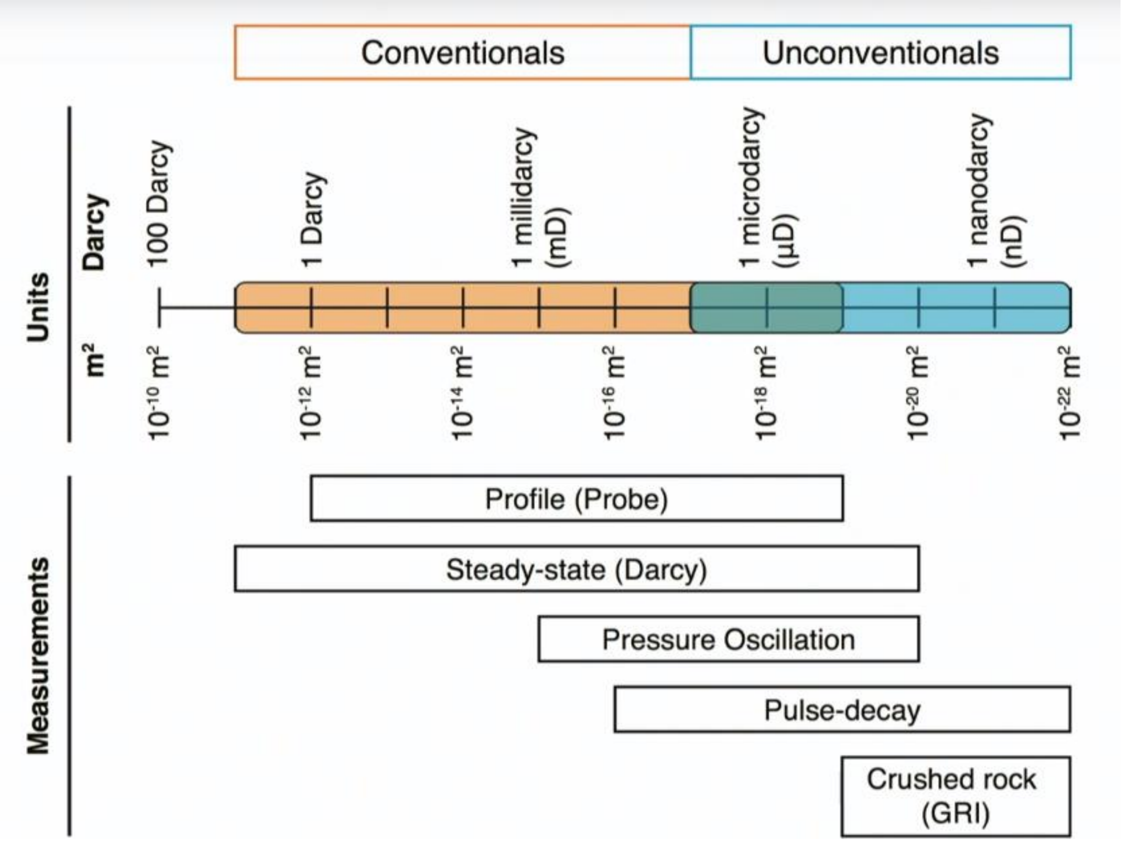

Zoback MD, Kohli AH, 2019, Unconventional Geomechanics, Cambridge Univ

Unconventional Resources
Permeability

- Permeability versus depth
  - Permeability is stress-dependent (especially for fractured rock)

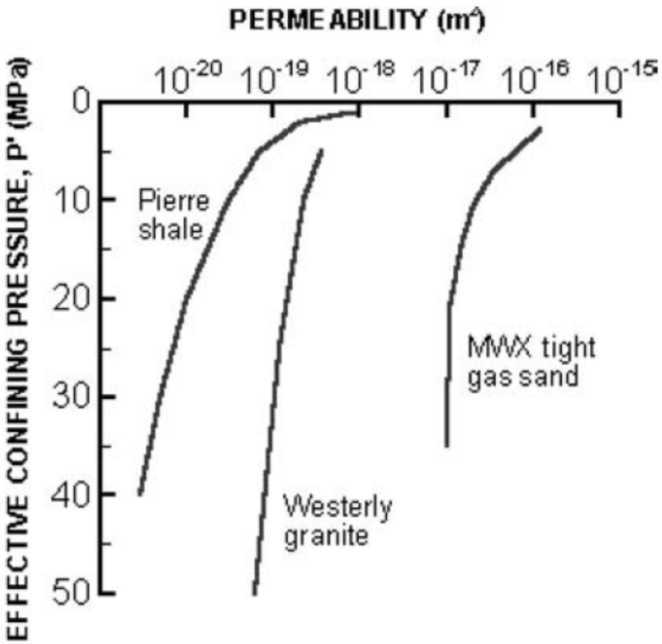

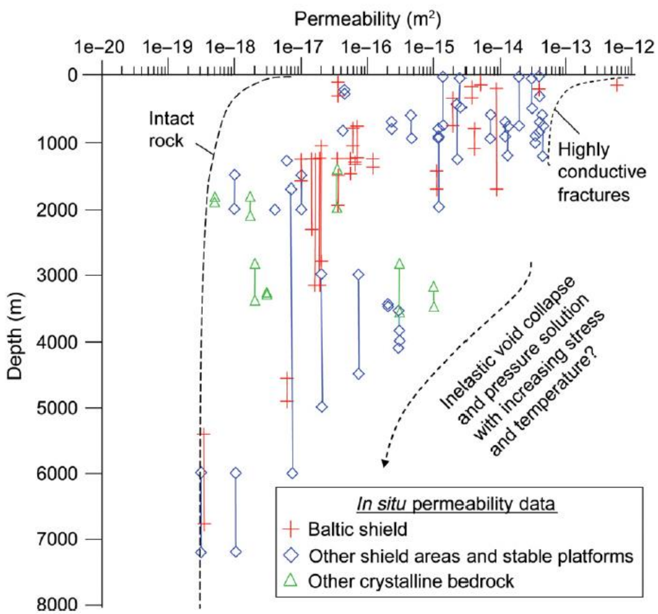

Rutqvist, J., O. Stephansson. The Role of Hydromechanical Coupling in Fractured Rock Engineering. *Hydrogeology Journal 11(1) 2003: 7-40.*
Rutqvist, J. , 2015, Fractured rock stress-permeability relationships from in situ data and effects of temperature and chemical-mechanical couplings. Geofluids 15(1-2): 48-66.

Hydraulic Fracturing
Introduction

SEOUL NATIONAL UNIVERSITY

- The purpose of hydraulic fracturing
  - to bypass near-wellbore damage and return a well to its "natural" productivity
  - to extend a conductive path deep into a formation and thus increase productivity beyond the natural level
  - to alter fluid flow in the formation.
- Complexity of HF
  - Fluid Mechanics: flow within the fracture
  - Rock Mechanics: deformation and stress in the rock
  - Fracture Mechanics: all aspects of the failure and fracture initiation/propagation
  - Thermal Process: exchange of heat between the fracturing fluid and the reservoir

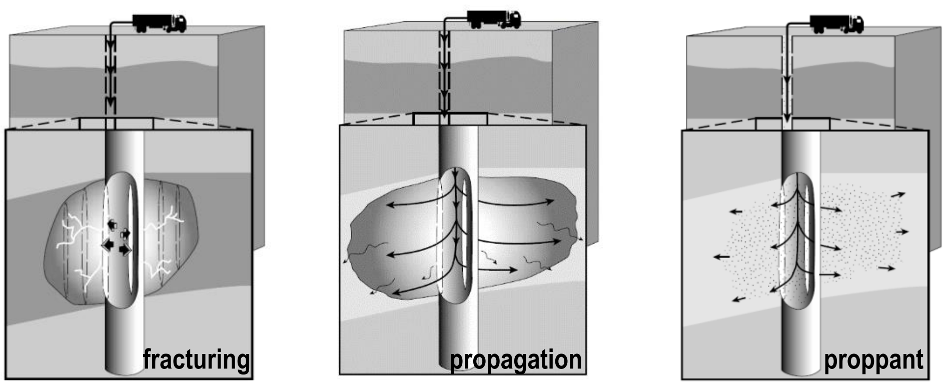

Smith & Shlyapobersky, 2000, Basics of HF, Eds: Economides & Nolte, Reservoir Stimulation, 3rd Ed., Wiley

Unconventional Resources
Horizontal Drilling

SEOUL NATIONAL UNIVERSITY

- Horizontal Drilling and multi-stage hydraulic fracturing

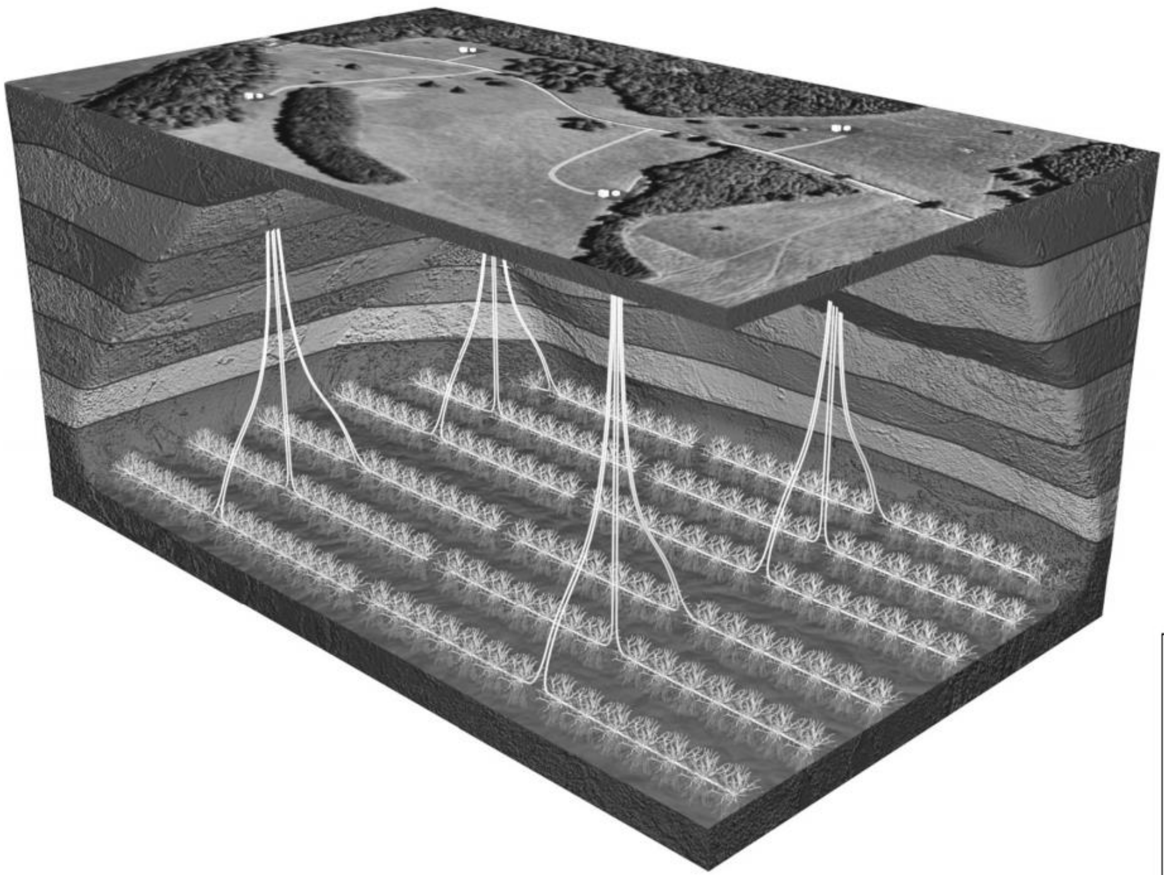

Zoback MD, Kohli AH, 2019, Unconventional Geomechanics, Cambridge Univ

wiki.aapg.org

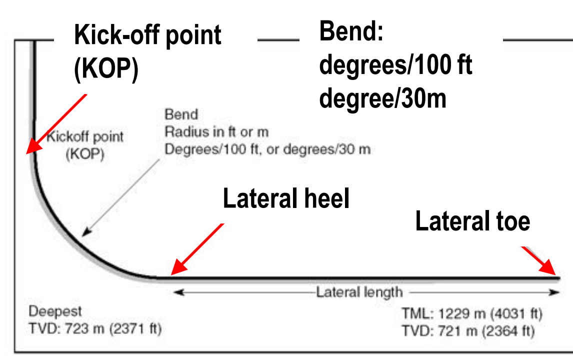

- Horizontal wells in the US
  - Depth: ~2.5 km up to ~4 km
  - Thickness: ~ tens of meters
  - Lateral lengths: 1,000~3,000 m

Table 1.3 General attributes of horizontal wells in different unconventional basins (from Kennedy et al. (2016) and other sources).

Formation	Depth range (m)	Thickness range (m)	Lateral lengths (m)
Bakken	2,920–3,200	12–22	2,650–3,050
Barnett	2,000–2,600	30–180	12,00–1,325
Duvernay	2,500–4,000	20–70	1,830–2,150
Eagle Ford	2,100–3,700	30–145	1,500–2,135
Fayetteville	300–2,150	6–61	1,430–1,680
Haynesville	3,200–4,100	61–91	1,340–1,430
Horn River	2,000–2,750	38–137	1,524–2,000
Marcellus	1,200–2,600	15–61	1,280–1,500
Montney	1,500–3,500	46–305	1,430–1,740
Niobrara	900–4,300	15–91	1,230–1,550
Utica	600–4,300	21–230	1,430–1,890
Wolfcamp	1,676–3,350	457–795	1,390–2,050

Zoback MD, Kohli AH, 2019, Unconventional Geomechanics, Cambridge Univ

Unconventional Resources
Horizontal Drilling

SEOUL NATIONAL UNIVERSITY

- Hydraulic fracturing parameters
  - Injection volume: 14~27 m3/m
  - Total injection volume: 19,000 m3 ~ 77,000 m3/well
  - Flowback recovery: 5% ~ 100%
  - Surface injection pressure: 45 ~ 62 MPa
  - Number of stages: 7~ 18 stages
  - Duration of fluid injection per stage: 1 ~ 4 hours
  - Average injection flow rate: 8~16 m3/min (132 ~ 264 l/sec)
  - Injected proppant mass per well: 400 ~ 4,000 tonnes
  - Fracture height: 100~500 m
  - Fracture horizontal length: 300~900 m

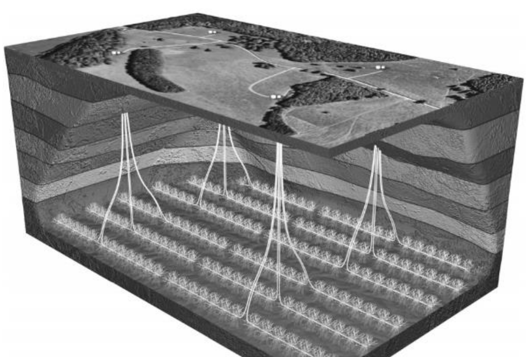

Table 8.2 Hydraulic fracturing in different formations.

Parameter	Value	Formation
Total injected fracturing fluid volume	20,000 m^3 (16,000–26,000 m^3)	Marcellus
	19,000 m^3 (11,000–23,000 m^3)	Barnett
	77,000 m^3 (mean), 66,000 m^3 (median) (35 wells) (2013–2014)	Horn River
	64,000 m^3 (2010–2012)	Haynesville
	19,000 m^3 (6,000–25,000 m^3)	Eagle Ford
	23,000 m^3	
Injected fluid volume normalized by horizontal well length	14 m^3 /m (235 wells)	Marcellus
	25 m^3 /m (2004)	Barnett
	19 m^3 /m (2006)	Horn River
	15 m^3 /m (2008–2012)	
	27 m^3 /m (35 wells) (2012–2014)	
Injected volume flowback recovery	1–50%	Marcellus
	65% (1 year)	Barnett
	90% (2 years)	Horn River
	100% (3 years)	Haynesville
	13% (8 wells)	
	5%	
Surface injection pressure	45–62 MPa	Marcellus
	54 MPa (max. 22 wells)	Horn River
	49 MPa (avg. 22 wells)	
Bottom-hole injection pressure	55–83 MPa (30–55 MPa surface injection pressure)	Woodford
	48–85 MPa	Unspecified
Number of stages	12 (7–24) (184 wells)	Marcellus
	18	Horn River
Fluid injection duration per stage	2–3 h	Marcellus
	3–4 h	Horn River
	2.5-3h	Woodford
Average injection flow rate (for the duration of each stage)	12 m^3 /min	Marcellus
	8–16 m^3 /min	Barnett
	16 m^3 /min (35 wells)	Horn River
	15 m^3 /min	Woodford
Injected proppant mass (per well)	2,100 tonnes (400–3,600 tonnes) (187 wells)	Marcellus
	3,000 tonnes (48 wells)	Horn River
	4,000 tonnes	
Fracture height inferred from microseismic measurements	~160 m (median), ~500 m (max.)	Marcellus
	~160 m (median)	Barnett
	250 m (12 wells)	Horn River
	~130 m (median)	Woodford
	~100 n (median)	Eagle Ford
Fracture horizontal length inferred from microseismic measurements	~300–400 m	Marcellus
	~600–900 m (12 wells)	Horn River

Zoback MD, Kohli AH, 2019, Unconventional Geomechanics, Cambridge Univ

- Wellbore completion
  - Plug-and-perf method
  - Sliding sleeve method in open holes

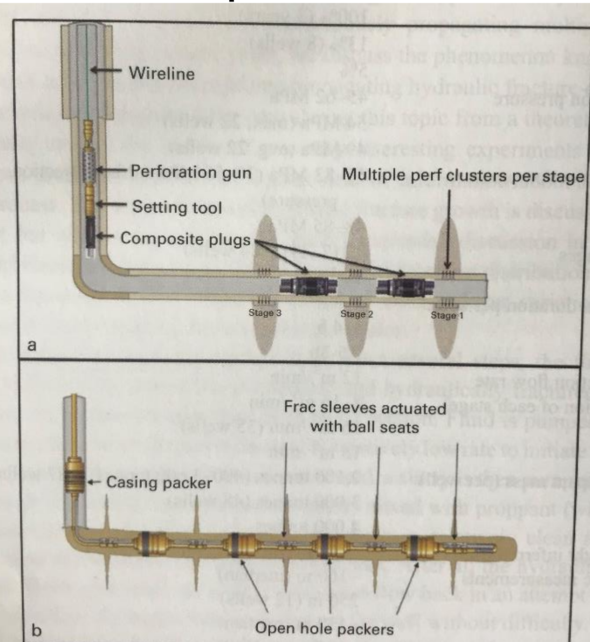

Figure 8.4 Schematic illustrations of the two most common wellbore completion methods. (a) The plug-and-perf method which utilizes separately deployed frac plugs to isolate sections of a cased and cemented well. After setting the plug, clusters of perforations are made at several places (usually tens of meters apart) before hydraulic fracturing. (b) The sliding sleeve method is usually used in open holes. A single piece of tubing with multiple packers is deployed. A given interval is pressurized by dropping a ball into a valve which slides open when pressurized. After Burton (2016).

Zoback MD, Kohli AH, 2019, Unconventional Geomechanics, Cambridge Univ

Unconventional Resources
Horizontal Drilling

SEOUL NATIONAL UNIVERSITY

- Direction of horizontal drilling & fracture propagation
  - Direction of fracture propagation: Parallel to the maximum horizontal stress
  - Direction of horizontal drilling: to the minimum horizontal stress

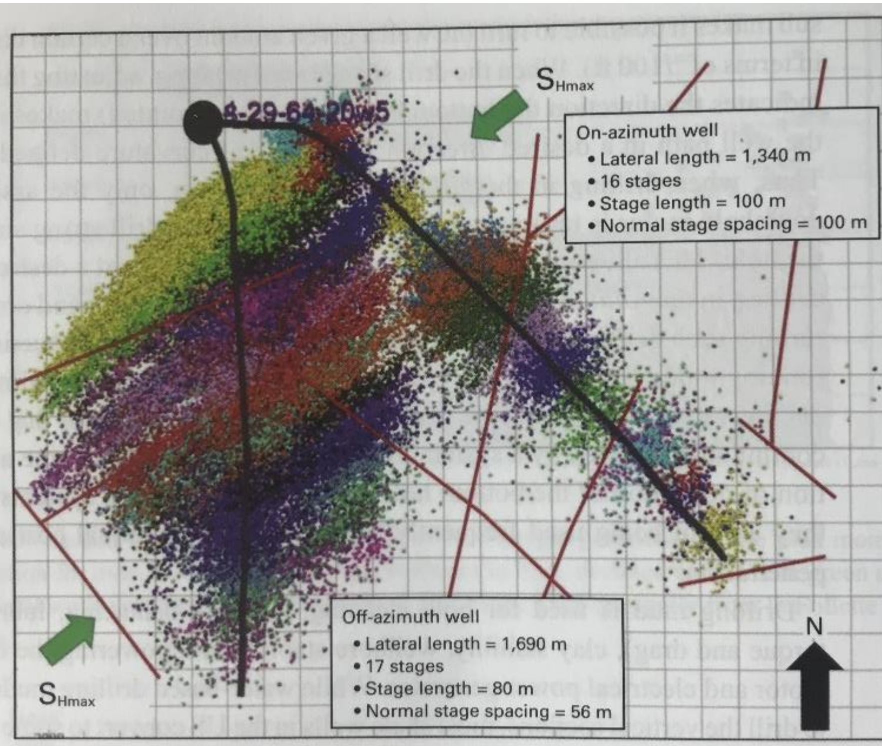

Figure 8.3 Microseismic events recorded by arrays deployed in the heel of each well associated with two wells drilled in the Duvernay formation. Events are colored by stage. Red lines represent lineaments (possible faults) interpreted from seismic data. From Stephenson et al. (2018)

Zoback MD, Kohli AH, 2019, Unconventional Geomechanics, Cambridge Univ

- Hydraulic fracturing
  - Well pad with parallel horizontal wells
  - Microseismic events located (essential component of locating the created reservoir)

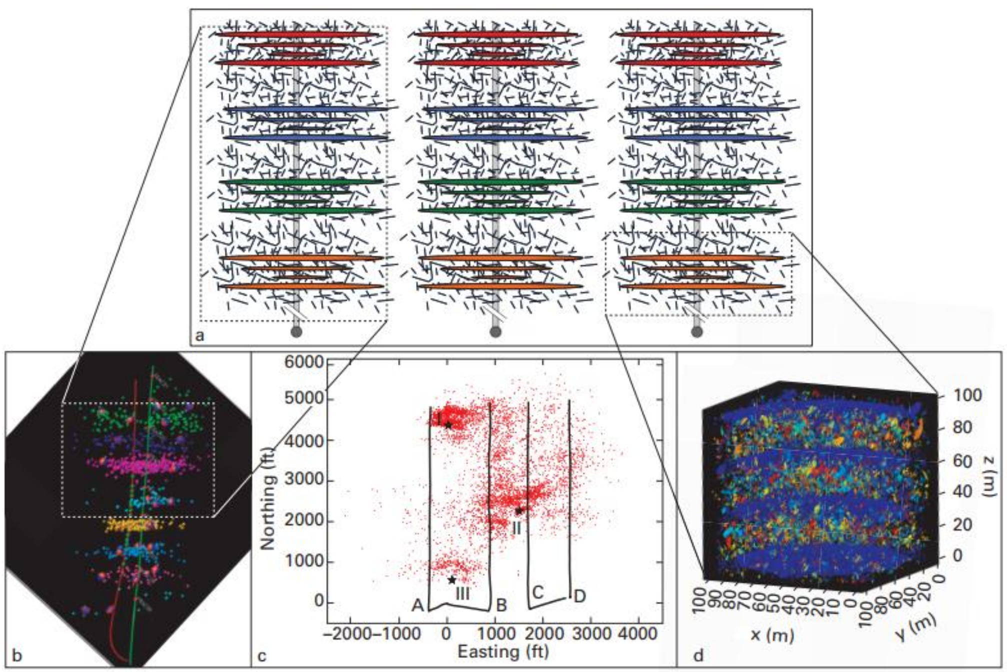

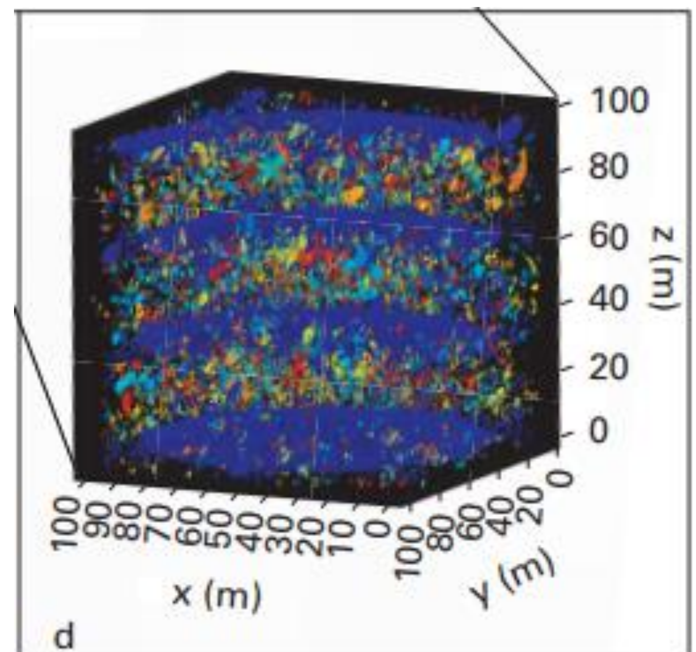

Theoretical model

Zoback MD, Kohli AH, 2019, Unconventional Geomechanics, Cambridge Univ

Unconventional Resources
Production

SEOUL NATIONAL UNIVERSITY

mscf: thousand standard cubic feet
mmscf: million standard cubic feet

- Average production per wells
  - Production rapidly drops with production
  - Efficiency is rapidly increasing

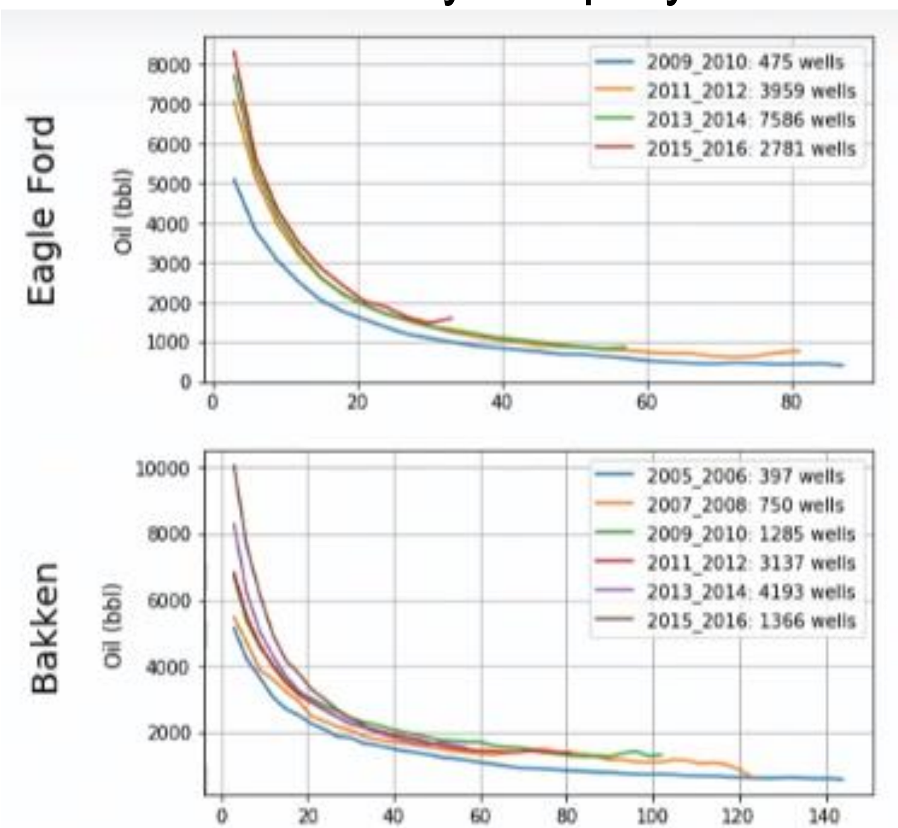

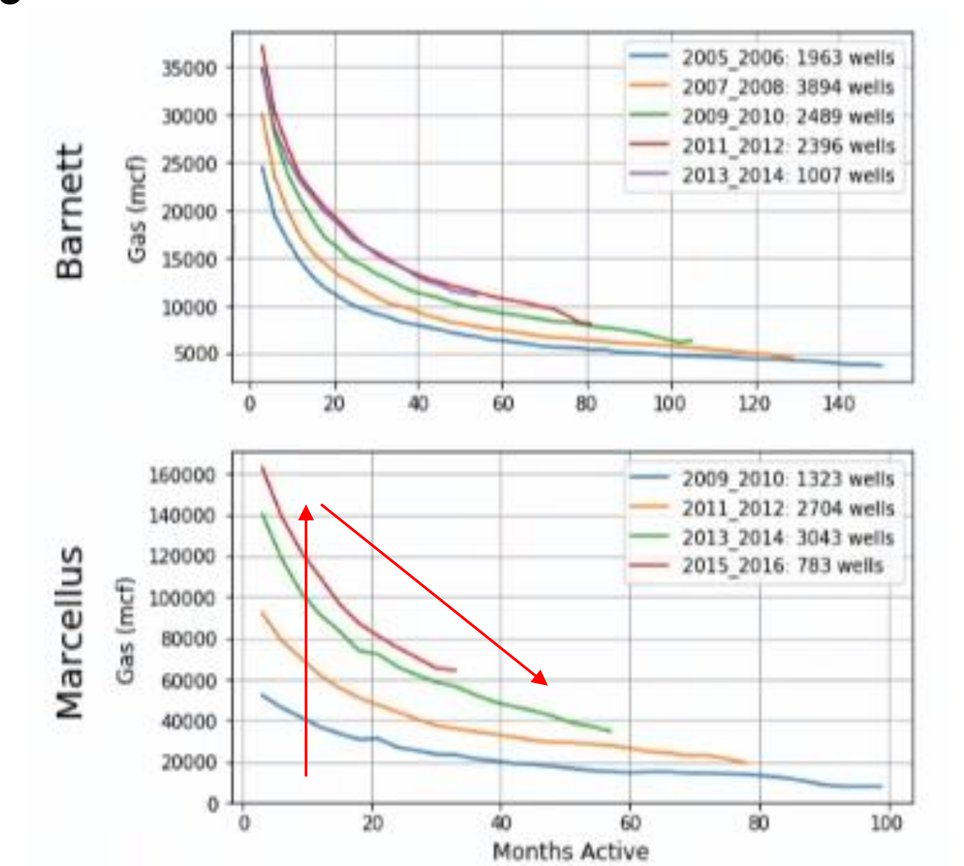

Zoback MD, Kohli AH, 2019, Unconventional Geomechanics, Cambridge Univ

Hydraulic Fracturing
Factors – Initiation and propagation direction

SEOUL NATIONAL UNIVERSITY

- Hydraulic fracture initiate at the minimum tangential stress

Hydrofracturing (tensile failure)
수압파쇄 (인장파괴)

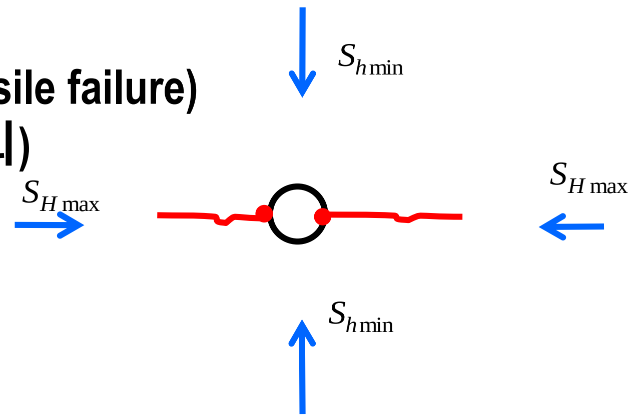

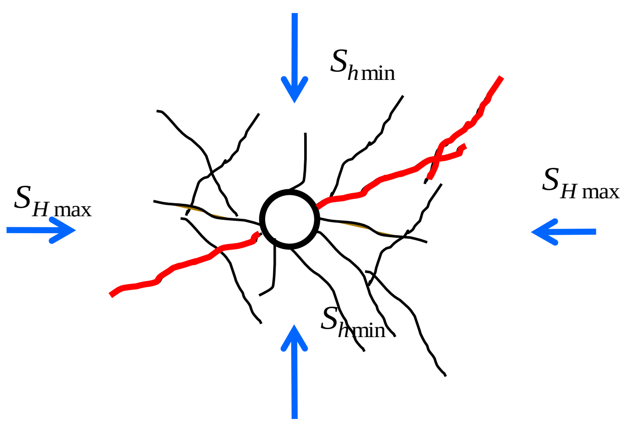

Hydroshearing (shear failure)
절리팽창 (전단파괴)

Hydraulic Fracturing
Factors - Confinement

- Confinement of a fracture between layers of higher stress

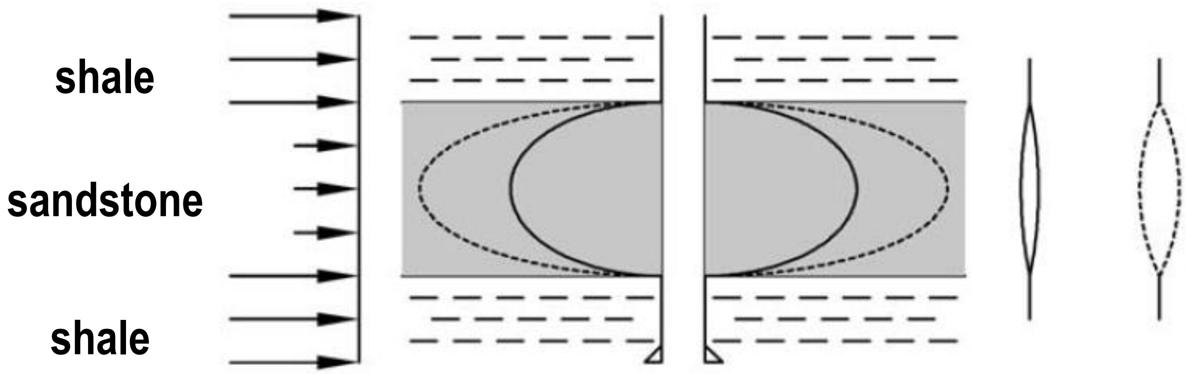

Fjaer et al., 2008, Petroleum related rock mechanics, 2nd ed., Elsevier

Hydraulic Fracturing
Factors - Confinement

SEOUL NATIONAL UNIVERSITY

- Growth of vertical hydraulic fractures in shale gas/tight oil
  - Barnett, Marcellus, Woodford and Eagle Ford
  - Monitored by microseismic events

Groundwater level

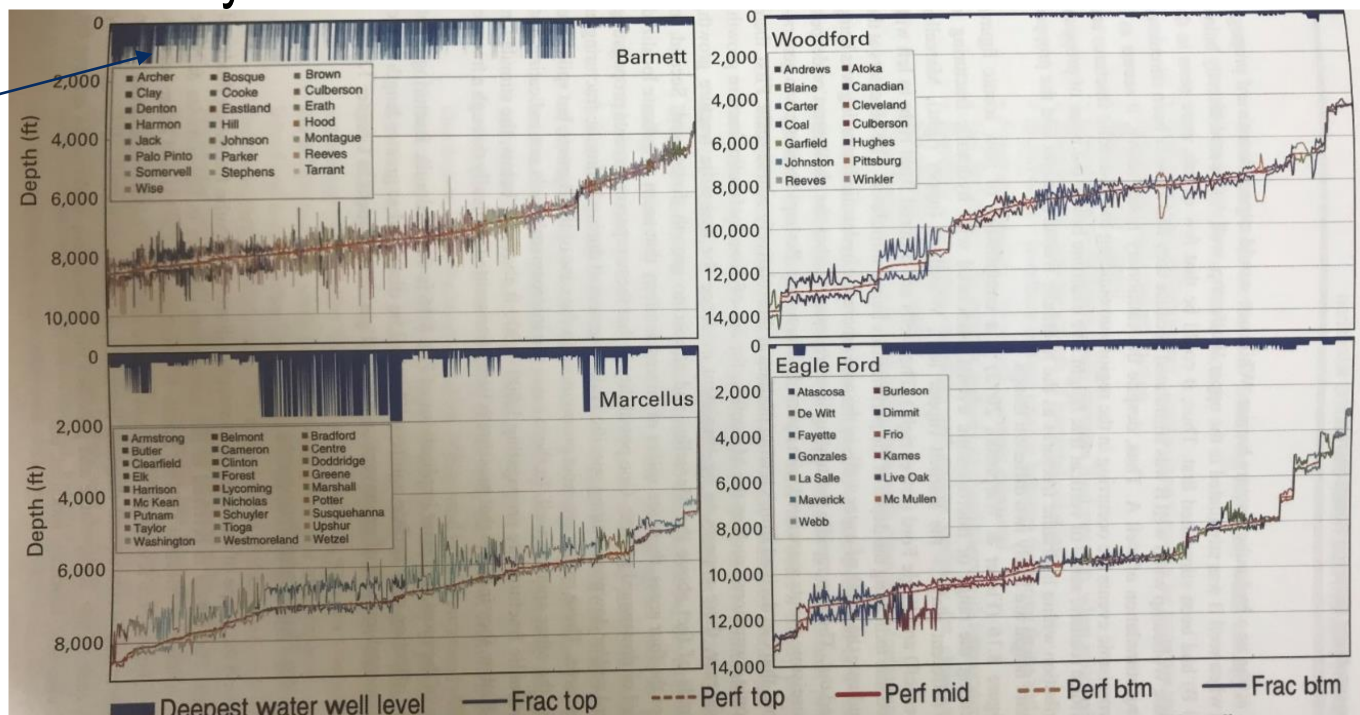

Figure 8.16 Depths of shallowest and deepest microseismic events associated with hydraulic fracturing in four unconventional plays. The wells are sorted by depth of the perforations (red line) from right to left. The counties in which the measurements are made is shown in each inset and are used to color the lines representing microseismic event depths. The blue bars indicate the depth of water wells in each area. From Fisher & Warpinski (2012).

Zoback MD, Kohli AH, 2019, Unconventional Geomechanics, Cambridge Univ

Hydraulic Fracturing
Factors – Required pressure

$$\frac{\partial p}{\partial x} = -\frac{12 q\mu}{h_f w^3}, \quad \frac{dp}{dx} = -\frac{64 q\mu}{\pi h_f w^3},$$

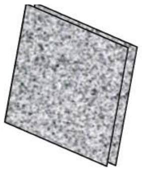

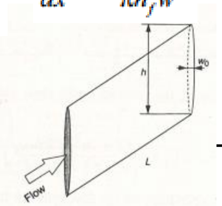

SEOUL NATIONAL UNIVERSITY

Pressure required to extend the fracture

$$p_e = p(\sigma_h) + p(\text{flow}) + p(\text{tip})$$

Keep the fracture open

Drive the fluid flow

Overcome the resistance at the fracture tip

- Stress intensity at the tip

$$K_i = (P_f - S_3)(\pi L)^{1/2} \quad (4.38)$$

half

where K_i is the stress intensity factor, P_f is the pressure within the fracture (taken to be uniform for simplicity), L is the length of the fracture and S_3 is the least principal stress. Fracture propagation will occur when the stress intensity factor K_i exceeds K_{ic},

  - Fracture propagation $K_i > K_{ic}$
    - K_{ic}: fracture toughness (=critical stress intensity), MPa m$^{1/2}$
    - K_{ic}: A material property ranging ~1.0 ~ 2.4 MPa m$^{1/2}$(Zang & Stephansson, 2010)
    - Important for propagation
  - Once fracture reaches a few tens of cm, small pressure in excess of S3 is required regardless of toughness.

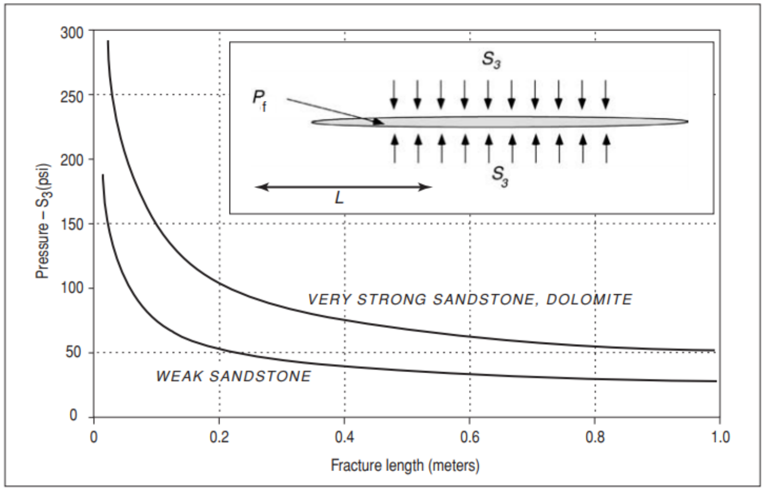

Figure 4.21. The difference between internal fracture pressure and the least principal stress as a function of fracture length for a Mode I fracture (see inset) for rocks with extremely high fracture toughness (such as very strong sandstone or dolomite) and very low fracture toughness (weakly cemented sandstone).

Zang & Stephansson, 2010, Stress Field of the Earth's Crust, Springer

Hydraulic Fracturing
Factors – Required pressure (fracture toughness)

- Crack-tip deformation mode
  - Mode I: crack opening model – mostly relevant to Hydraulic Fracturing
  - Mode II: sliding model
  - Mode III: tearing model

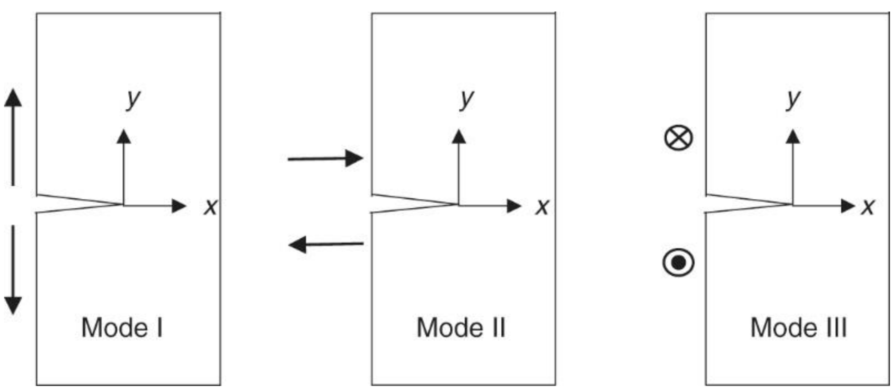

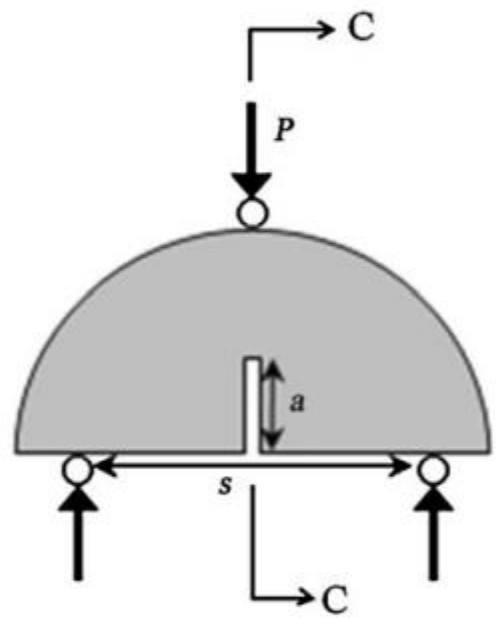

Fracture toughness test on semi-circular bend specimen (Kuruppu et al., 2014)

Jaeger, Cook & Zimmerman, 2007, Fundamentals of Rock Mechanics, 4th ed, Blackwell Publishing
Kuruppu MD et al., 214, ISRM-Suggested Method for Determining the Mode I Static Fracture Toughness Using Semi-Circular Bend Specimen, Rock Mech Rock Engng, 47:267–274

Hydraulic Fracturing
Factors – Initiation and propagation direction

SEOUL NATIONAL UNIVERSITY

- Breakdown Pressure

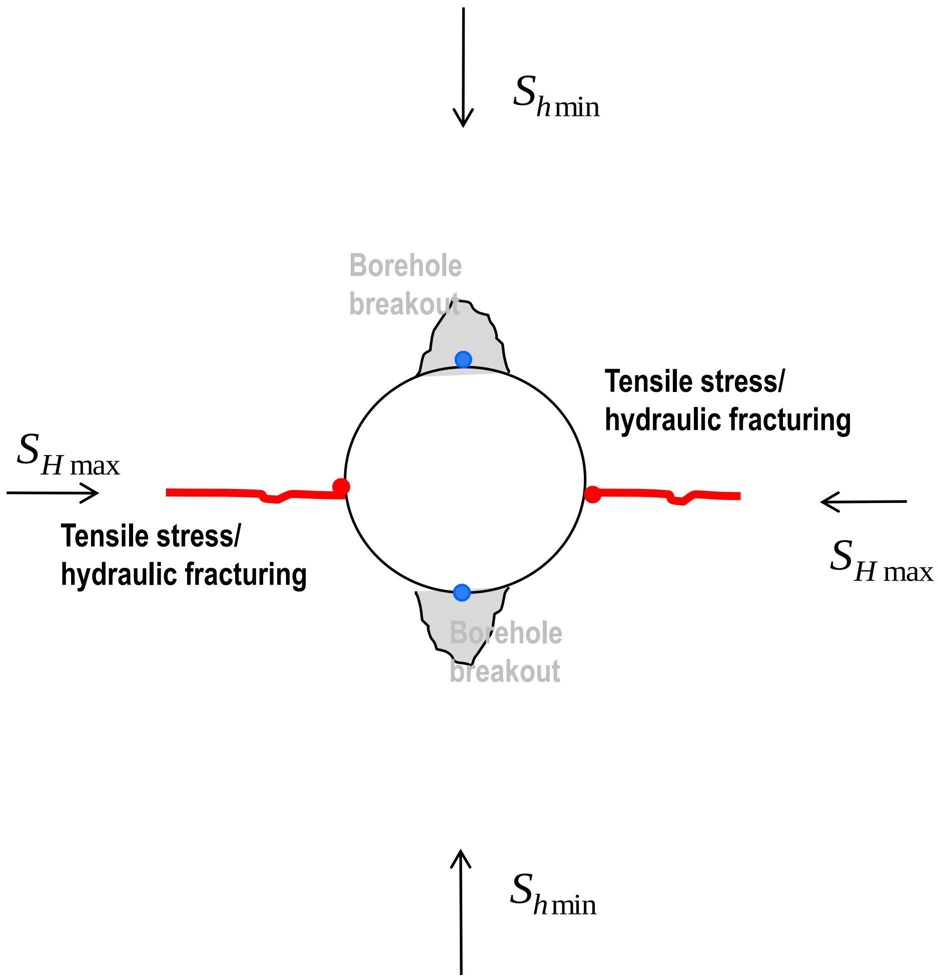

– Required internal hydraulic pressure to induce hydraulic fracturing (assuming that the formation is impermeable)

  - Impermeable, fast pressurization (upper limit)

$$P_w = 3S_{h\min} - S_{H\max} + T_0$$

  - Permeable, slow pressurization (lower limit)

$$P_w - P_f = \frac{3S_{h\min} - S_{H\max} + T_0}{2 - \alpha\left(1 - 2\nu\right) / (1 - \nu)}$$

– Fracturing occurs perpendicular to the minimum horizontal stress

Hydraulic Fracturing
Factors – Initiation and propagation direction

SEOUL NATIONAL UNIVERSITY

- Pressure response during hydraulic fracturing
  - Distinct breakdown pressure may/may not be observed

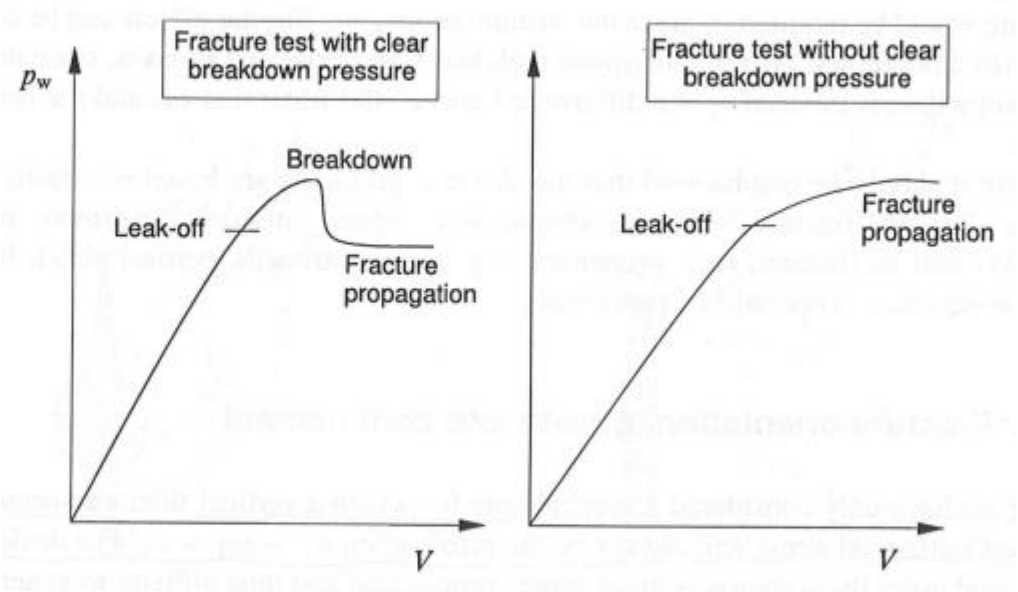

Fjaer et al., 2008, Petroleum related rock mechanics, 2nd ed., Elsevier

Hydraulic Fracturing
Factors – Initiation and propagation direction

- Hydraulic fracture propagate normal to the minimum stress

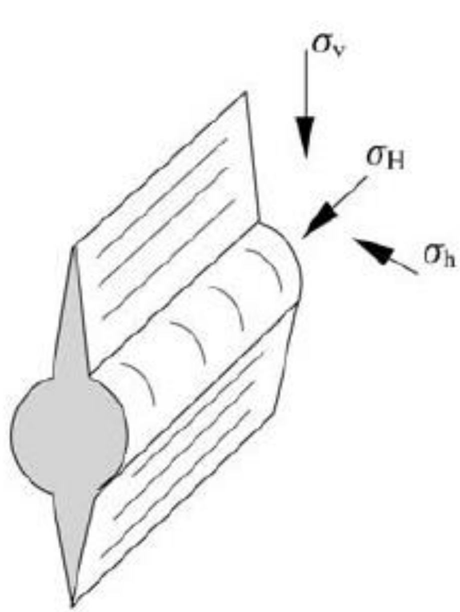

Fracture parallel to the borehole

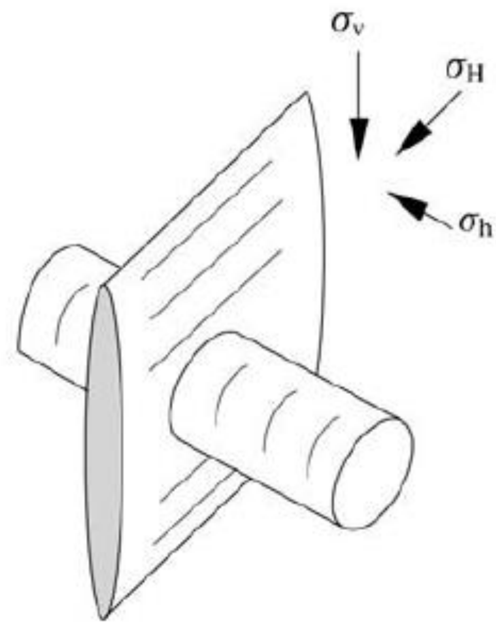

Fracture normal to the borehole

Fjaer et al., 2008, Petroleum related rock mechanics, 2nd ed., Elsevier

Hydraulic Fracturing
Factors – Initiation and propagation direction

SEOUL NATIONAL UNIVERSITY

- Hydraulic fracture propagate normal to the minimum stress

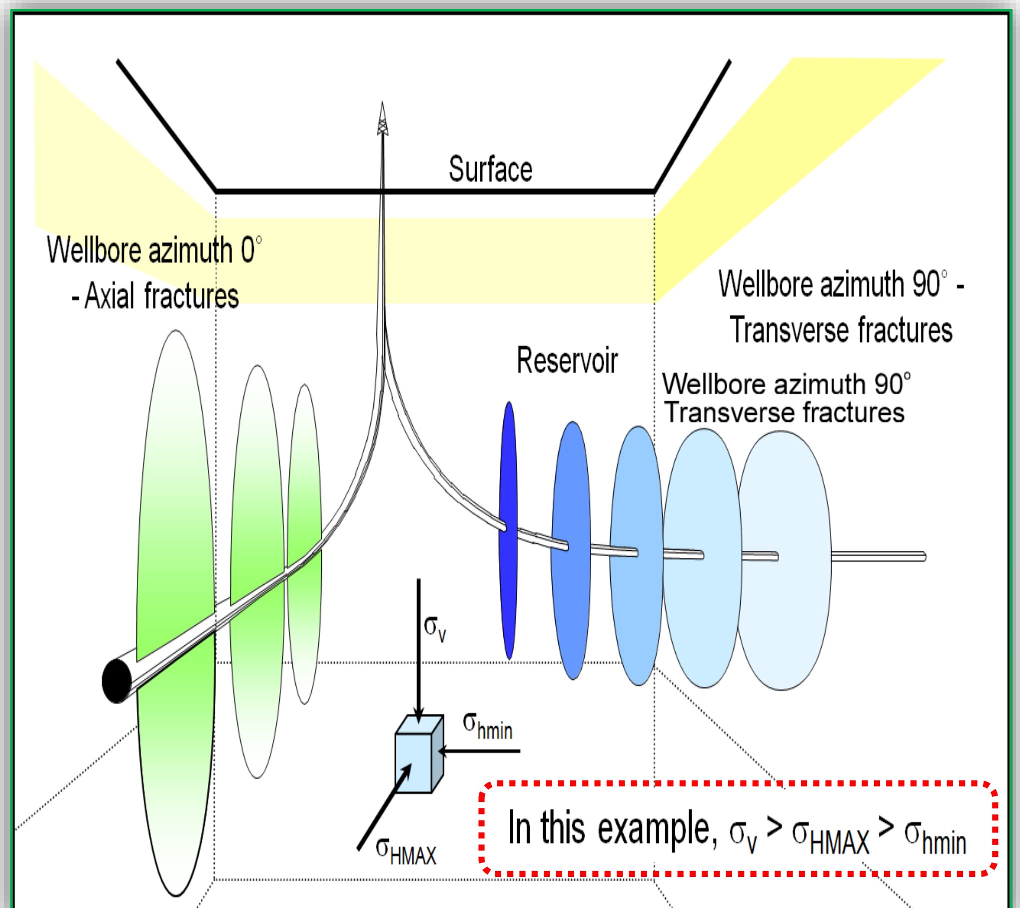

(MA Dusseault, 2011)

State of in situ "dictates" the direction of hydraulic fracturing

Hydraulic Fracturing
Factors – Initiation and propagation direction

SEOUL NATIONAL UNIVERSITY

- Evidence of tensile fracture: Observed tensile fractures from multistage hydraulic fracturing
  - Core
  - Image logs

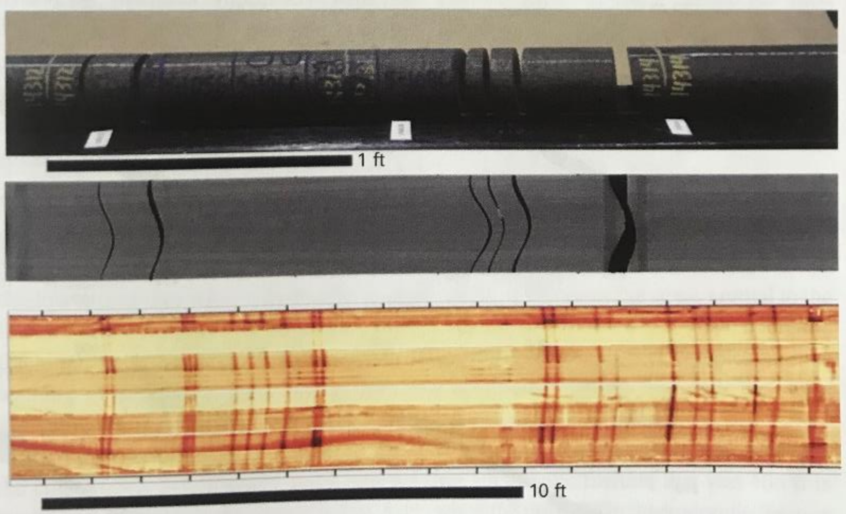

Figure 8.8 Hydraulic fractures observed in core and image logs in the ConocoPhillips drill through/core through experiment. After Raterman et al. (2017).

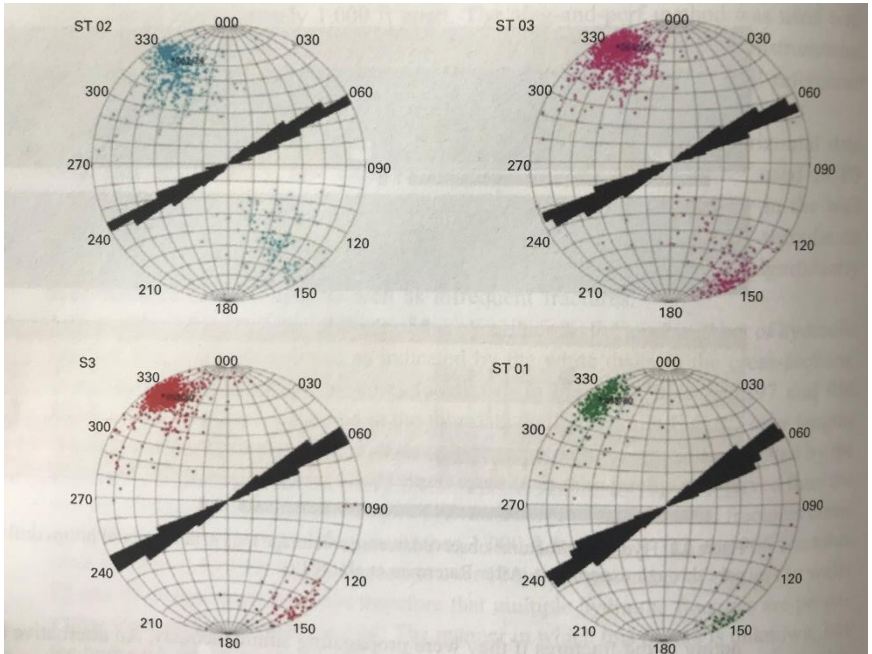

Figure 8.9 The orientation of hydraulic fractures observed in core and image logs in the ConocoPhillips drill through/core through experiment. After Raterman et al. (2017). Note that the hydraulic fracture orientations are perfectly aligned with the stress field in this region as shown in Fig. 7.2.

Zoback MD, Kohli AH, 2019, Unconventional Geomechanics, Cambridge Univ

Hydraulic Fracturing
Factors – Initiation and propagation direction

- Initiation vs. propagation
- Hydraulic fractures away from the well propagate normal to the minimum stress (Valkó & Economides, 1995)
  - The plane of fracture initiation is affected greatly by the perforation patterns
  - Near-well effect leads to ‘choke’ effect (near well tortuosity)
  - In the below, the second wing may be generated
  - With excessive resistance ahead of a second wing may result in only one wing of a fracture

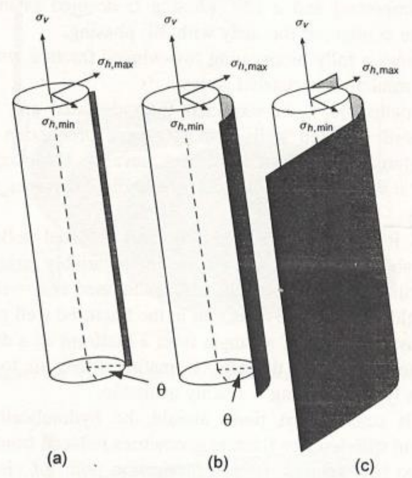

Figure 4.5 Fracture initiation from a vertical well (a), turning normal to the least resistance, in most cases, the minimum horizontal stress (b) and, finally, once the resistance is overcome, evolving into a two-winged fracture (c)

Valkó P & Economides MJ, 1995, Hydraulic fracture mechanics, John Wiley & Sons

Hydraulic Fracturing
Factors – Initiation and propagation direction

- <u>Initiation vs. propagation</u>
- Direction of fracture initiation and propagation is closely related to the production characteristics (Valkó & Economides, 1995)
  - Vertical well – vertical fracture: linear flow
  - Horizontal well – transverse vertical fracture: linear + radial flow
    - Although radial flow reduce the production, composite flowrates from multiple treatment is larger than from a single fracture
  - Entry from the well to the fracture needs to be minimized
    - Problem in the right can happen even if drilling was pr

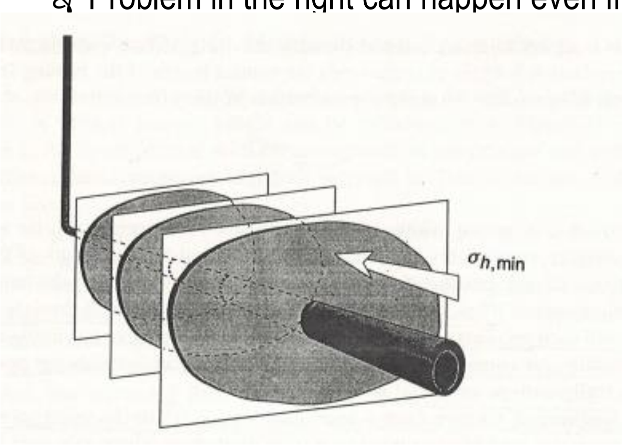

Transverse fracture from a horizontal well

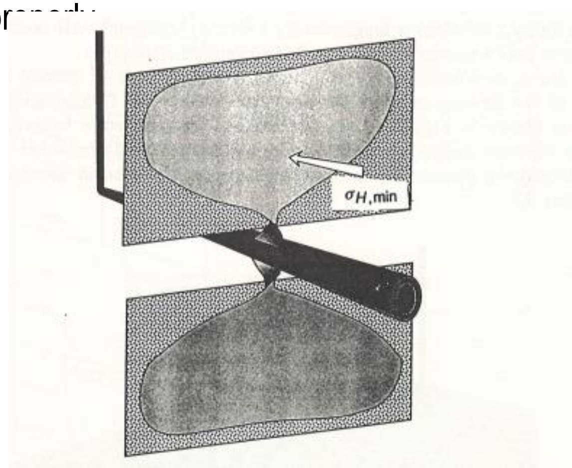

Turning from longitudinal initiation to transverse direction

Valkó P & Economides MJ, 1995, Hydraulic fracture mechanics, John Wiley & Sons

Hydraulic Fracturing
Factors – Initiation and propagation direction

SEOUL NATIONAL UNIVERSITY

- Pressure response monitoring during fracturing is important
  - Growth direction
  - Abnormal pressure increase due to proppant bridging

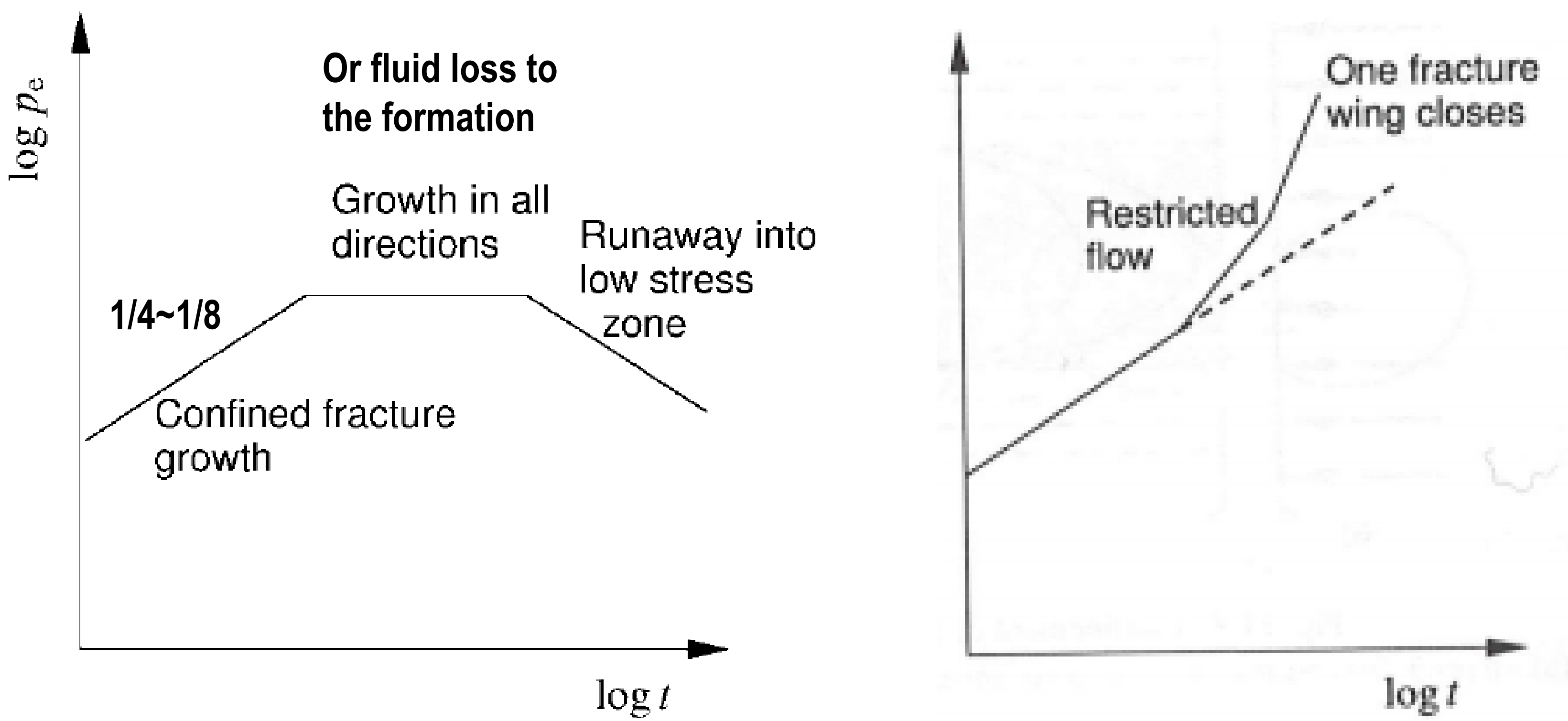

Fjaer et al., 2008, Petroleum related rock mechanics, 2nd ed., Elsevier

Models of hydraulic fracturing

- Models of hydraulic fracturing
  - Economic optimization
  - Design of a pump schedule
  - Simulation of the fracture geometry and proppant placement
  - Evaluation of treatment
    - comparison of prediction with actual behavior
  - Estimation of fluid volume and proppant to create a fracture with a desired conductivity and geometry

Models of hydraulic fracturing – circular crack

SEOUL NATIONAL UNIVERSITY

Circular Penny shaped crack model by Sneddon (1946)

- ✓ **Pressure** required to extend a Crack Radius of R ($p_{net} = p_{crack}$ – pressure against crack opening)

$$p_{net} = \sqrt{\frac{\pi \gamma_F E}{2(1-v^2)R}}$$

Derived using linear elastic fracture mechanics

- ✓ **Volume** of Crack

$$V = \frac{16(1-v^2)R^3}{3E} p_{net}$$

- ✓ **Width** of a Static Penny-shaped Crack (R = penny-shaped crack radius)

$$w(r) = \frac{8 p_{net} R(1-v^2)}{\pi E} \sqrt{a-(r/R)^2}$$

Derived using theory of linear elasticity

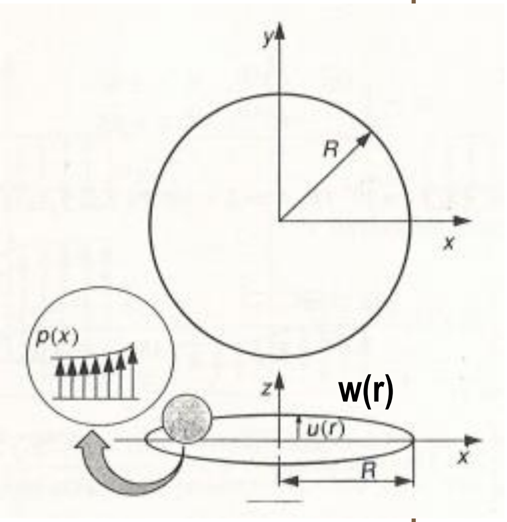

Hydraulic Fracturing
Models of hydraulic fracturing – elliptical shape

SEOUL NATIONAL UNIVERSITY

- Fracture with fixed height, infinite extent and elliptical shape

Sneddon and Elliot (1946) also showed that for fractures of a fixed height h_f and infinite extent (i.e., plane strain), the maximum width is

$$w = \frac{2 p_{net} h_f \left(1 - \nu^2\right)}{E} \qquad (6\text{-}7)$$

and the shape of the fracture is elliptical, so that the average width $\overline{w} = (\pi/4)w$. The term $E/(1 - \nu^2)$ appears so commonly in the equations of hydraulic fracturing that it is convenient to define the plane strain modulus E' as

$$E' = \frac{E}{1 - \nu^2}, \qquad (6\text{-}8)$$

$$\frac{dp}{dx} = -\frac{64 q \mu}{\pi h_f w^3}, \qquad (6\text{-}9)$$

where p is the pressure, x is the distance along the fracture, and μ is the fluid viscosity.

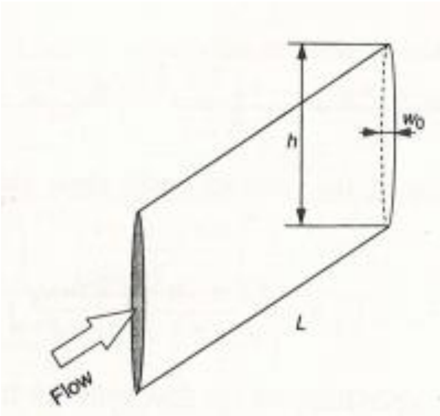

Mack & Warpinski, 2000, Mechanics of hydraulic fracturing, Eds: Economides & Nolte, Reservoir Stimulation, 3rd Ed., Wiley

Hydraulic Fracturing

Models of hydraulic fracturing –KGD vs. PKN Model

SEOUL NATIONAL UNIVERSITY

	KGD Model	*PKN Model*
	Khristianovich *et al.* (1959) Geertsma and de Klerk (1969)	Perkins and Kern (1961) Nordgren (1972)
3D -> 2D	• Plane strain in Horizontal Direction - Independent horizontal cross section • Fracture Height >> Fracture Length • Completely Confined Fracture	• Plane strain in Vertical Direction - Independent vertical cross section • Fracture Height << Fracture Length • Fixed Height
Focus on	• Fracture Mechanics and Fracture Tip	• Fluid Flow and Pressure Gradient
Ignore	• Flow Rate and Pressure in Fracture	• Fracture Mechanics and Tip Region Play

Similar to

- Planar Fracture
- 1D-Direction Fluid Flow : along the length of the fracture
- Newtonian Fluids
- Leakoff Behavior : Governed by filtration theory (Carter, 1957)
- Fracture Propagation : Continuous, Homogeneous, Isotropic Linear Elastic Solid

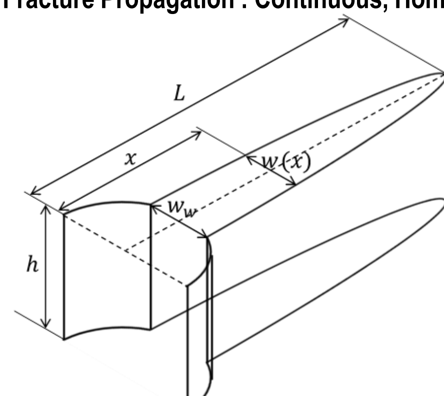

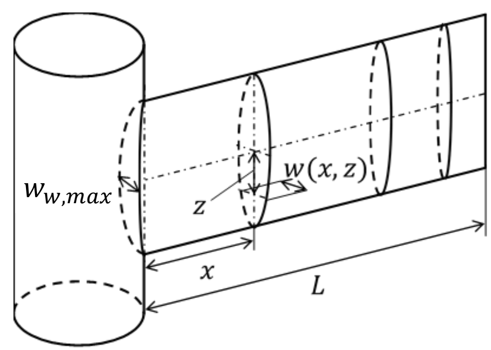

Hydraulic Fracturing
Models of hydraulic fracturing –KGD vs. PKN Model

KGD Model

Khristianovich *et al.* (1959)

Geertsma and de Klerk (1969)

PKN Model

Perkins and Kern (1961)

Nordgren (1972)

3D -> 2D

Focus on

Ignore

Similar to

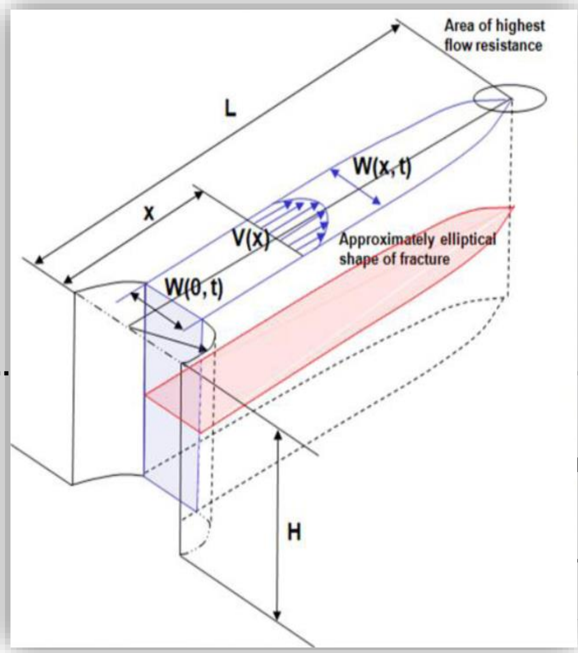

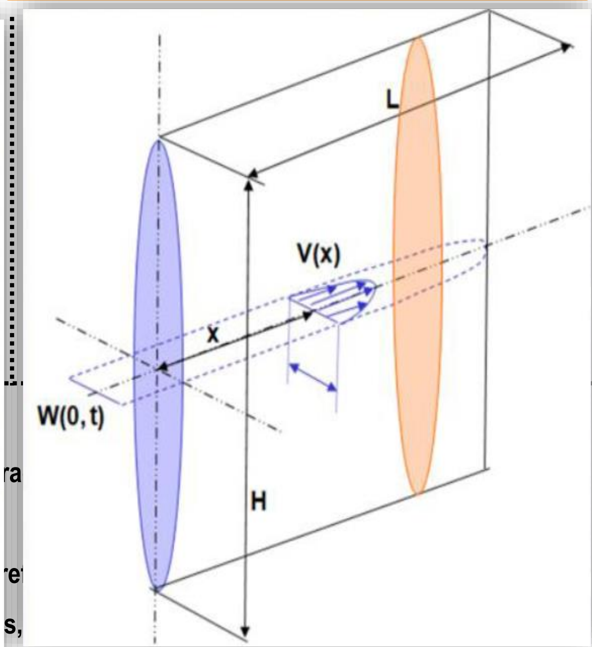

Mack & Warpinski, 2000, Mechanics of hydraulic fracturing, Eds: Economides & Nolte, Reservoir Stimulation, 3rd Ed., Wiley

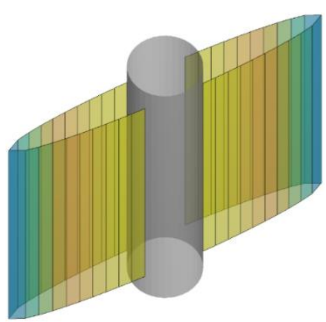

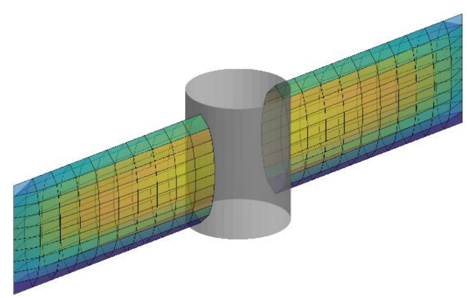

Hydraulic Fracturing
Models of hydraulic fracturing – PKN model

- Perkins and Kern (1961) & Nordgren (1972)
- Assumptions
  - Fully confined fractures (no change in the height)
    - Stresses in layers above and below the pay zone (reservoir) is large
  - Fracture cross section is elliptical
    - Maximum width proportional to the net pressure
  - Plane strain in vertical plane
  - Neglect fracture mechanics effects since pressure resulting from fluid flow is larger than the minimum pressure to extend the fracture

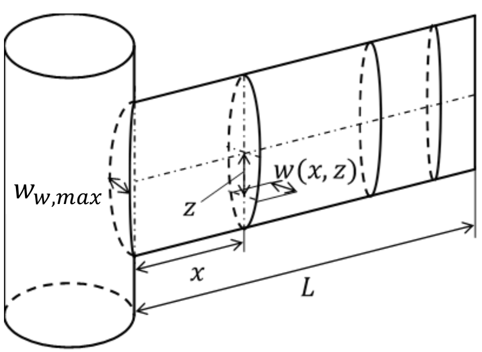

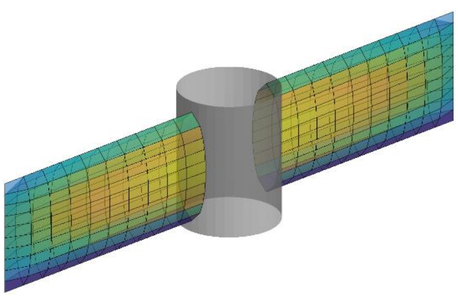

Models of hydraulic fracturing – PKN Model

Perkins & Kern (1961)

- ✓ **Pressure required to extend a Crack Radius of R = Work done by the pressure in the crack to open the additional width**

$$p_{net} = \sqrt{\frac{\pi \gamma_F E}{2(1-v^2)R}} \longrightarrow p_{net} = \left(\frac{2\pi^3 \gamma_F^3 E^2}{3(1-v^2)^2 V} \right)^{\frac{1}{5}}$$

- ✓ **Volume of Crack (q_i : constant injection rate, t : time)**

$$V = q_i t = \frac{16(1-v^2)R^3}{3E} \left(\frac{2\pi^3 \gamma_F^3 E^2}{3(1-v^2)^2 q_i t} \right)^{\frac{1}{5}}, \quad R = \left[\frac{9 E q_i^2 t^2}{128 \pi \gamma_F (1-v^2)} \right]^{\frac{1}{5}}$$

- ✓ **Max. Width of a Static Penny-shaped Crack (h_f : fixed height)**

$$w = \frac{2 p_{net} h_f (1-v^2)}{E}$$

Mack & Warpinski, 2000, Mechanics of hydraulic fracturing, Eds: Economides & Nolte, Reservoir Stimulation, 3rd Ed., Wiley

Models of hydraulic fracturing –Inclusion of leakoff

SEOUL NATIONAL UNIVERSITY

- Leakoff model
  - Presence of think layer (filter cake) may prevent loss of fluid through fracture face. In reality, fluid leakoff into the formation occurs

$$u_L = \frac{C_L}{\sqrt{t}},\qquad \frac{V_L}{A_L} = 2C_L\sqrt{t} + S_p,$$

u_L: leakoff velocity (m/s)
C_L: leakoff coefficient, m/s$^{1/2}$
S_p: spurt loss coefficient (m), width of the fluid body passing through the surface instantaneously at the very beginning of the leakoff process

t min	V_L cm^3.
1	5.2
2	6.7
4	7.3
10	8.6
20	9.7
30	10.6
40	11.4
50	12.5
60	13.2

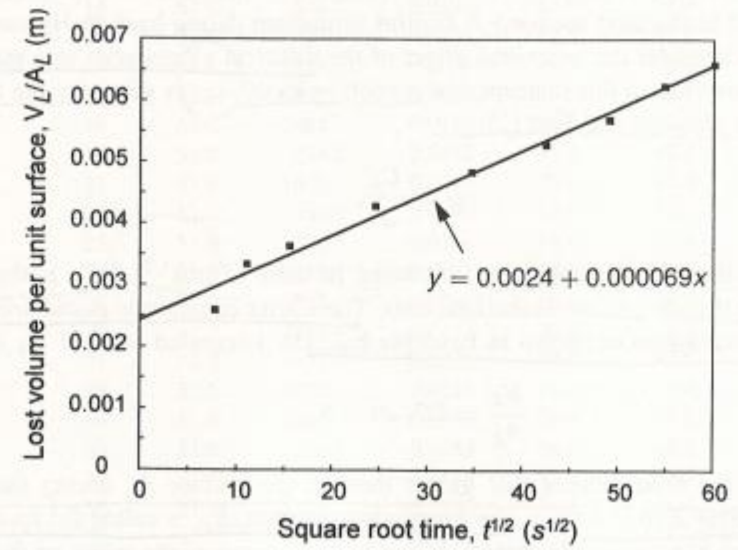

Leakoff laboratory test on core sample (cross sectional area 20 cm^2)

Valkó P & Economides MJ, 1995, Hydraulic fracture mechanics, John Wiley & Sons

Hydraulic Fracturing
Models of hydraulic fracturing –Inclusion of leakoff

SEOUL NATIONAL UNIVERSITY

Mechanisms of overpressure generation
Disequilibrium compaction (undercompaction)

SEOUL NATIONAL UNIVERSITY

- Characteristic time for linear diffusion

storativity

$$\frac{k}{\mu}\left(\frac{\partial^2 p}{\partial x^2}+\frac{\partial^2 p}{\partial y^2}+\frac{\partial^2 p}{\partial z^2}\right) = S\frac{\partial p}{\partial t}$$

$$\frac{\partial^2 p}{\partial x^2}+\frac{\partial^2 p}{\partial y^2}+\frac{\partial^2 p}{\partial z^2} = \frac{\mu S}{k}\cdot\frac{\partial p}{\partial t} = \frac{1}{c}\frac{\partial p}{\partial t}$$

$$S = \phi\beta_f + \beta_r \approx \phi\beta_f$$

$$\beta_f \approx 5\times10^{-4}/\mathrm{MPa} = 5\times10^{-10}/\mathrm{Pa}$$

$$\mu\ (\eta) \approx 10^{-3}\ \mathrm{Pa\cdot s} = 1\ \mathrm{cp}$$

Diffusion equation
Dimensional Analysis

- Dimensionless group dictate the nature of diffusion process or demonstrate the competition between two rate process

$$\nabla^2 p = \frac{\mu S}{k}\frac{\partial p}{\partial t}$$

$$\nabla^{2+} p^+ = \frac{\mu S}{k}\frac{L^2}{t_0}\frac{\partial p^+}{\partial t^+} = \tau\cdot\frac{1}{t_0}\frac{\partial p^+}{\partial t^+}$$

$$\tau = \frac{l^2}{\kappa} = \frac{(\phi\beta_f+\beta_r)\eta l^2}{k} \qquad (2.2)$$

where l is a characteristic length-scale of the process, $\kappa \approx k/\eta(\phi\beta_f+\beta_r)$ is the hydraulic diffusivity, β_f and β_r are the fluid and rock compressibilities, respectively, ϕ is the rock porosity, k is the permeability in m^2 ($10^{-12}\ m^2 = 1$ Darcy), and η is the fluid viscosity.

1 D (darcy) = $0.987\times10^{-12}\ m^2 \sim 10^{-12}\ m^2$

Hydraulic Fracturing
Models of hydraulic fracturing –Inclusion of leakoff

SEOUL NATIONAL UNIVERSITY

- Effect of leakoff
  - Fluid leak off into the formation
  - Not desirable for typical HF but serves good for shale gas HF (increased shear slip)
- Effect of stress shadow
  - When a hydraulic fracture opens, it increases the stress normal to the fracture facee
  - Shorter fracture length in the center than outside

No leakoff

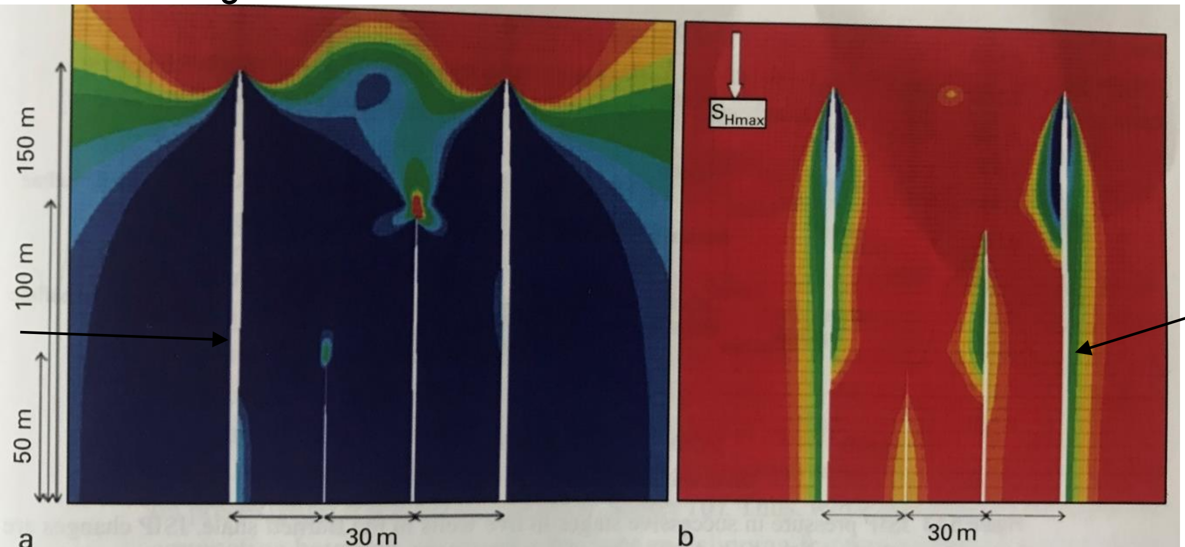

leakoff

Numerical modeling of HF with & without leakoff

Figure 8.12 (a) Numerical model of four hydraulic fractures propagating simultaneously from four perforation clusters 30 m apart with no leak-off of pressure from the fractures. (b) The same model with leak-off. The color indicates the tendency of the induced change in stress and pressure to stimulate shear on optimally oriented pre-existing fractures. From Agarwal et al. (2012).

Zoback MD, Kohli AH, 2019, Unconventional Geomechanics, Cambridge Univ.

Models of hydraulic fracturing –Inclusion of leakoff

SEOUL NATIONAL UNIVERSITY

- Effect of HF fluid on leakoff
  - In multistage HF, slickwater HF (with lower viscosity) is considered to be a key process

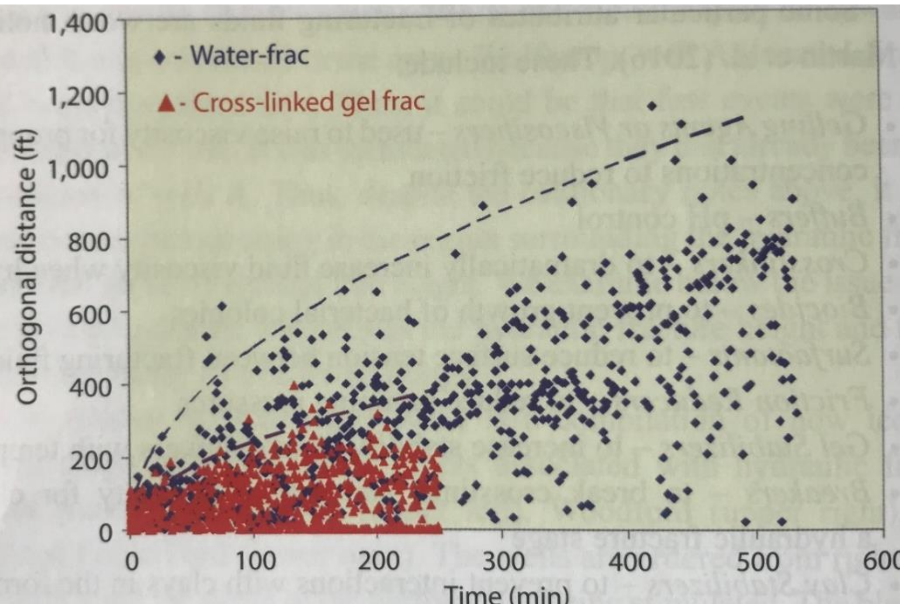

Figure 8.17 The number of microseismic events accompanying fracturing with water or cross-linked gel as a function of time and orthogonal distance from perforations. After Cipolla et al. (2008).

Zoback MD, Kohli AH, 2019, Unconventional Geomechanics, Cambridge Univ

Models of hydraulic fracturing – Continuity Equation

- Continuity equation

$$\frac{\partial q}{\partial x} + q_L + \frac{\partial A}{\partial t} = 0$$

where q is the volume flow rate through a cross section, A is the cross-sectional area of the fracture ($\pi w h_f/4$ for the PKN model), and q_L is the volume rate of leakoff per unit length:

$$q_L = 2h_f u_L \,, \tag{6-22}$$

where u_L is from Eq. 6-14. The cross-sectional area

$$\frac{E'}{128\mu h_f}\frac{\partial^2 w^4}{\partial x^2} = \frac{8C_L}{\pi\sqrt{t - t_{exp}(x)}} + \frac{\partial w}{\partial t}.$$

Mack & Warpinski, 2000, Mechanics of hydraulic fracturing, Eds: Economides & Nolte, Reservoir Stimulation, 3rd Ed., Wiley

Hydraulic Fracturing
Models of hydraulic fracturing – PKN Model

SEOUL NATIONAL UNIVERSITY

- PKN model

Harrington and Hannah (1975) introduced efficiency as:

$$\eta = \frac{V_f}{V_i} = \frac{V_f}{V_f + V_L}, \qquad (6A\text{-}2)$$

where V_f is the fracture volume, V_i is the volume of fluid injected, and V_L is the leaked-off volume, which in terms of Eq. 6-20 becomes

$$\eta = \frac{\overline{w}}{\overline{w} + 2C_L\sqrt{2t}} \qquad (6A\text{-}3)$$

6B. Approximations to Nordgren's equations

Nordgren (1972) derived two limiting approximations, for storage-dominated, or high-efficiency ($t_D < 0.01$), cases and for leakoff-dominated, or low-efficiency ($t_D > 1.0$), cases, with t_D defined by Eq. 6-24. They are useful for quick estimates of fracture geometry and pressure within the limits of the approximations. Both limiting solutions overestimate both the fracture length and width (one neglects fluid loss and the other neglects storage in the fracture), although within the stated limits on t_D, the error is less than 10%.

The storage-dominated ($\eta \to 1$) approximation is

$$L(t) = 0.39\left[\frac{E' q_i^3}{\mu h_f^4}\right]^{1/5} t^{4/5} \qquad (6B\text{-}1)$$

$$w_w = 2.18\left[\frac{\mu q_i^2}{E' h_f}\right]^{1/5} t^{1/5}, \qquad (6B\text{-}2)$$

and the high-leakoff ($\eta \to 0$) approximation is

$$L(t) = \frac{q_i t^{1/2}}{2\pi C_L h_f} \qquad (6B\text{-}3)$$

$$w_w = 4\left[\frac{\mu q_i^2}{\pi^3 E' C_L h_f}\right]^{1/4} t^{1/8}. \qquad (6B\text{-}4)$$

Equation 6B-3 could also be obtained from the approximation in Sidebar 6A, with the fracture width set to zero and $2\sqrt{2t}$ replaced by $\pi\sqrt{t}$, which is more correct. Once the width is determined from Eq. 6B-2 or 6B-4, the pressure can be found from Eq. 6-7.

Mack & Warpinski, 2000, Mechanics of hydraulic fracturing, Eds: Economides & Nolte, Reservoir Stimulation, 3rd Ed., Wiley

Hydraulic Fracturing
Models of hydraulic fracturing – PKN Model

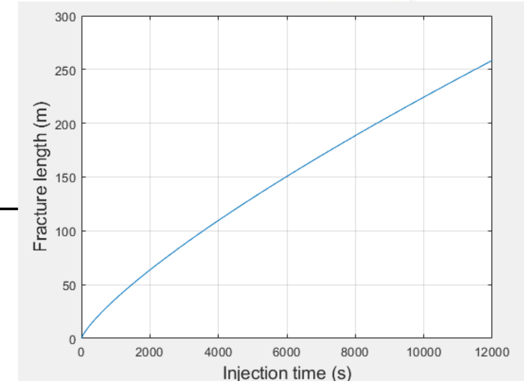

- Example

input

C_L	9.84×10^{-6} $\mathrm{m/s^{1/2}}$	0.00025 $\mathrm{ft/min^{1/2}}$
S_p	0 m	0 in
h_f	51.8 m	170 ft
E'	6.13×10^{10} Pa	8.89×10^{6} psi
μ	0.2 Pa·s	200 cp
i	0.0662 $\mathrm{m^3/s}$	50/2 = 25 bpm
t_e	12 000 s	200 min

→

Output

- **Fracture length (L)**
- **Fracture width(aperture): Max/average**
- **Net fluid Pressure**

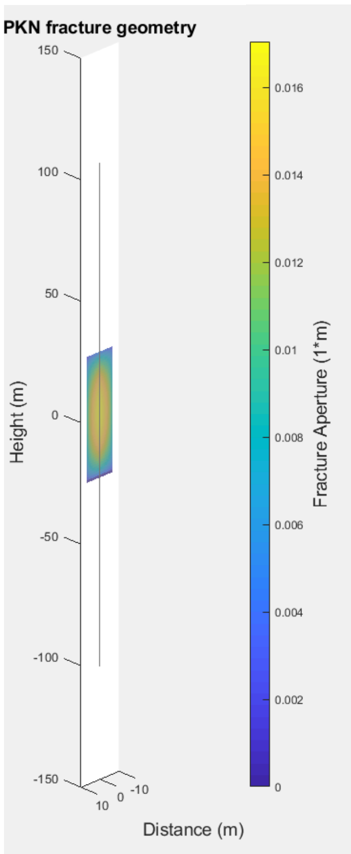

t=2 min

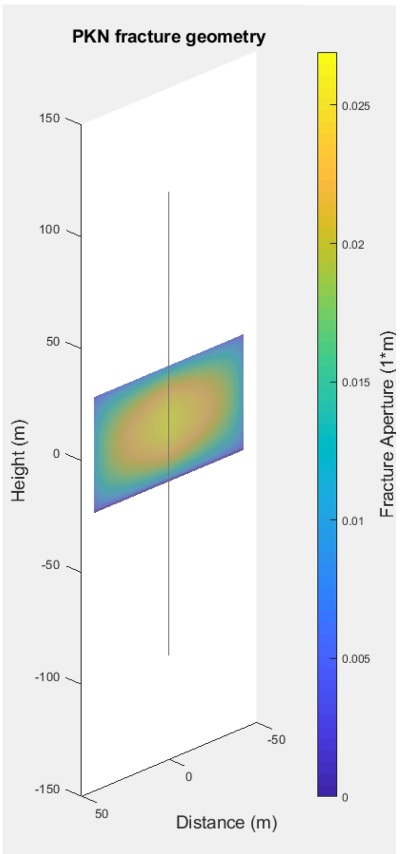

t=20 min

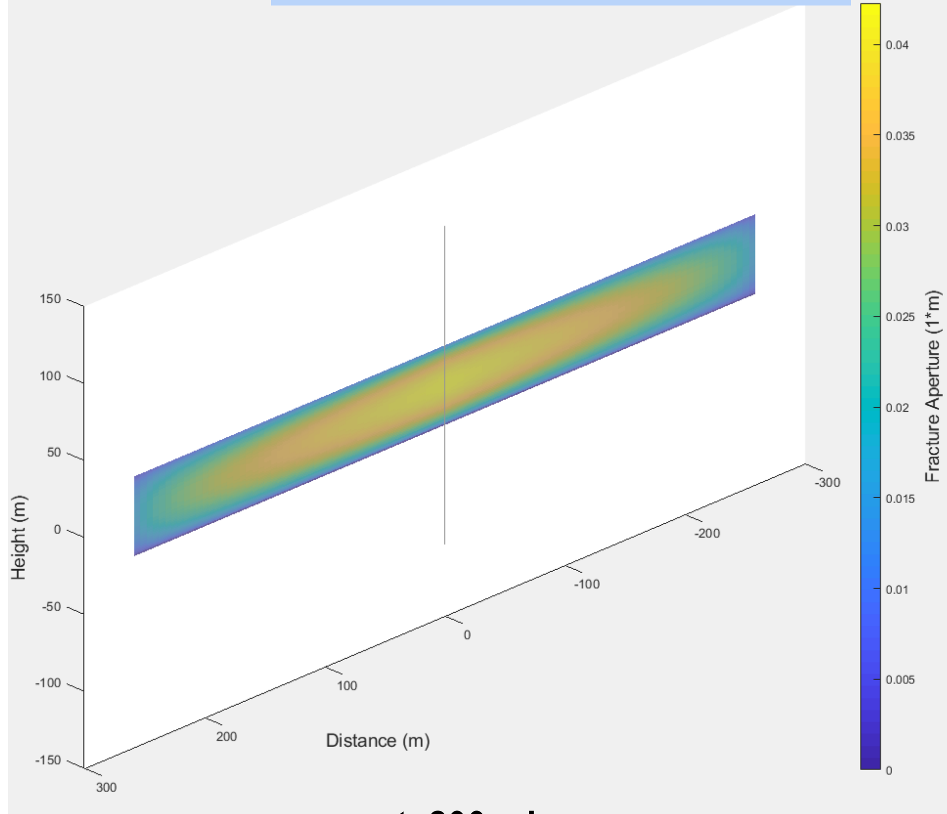

t=200 min

Hydraulic Fracturing
Models of hydraulic fracturing – PKN Model

- Example

C_L	9.84×10^{-6} m/s$^{1/2}$	0.00025 ft/min$^{1/2}$
S_p	0 m	0 in
h_f	51.8 m	170 ft
E'	6.13×10^{10} Pa	8.89×10^{6} psi
μ	0.2 Pa·s	200 cp
i	0.0662 m^3/s	50/2 = 25 bpm
t_e	12 000 s	200 min

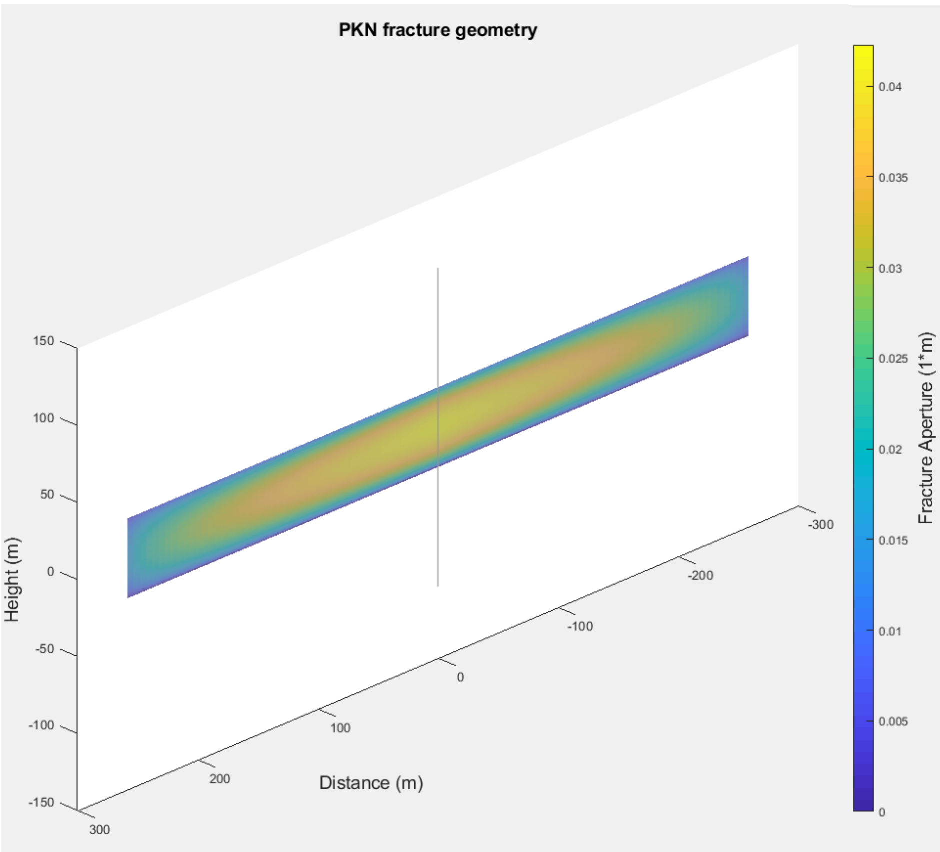

t=200 min

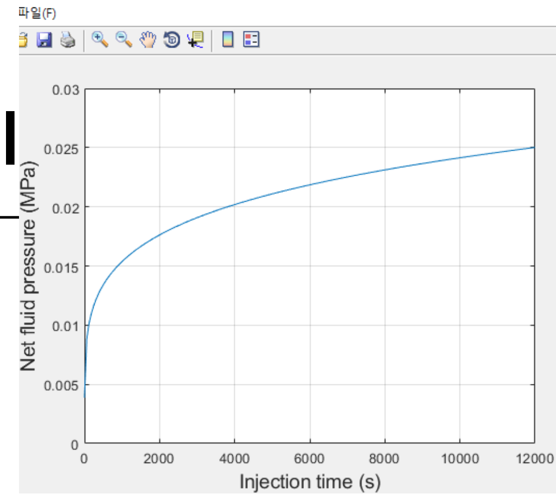

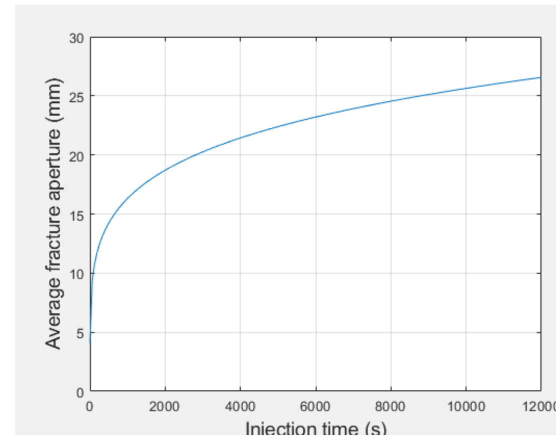

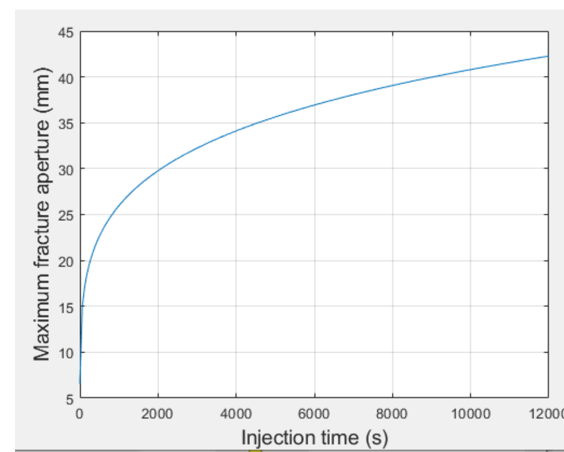

Hydraulic Fracturing
Models of hydraulic fracturing – PKN Model

- Example

C_L	9.84×10^{-6} m/s$^{1/2}$	0.00025 ft/min$^{1/2}$
S_p	0 m	0 in
h_f	51.8 m	170 ft
E'	6.13×10^{10} Pa	8.89×10^6 psi
μ	0.2 Pa·s	200 cp
i	0.0662 m^3/s	50/2 = 25 bpm
t_e	12 000 s	200 min

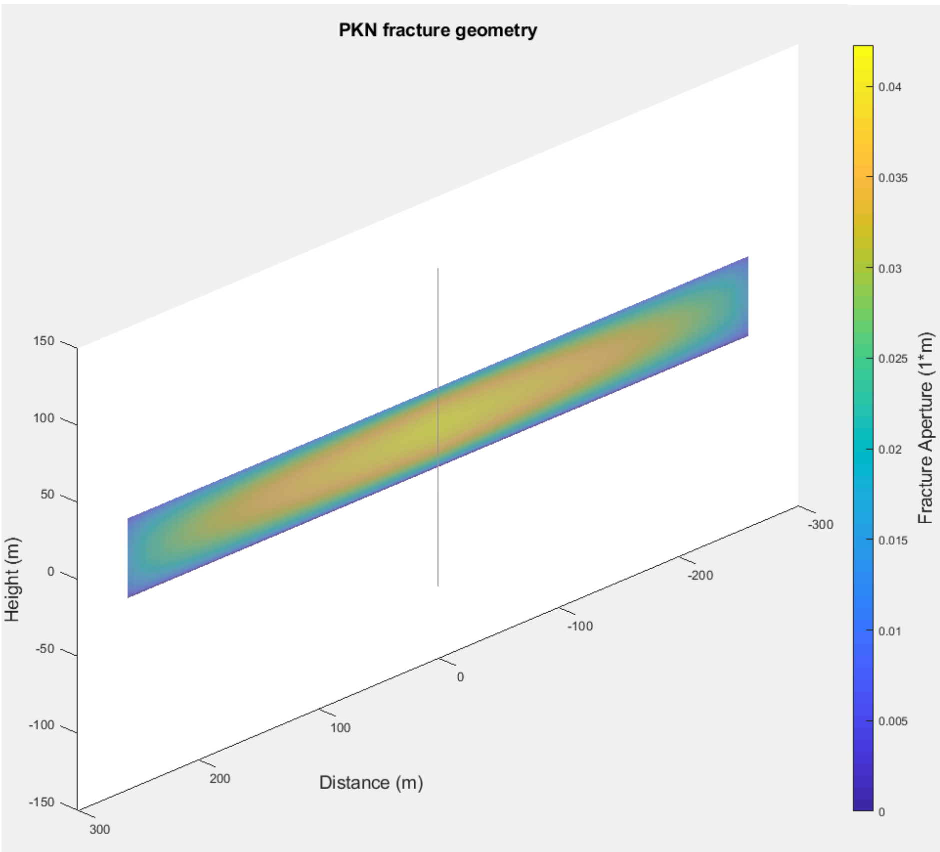

t=200 min

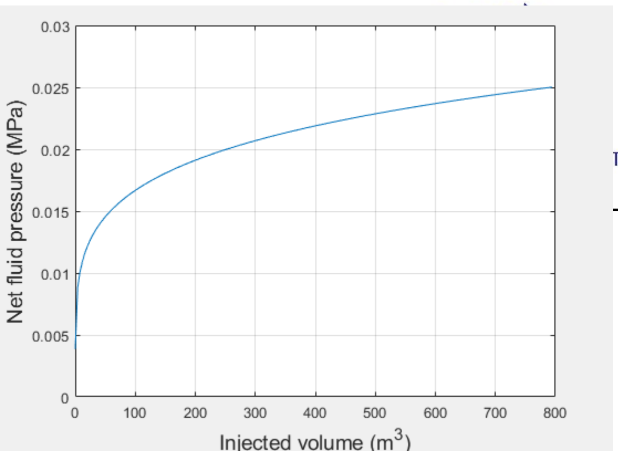

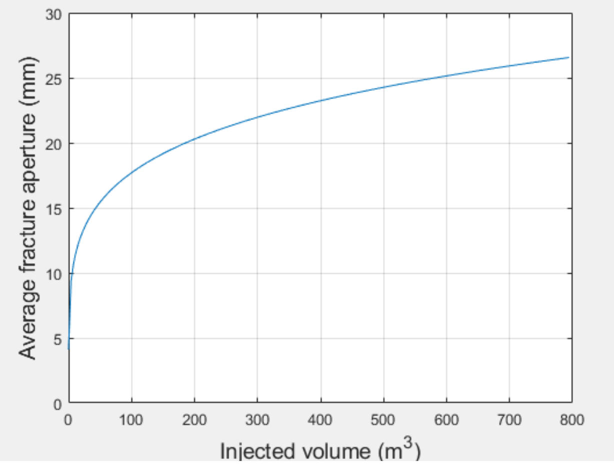

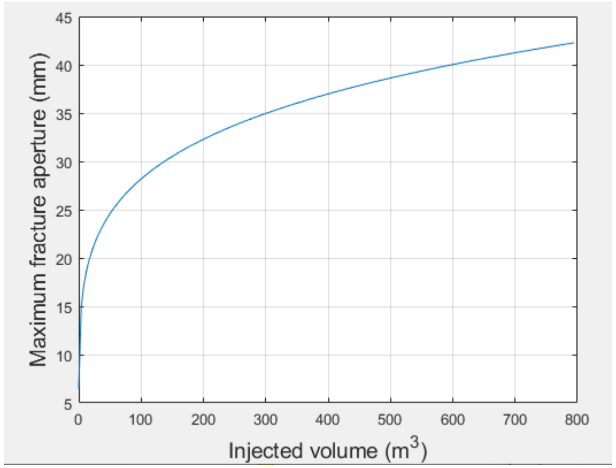

Hydraulic Fracturing
Models of hydraulic fracturing – KGD Model

SEOUL NATIONAL UNIVERSITY

- Khristianovich et al. (1959) & Geertsma and de Klerk (1969)
- Assumptions
  - Rectangular cross section - Width of the crack at any position from the well is independent of vertical position (h . L)
  - Plane strain condition in horizontal plane

$$\frac{\partial p}{\partial x} = -\frac{12 q \mu}{h_f w^3}, \qquad (6\text{-}25)$$

which can be written in integral form as

$$p_{net} = \frac{6 \mu q_i}{h_f} \int_0^L \frac{dx}{w^3}. \qquad (6\text{-}26)$$

For no leakoff, the equations can be solved for length and width, respectively:

$$L(t) = 0.38 \left[\frac{E' q_i^3}{\mu h_f^3} \right]^{1/6} t^{2/3} \qquad (6\text{-}31)$$

$$w_w = 1.48 \left[\frac{\mu q_i^3}{E' h_f^3} \right]^{1/6} t^{1/3}. \qquad (6\text{-}32)$$

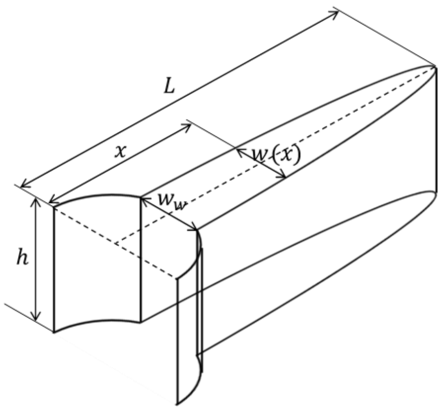

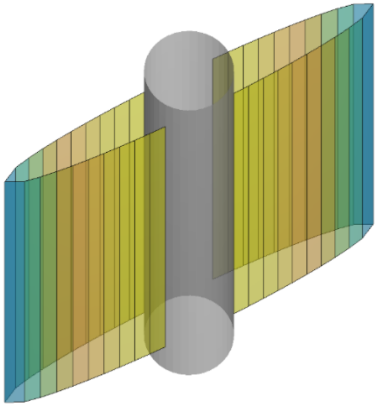

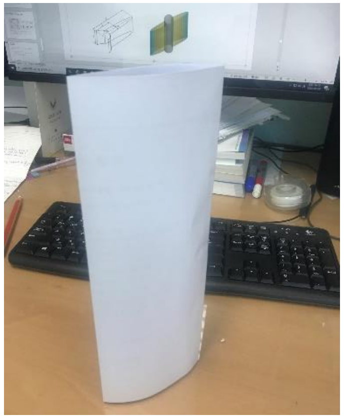

Hydraulic Fracturing
Models – KGD vs. PKN Model

SEOUL NATIONAL UNIVERSITY

	KGD Model	*PKN Model*
	Khristianovich *et al.* (1959) Geertsma and de Klerk (1969)	Perkins and Kern (1961) Nordgen (1972)
Fluid Flow Rate	$\frac{\partial p}{\partial x} = -\frac{12q\mu}{h_h w^3}$	$\frac{dp}{dx} = -\frac{64q\mu}{\pi h_h w^3}$
Net Pressure	$p_w(\mathrm{t}) = S + 1.09\left[\frac{\mu E^2}{(1-\nu^2)^2}\right]^{1/3} t^{-1/3}$	$p_w(\mathrm{t}) = S + 1.09\left[\frac{E^4\mu Q^2}{(1-\nu^2)^4 h^6}\right]^{1/5} t^{1/5}$
Width at Wellbore	$\mathrm{w}_w(\mathrm{t}) = 1.67\left[\frac{(1-\nu^2)\mu Q^3}{Eh^3}\right]^{1/6} t^{1/3}, \quad \bar{w} = \frac{\pi}{4}\mathrm{w}_w$	$\mathrm{w}_{w,max}(\mathrm{t}) = 2.18\left[\frac{(1-\nu^2)\mu Q^2}{Eh}\right]^{1/5} t^{1/5}, \quad \bar{w} = \frac{\pi}{5}\mathrm{w}_{w,max}$
Fracture Length (fn of time)	$\mathrm{L(t)} = 0.38\left[\frac{EQ^3}{(1-\nu^2)\mu h^3}\right]^{1/6} t^{2/3}$	$\mathrm{L(t)} = 0.39\left[\frac{EQ^3}{(1-\nu^2)\mu h^4}\right]^{1/5} t^{4/5}$

Width, fracture length, net pressure without leakoff

Mack & Warpinski, 2000, Mechanics of hydraulic fracturing, Eds: Economides & Nolte, Reservoir Stimulation, 3rd Ed., Wiley

Hydraulic Fracturing
SNU Geomechanics Toolbox

SEOUL NATIONAL UNIVERSITY

- KGD model
- PKN model
- Radial model

- Critical pressure for shearing

- Statistical Generation of fracture in 3D
- Self verification

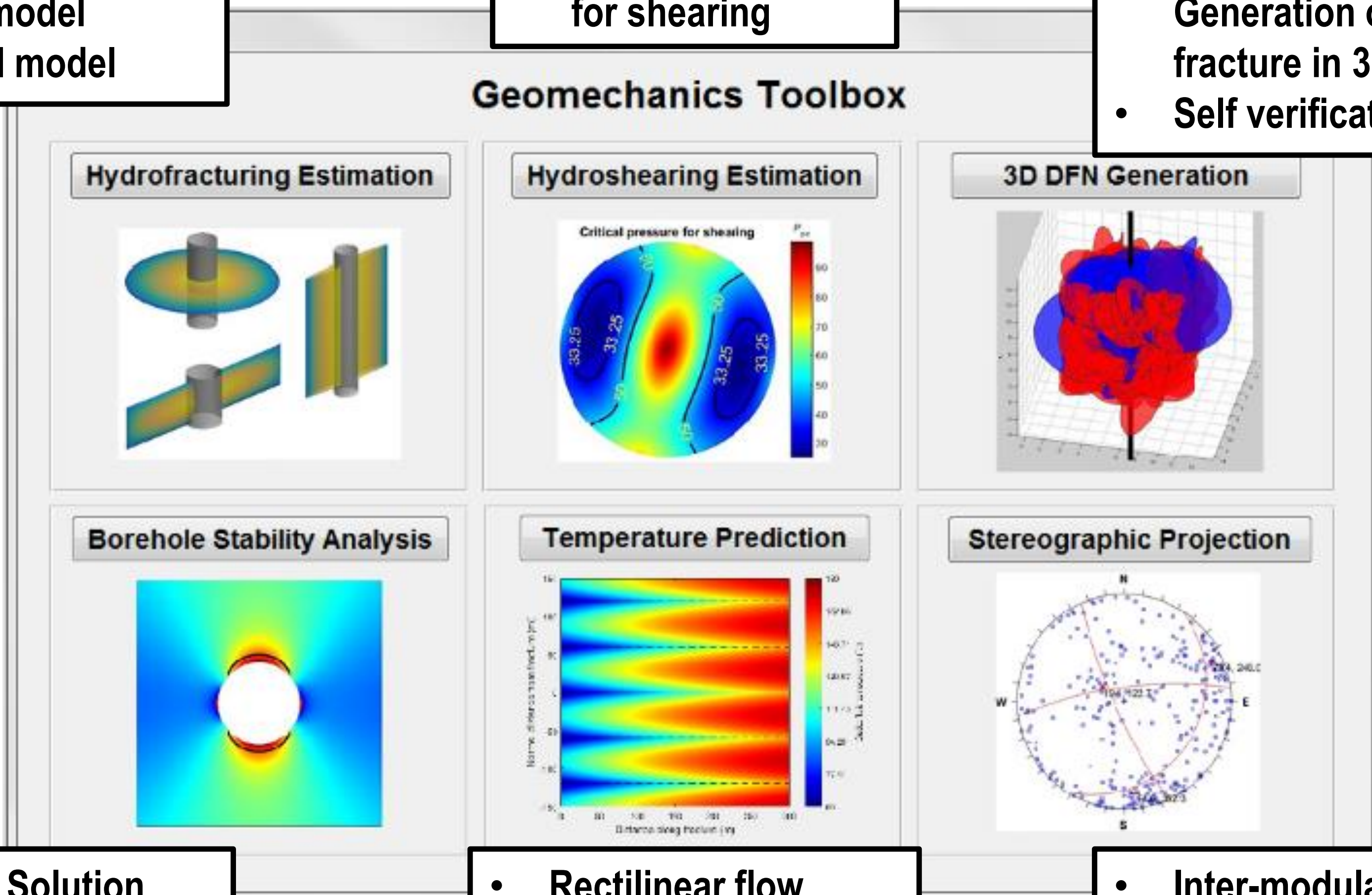

- Analytic Solution
- FEM
- Thermal stress

- Rectilinear flow
- Radial flow
- Temperature drawdown

- Inter-modular data transfer
- Generating compatible data

Park S, Kim KI, Kwon S, Yoo H, Xie L, Min K-B*, Kim KY, Development of a hydraulic stimulation simulator toolbox for enhanced geothermal system design. Renewable Energy, 2018, 118C: 879-895

Hydraulic Fracturing
SNU Geomechanics Toolbox

SEOUL NATIONAL UNIVERSITY

- SNU Geomechanics Toolbox - Hydraulic Fracturing Module

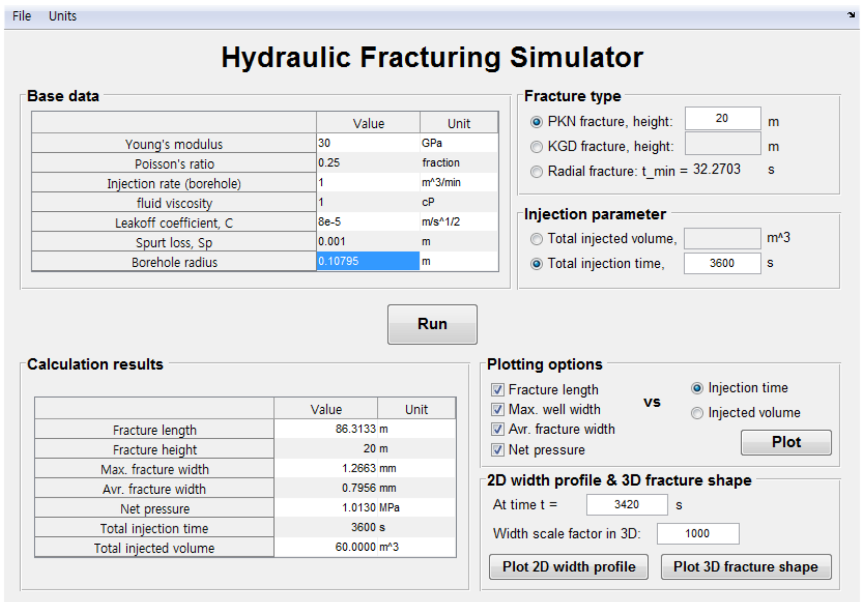

Main window

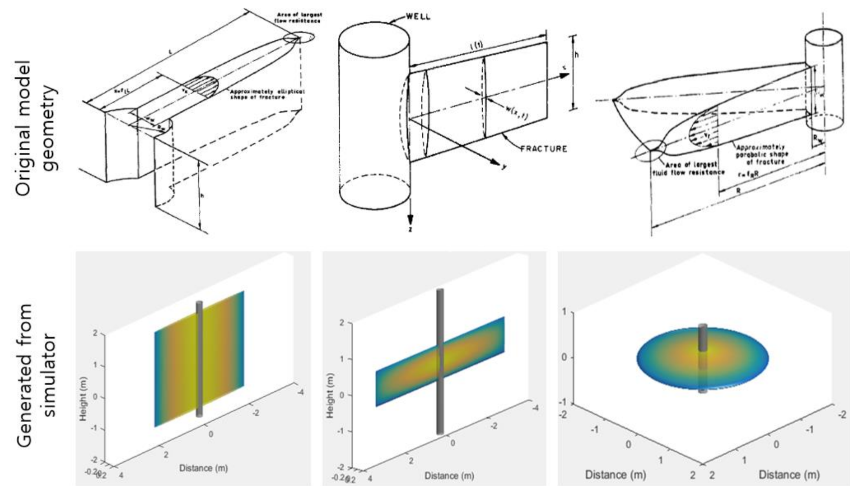

KGD model PKN model Radial model

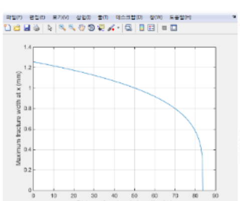

2D width profile

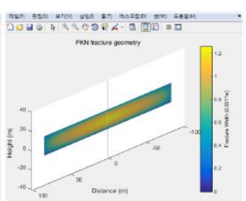

3D visualization

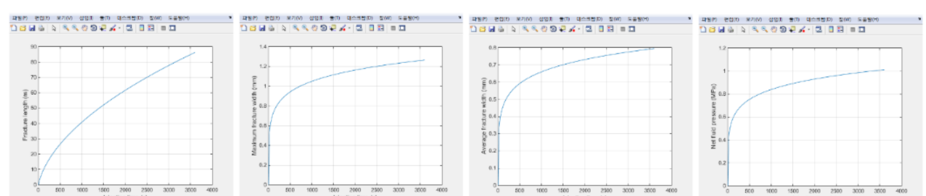

Length, max. aperture, min. aperture, net pressure curves

Hydraulic Fracturing
SNU Geomechanics Toolbox

SEOUL NATIONAL UNIVERSITY

- PKN vs. KGD models

Longitudinal fracture models
- KGD model
  - 1) Assumption of no leak-off
  - 2) Carter's leak-off eqs.
- PKN model
  - 3) Assumption of no leak-off
  - 4) Assumption of high leak-off
  - 5) Carter's leak-off eqs.

Transverse fracture model
- Radial model
  - 6) Carter's leak-off eqs.

1) KGD model with assumption of no leak-off

$$L(t) = 0.38\left[\frac{EQ^3}{(1-\nu^2)\mu h^3}\right]^{1/6} t^{2/3}$$

$$W_{w,max}(t) = 1.67\left[\frac{(1-\nu^2)\mu Q^3}{Eh^3}\right]^{1/6} t^{1/3}, \quad \bar{w} = \frac{\pi}{4}W_{w,max}$$

$$p_w(t) = S + 1.09\left[\frac{\mu E^2}{(1-\nu^2)^2}\right]^{1/3} t^{-1/3}$$

3) PKN model with assumption of no leak-off (error $< 10\%$ when $t_D < 0.01$)

$$L(t) = 0.39\left[\frac{EQ^3}{(1-\nu^2)\mu h^4}\right]^{1/5} t^{4/5}$$

$$W_{w,max}(t) = 2.18\left[\frac{(1-\nu^2)\mu Q^2}{Eh}\right]^{1/5} t^{1/5}, \quad \bar{w} = \frac{\pi}{5}W_{w,max}$$

$$p_w(t) = S + 1.09\left[\frac{E^4\mu Q^2}{(1-\nu^2)^4 h^6}\right]^{1/5} t^{1/5}$$

Explicit form
(no leakoff)

2) KGD model with Carter's leak-off equations

$$W_{w,max} = 2.708\left[\frac{(1-\nu^2)\mu Q L^2}{hE}\right]^{1/4}, \quad \bar{w} = \frac{\pi}{4}W_{w,max}$$

$$L = \frac{(\pi w_w + 8S_p)Q}{32C^2\pi h}\left[\exp(\alpha^2)\,erfc(\alpha) + \frac{2\alpha}{\sqrt{\pi}} - 1\right], \quad \alpha = \frac{8C\sqrt{\pi t}}{\pi w_w + 8S_p}$$

By using root-finding method, first find the consistent set of $\bar{w}$ and L at certain time t, then

$$p_w = S + \frac{E}{4(1-\nu^2)L}W_{w,max}$$

5) PKN model with Carter's leak-off equations

$$W_{w,max} = 2.75\left[\frac{(1-\nu^2)\mu Q L}{E}\right]^{1/4}, \quad \bar{w} = \frac{\pi}{5}W_{w,max}$$

$$L = \frac{(\pi w_w + 10S_p)Q}{40C^2\pi h}\left[\exp(\beta^2)\,erfc(\beta) + \frac{2\beta}{\sqrt{\pi}} - 1\right], \quad \beta = \frac{10C\sqrt{\pi t}}{\pi w_w + 10S_p}$$

By using root-finding method, first find the consistent set of $\bar{w}$ and L at certain time t, then

$$p_w = S + \frac{E}{2(1-\nu^2)h}W_{w,max}$$

6) Radial model with Carter's leak-off equations

$$W_{w,max} = 3.532\left[\frac{(1-\nu^2)\mu Q R}{E}\right]^{1/4}, \quad \bar{w} = \frac{8}{15}W_{w,max}$$

$$R = \sqrt{\frac{(4w_w + 15S_p)Q}{60C^2\pi^2}\left[\exp(\beta^2)\,erfc(\beta) + \frac{2\beta}{\pi} - 1\right]}, \quad \beta = \frac{15C\sqrt{\pi t}}{4w_w + 15S_p}$$

By using root-finding method, first find the consistent set of $\bar{w}$ and L at certain time t, then

$$p_w = S + \frac{\pi E}{8(1-\nu^2)R}W_{w,max}$$

Implicit form
(consideration of leakoff)

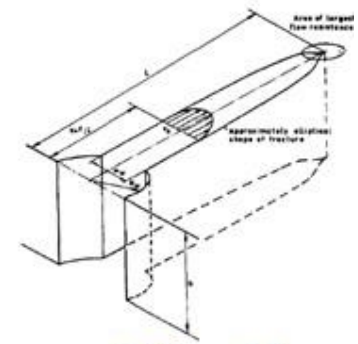

KGD model

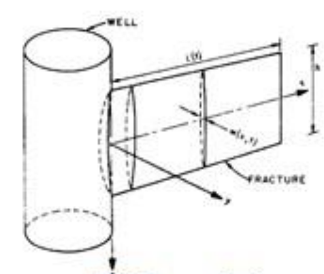

PKN model

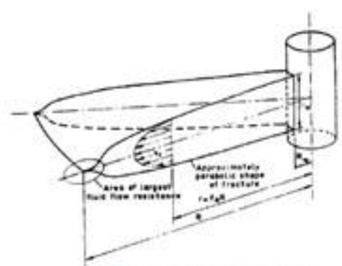

Radial model

Park S, Kim KI, Kwon S, Yoo H, Xie L, Min K-B*, Kim KY, Development of a hydraulic stimulation simulator toolbox for enhanced geothermal system design. Renewable Energy, 2018, 118C: 879-895

Hydraulic Fracturing
Proppant

SEOUL NATIONAL UNIVERSITY

- Proppants
  - Used to hold the walls of the fracture apart to create a conductive path to the wellbore
  - Placing the appropriate concentration and type of proppant in the fracture is critically important – effect on fluid rheology, effect of gravity…
  - Usually sand or ceramic material

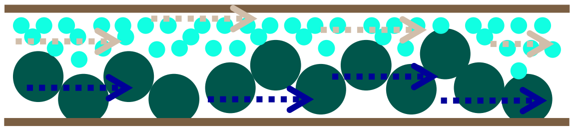

- Factors affecting the fracture conductivity
  - Proppant composition
  - Physical properties of the proppant – strength,
  - Proppant-pack permeability
  - Movement of formation fines
  - Long-term degradation of proppant

Proppant

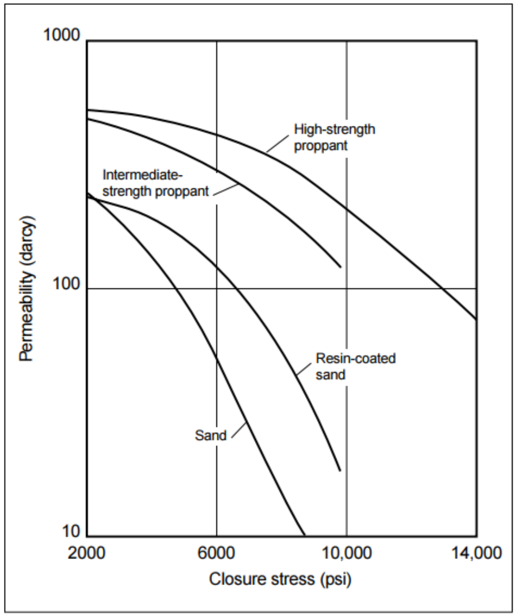

Strengfth vs permeability of various proppants

Gulbis & Hodge, 2000, Fracturing fluid chemistry and proppants, Eds: Economides & Nolte, Reservoir Stimulation, 3rd Ed., Wiley

Hydraulic Fracturing
Shear stimulation (Hydraulic shearing)

- Shear stimulation (or hydraulic shearing or hydroshearing)
  - Shearing of existing fractures through hydraulic pressure
  - Shear slip and dilation in the fracture is a main mechanism
  - Fluid flow through fracture ~ b^3.
  - In general proppant is not necessary ← irreversible process

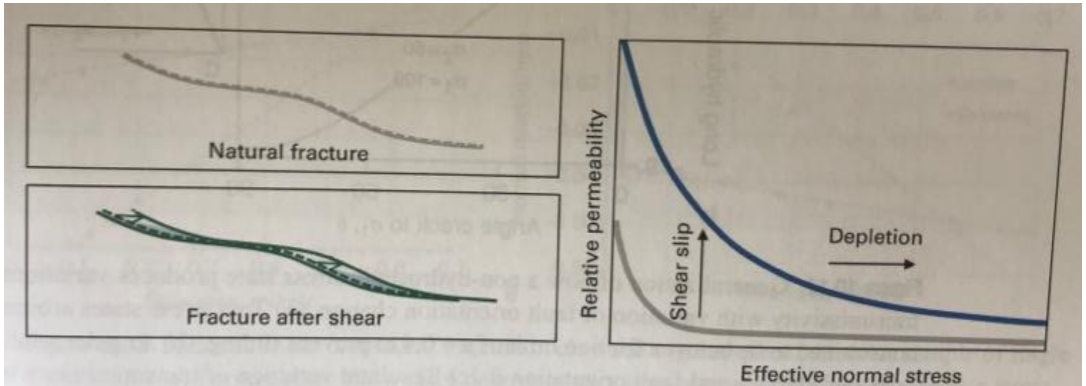

Figure 10.11 Generalization of the way in which slip on a pre-existing natural fracture is likely to increase its initial permeability and decrease the sensitivity of the permeability to depletion (after Barton et al., 2009).

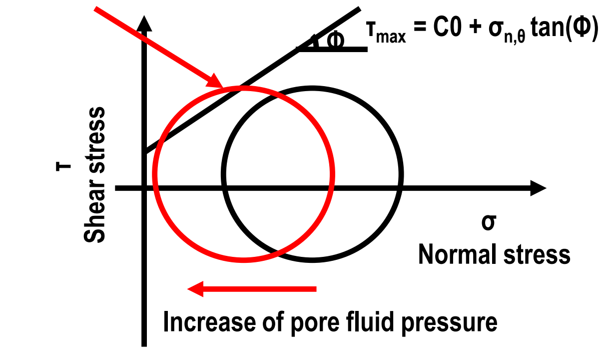

Zoback MD, Kohli AH, 2019, Unconventional Geomechanics, Cambridge Univ

Hydraulic Fracturing
Shear stimulation (Hydraulic shearing)

SEOUL NATIONAL UNIVERSITY

Real rock fracture

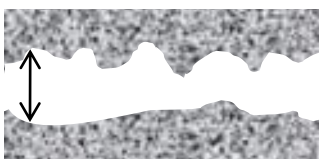

Idealization

Conceptual model

Idealized rock fracture

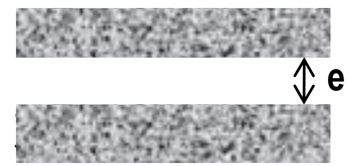

Aperture (e, or b): size of opening measured normal to the fracture wall

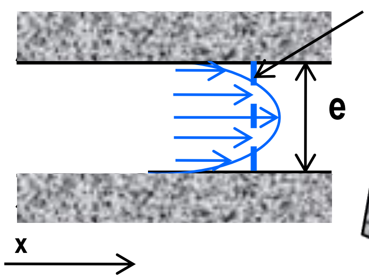

$$v = -\frac{1}{8\mu}\left(e^2 - 4y^2\right)\frac{d(\rho_w gh)}{dx}$$

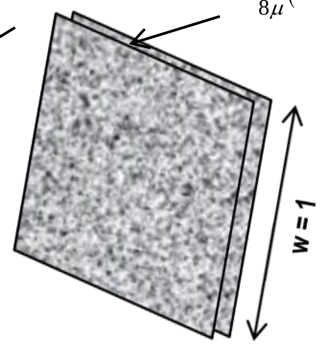

$$Q = \int_{-\frac{e}{2}}^{\frac{e}{2}} v(wdy) = -\frac{we^3}{12\mu}\frac{d}{dx}(\rho_w gh)$$

$$Q = -\frac{e^3}{12\mu}\frac{d}{dx}(\rho_w gh) = -\frac{\rho_w ge^3}{12\mu}\frac{dh}{dx}$$

$$K = \frac{\rho gk}{\mu}$$

$\rho ge^2/12\mu$ = hydraulic conductivity (K) of a fracture
$\rho ge^3/12\mu$ = transmissivity (T) of a fracture
$e^2/12$ = permeability (k) of a fracture

$$\boxed{Q = -\frac{\rho_w ge^3}{12\mu}\frac{\partial h}{\partial x}}$$

$$\boxed{Q = -\frac{e^3}{12\mu}\frac{\partial p}{\partial x}} \leftarrow$$

with zero elevation

ρ_w: density of fluid
g: acceleration of gravity
μ: viscosity (=η)

– Cubic law: for a given gradient in pressure and unit width (w), flow rate through a fracture is proportional to the **cube** of the fracture aperture.

plate approximation for fluid flow through a planar fracture. For a given fluid viscosity, η, the volumetric flow rate, Q, resulting from a pressure gradient, ∇P, is dependent on the cube of the separation between the plates, b,

$$Q = \frac{b^3}{12\eta}\nabla P \qquad (5.1)$$

Hydraulic Fracturing
Shear stimulation (Hydraulic shearing)

SEOUL NATIONAL UNIVERSITY

- Shear dilation observation (Olsson & Barton, 2001)

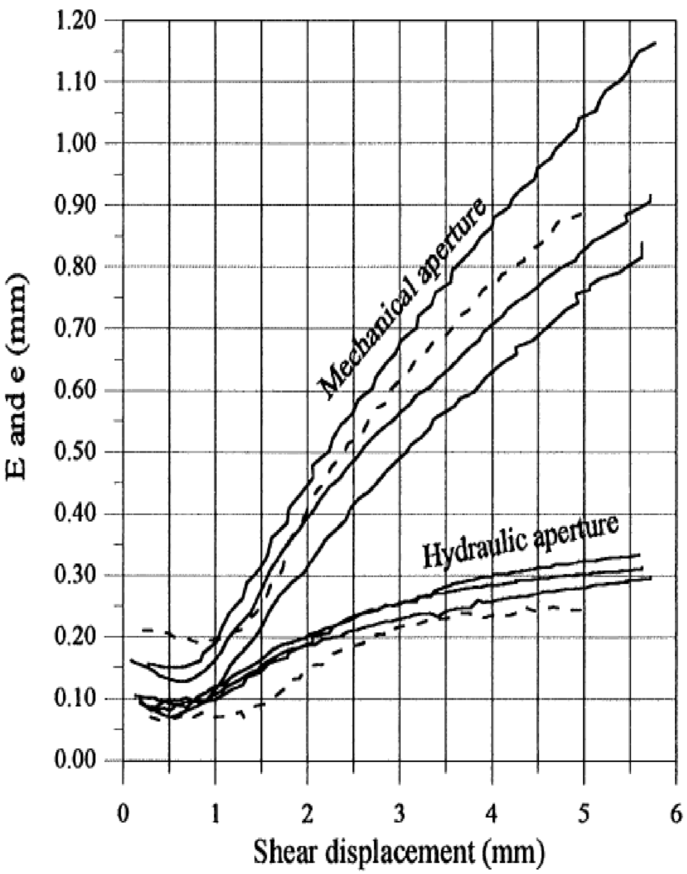

Shear dilation

Rothert & Baisch (2010)

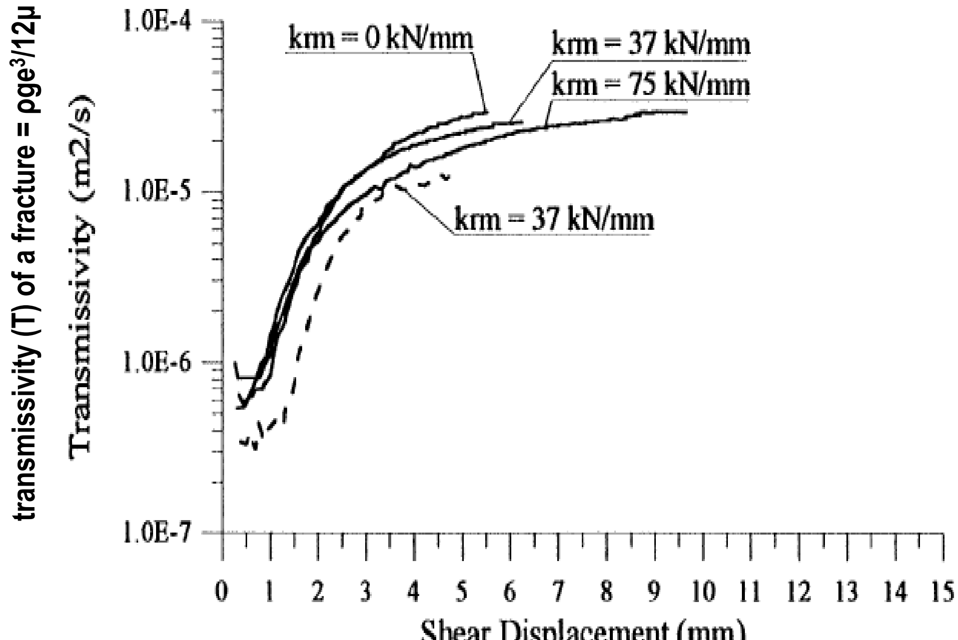

Olsson, R. and N. Barton (2001). "An improved model for hydromechanical coupling during shearing of rock joints." International Journal of Rock Mechanics and Mining Sciences 38(3): 317-329.

Rothert E & Baisch S, 2010, Passive Seismic Monitoring: Mapping Enhanced Fracture Permeability, 10th World Geothermal Congress, Paper No.3161

Hydraulic Fracturing
Shear stimulation (Hydraulic shearing)

SEOUL NATIONAL UNIVERSITY

- Normal mechanical behavior
  - Unit: Stress/length (MPa/m)
  - Linear model $\sigma_n = K_n \delta_n$
  - Non-linear model

$$\delta_n = \frac{\sigma_n}{c + d\sigma_n}$$

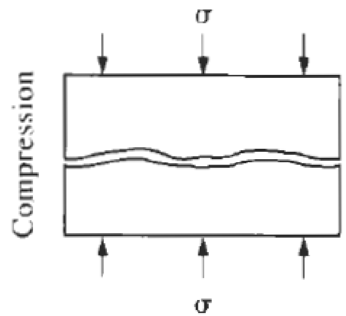

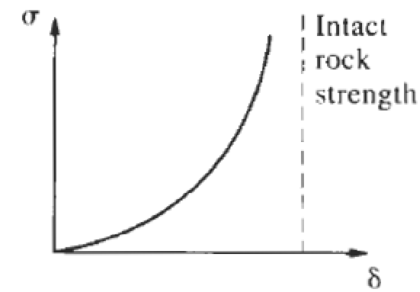

- Shear mechanical behavior
  - Unit: Stress/length (MPa/m)
  - Linear model $\sigma_s = K_s \delta_s$
  - Non-linear model: e.g., Barton's equation
  - Dilation angle $\phi_{dilation} = \tan^{-1}\left(\frac{\text{normal dilation}}{\text{shear displacement}}\right)$

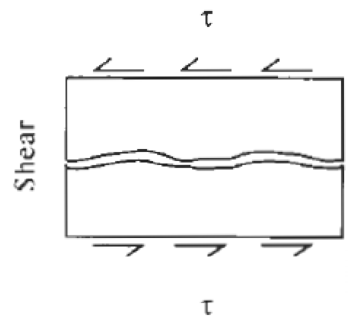

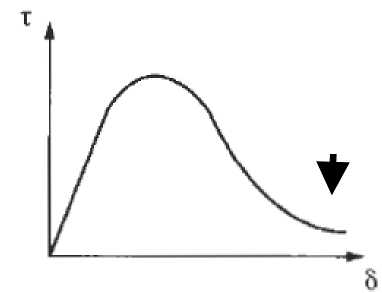

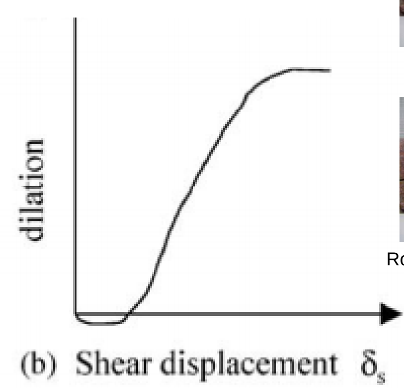

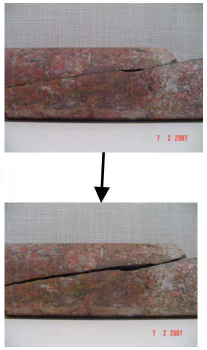

Rothert & Baisch (2010)

Rothert E & Baisch S, 2010, Passive Seismic Monitoring: Mapping Enhanced Fracture Permeability, 10th World Geothermal Congress, Paper No.3161

Hydraulic Fracturing
Shear stimulation (Hydraulic shearing)

SEOUL NATIONAL UNIVERSITY

- Direct shear test on 57 single fractures (Glamheden, 2007)

	0.5 MPa	5 MPa	20 MPa
σ_n =	0.5 MPa	5 MPa	20 MPa
Ψ_{mean} =	14.6°	7.7°	3.2°

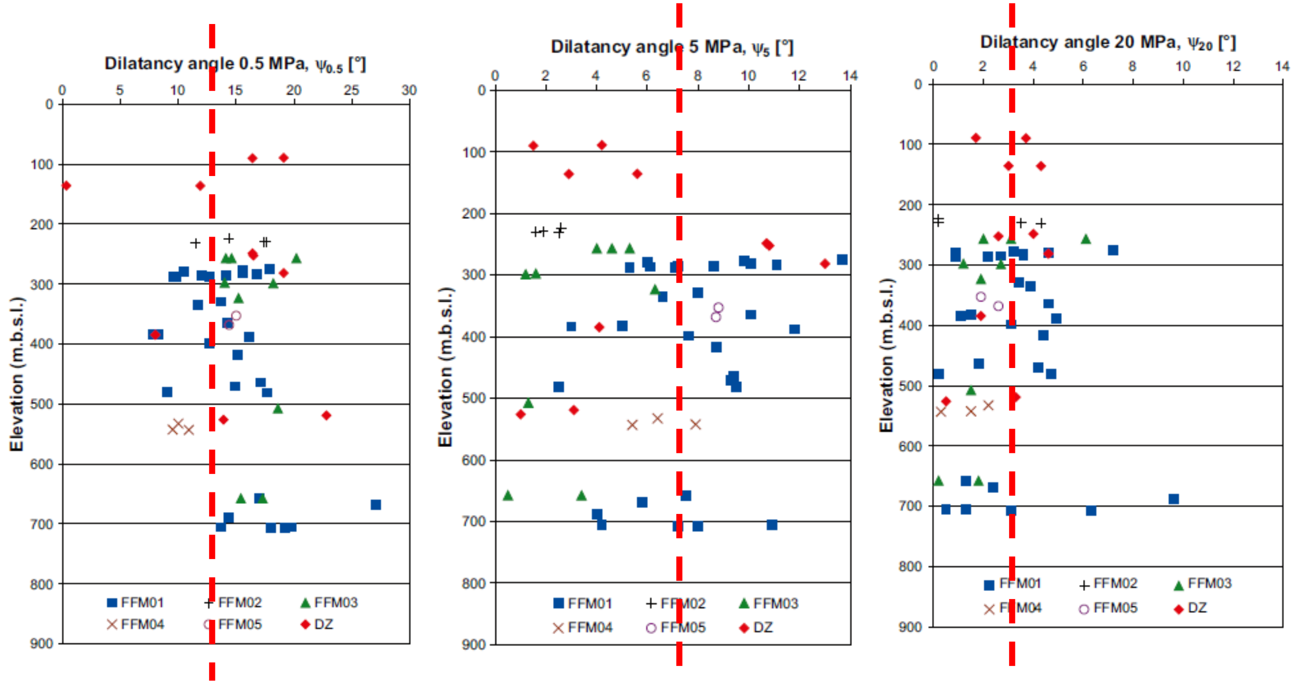

- Shear dilation varies a lot at moderate normal stress (~ 20 MPa, ~ 500 m)

- At deep depth, dilation seems fairly small but it still enhances permeability a great deal

Glamheden R, Fredriksson A, Röshoff K, Karlsson J, Hakami H and Christiansson R (2007), Rock Mechanics Forsmark. Site descriptive modelling Forsmark stage 2.2. SKB.

Hydraulic Fracturing
Shear stimulation (Hydraulic shearing)

- Examples of critically stressed faults
  - Majorities of hydraulically conductive faults are critically stressed

Hydraulically conductive **Hydraulically non-conductive**

Orientation of wells that would intersect the greatest number of critically stresses faults

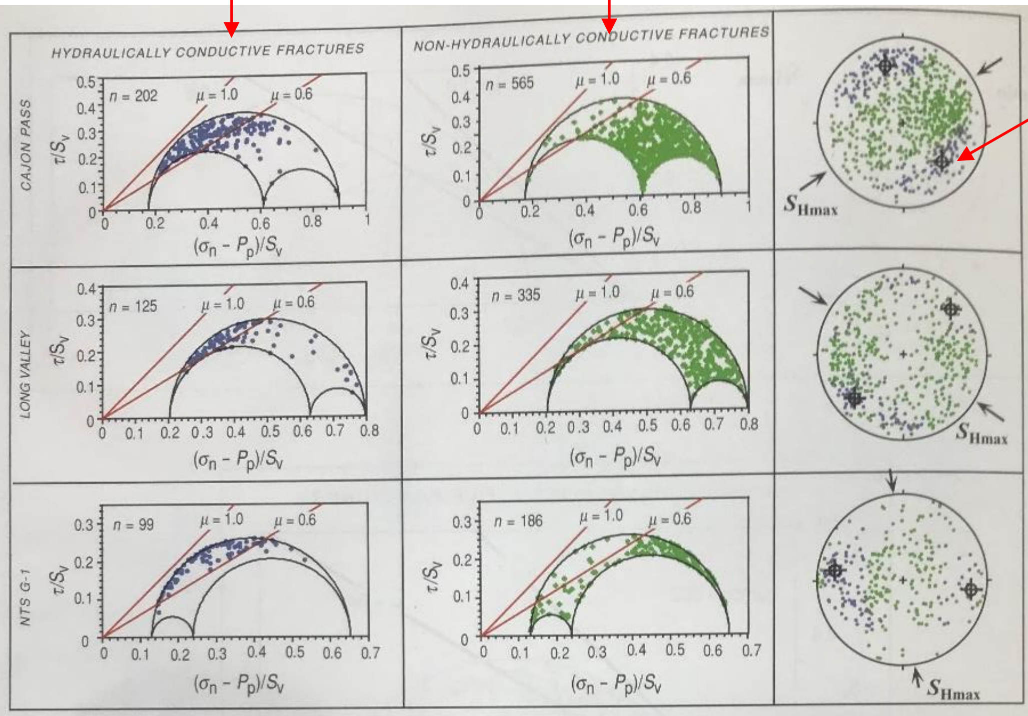

Figure 11.2. Normalized Mohr diagrams of the three wells that illustrate that most hydraulically conductive faults are critically stressed faults (left column) and faults that are not hydraulically conductive are not critically stressed (center column) along with stereonets that show the orientations of the respective fracture sets. The first row shows data from the Cajon Pass well (same Mohr diagrams as in Figure 11.1b), the second from the Long Valley Exploration Well and the third from well G-1 at the Nevada Test Site. After Barton, Zoback et al. (1995).

Cajon Pass
- Fractured Granite/granodiorate
- ~ 3.5 km
- ~ 4 km from the San Andreas fault
- Strike-slip ~ normal faulting

Long Valley:
- Fractured metamorphic rock
- drilled ~ 2 km
- Investigation of the structure/caldera
- Strike-slip ~normal-slip stress regime

Nevada Test Site (Yucca Mountain project)
- Tuffaceous rock
- potential site for nuclear waste repository
- Hole was drilled >1.7 km
- Normal faulting

Zoback MD, 2007, Reservoir Geomechanics, Cambridge University Press

Hydraulic Fracturing
Shear stimulation – Analytical model

SEOUL NATIONAL UNIVERSITY

- **Critical fluid pressure** (P_c) for shearing specific joint and **minimum critical fluid pressure** (P_{cm}) for optimally oriented joint:

$$P_c = \sigma - \frac{\tau}{\mu}, \quad \sigma = l^2\sigma_1 + m^2\sigma_2 + n^2\sigma_3$$

$$\tau = [(\sigma_1-\sigma_2)^2 l^2 m^2 + (\sigma_2-\sigma_3)^2 m^2 n^2 + (\sigma_3-\sigma_1)^2 l^2 n^2]^{1/2}$$

$$P_{cm} = \frac{k_c - k}{k_c - 1}\sigma_3, \quad k = \frac{\sigma_1}{\sigma_3}, \quad k_c = \frac{1+sin\phi}{1-sin\phi}$$

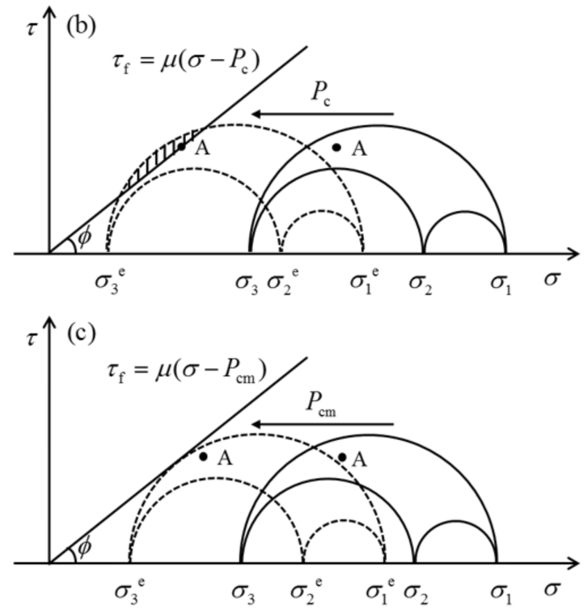

- Shearing onset location and migration direction can be estimated by the **depth gradient of critical pressure (dPc/dz),** if σ_1, σ_2, σ_3 $\propto$ depth:

$$\sigma_1 = k_1 S_v \quad \sigma_2 = k_2 S_v \quad \sigma_3 = k_3 S_v$$

$$P_c' = \sigma' - \frac{1}{\mu}\tau' \qquad P_c' = \gamma_\sigma g - \frac{\gamma_\tau g}{\mu} = \gamma g$$

Shearing at casing shoe with upward growth $\quad \gamma > \rho_w$

Shearing at well toe with downward growth $\quad \gamma < \rho_w$

- **Cut-off pressure (**P_{co}**):** fluid pressure sufficient to activate shearing in typical jointed rock mass

$$P_{co} = P_{cm} + \alpha(P_{cf} - P_{cm}), \qquad 0 \le \alpha \le 1$$

Where P_{cf} is fracture opening pressure,
Satisfying $P_{cm} < P_{co} < P_{cf}$

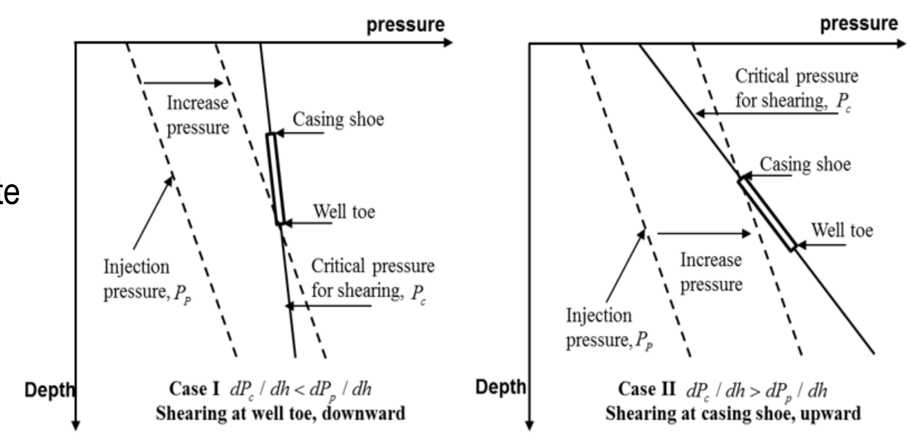

Xie, L., Min, K.B., 2016. Initiation and propagation of fracture shearing during hydraulic stimulation in enhanced geothermal system. Geothermics 59, 107-120.

Hydraulic Fracturing
Shear stimulation – SNU Geomechanics Toolbox

SEOUL NATIONAL UNIVERSITY

(1) In-situ stress condition input
- Magnitudes and orientations

(2) Reservoir condition input
3D DFN, rock & fluid density, friction angle, P_{co} evaluation coefficient

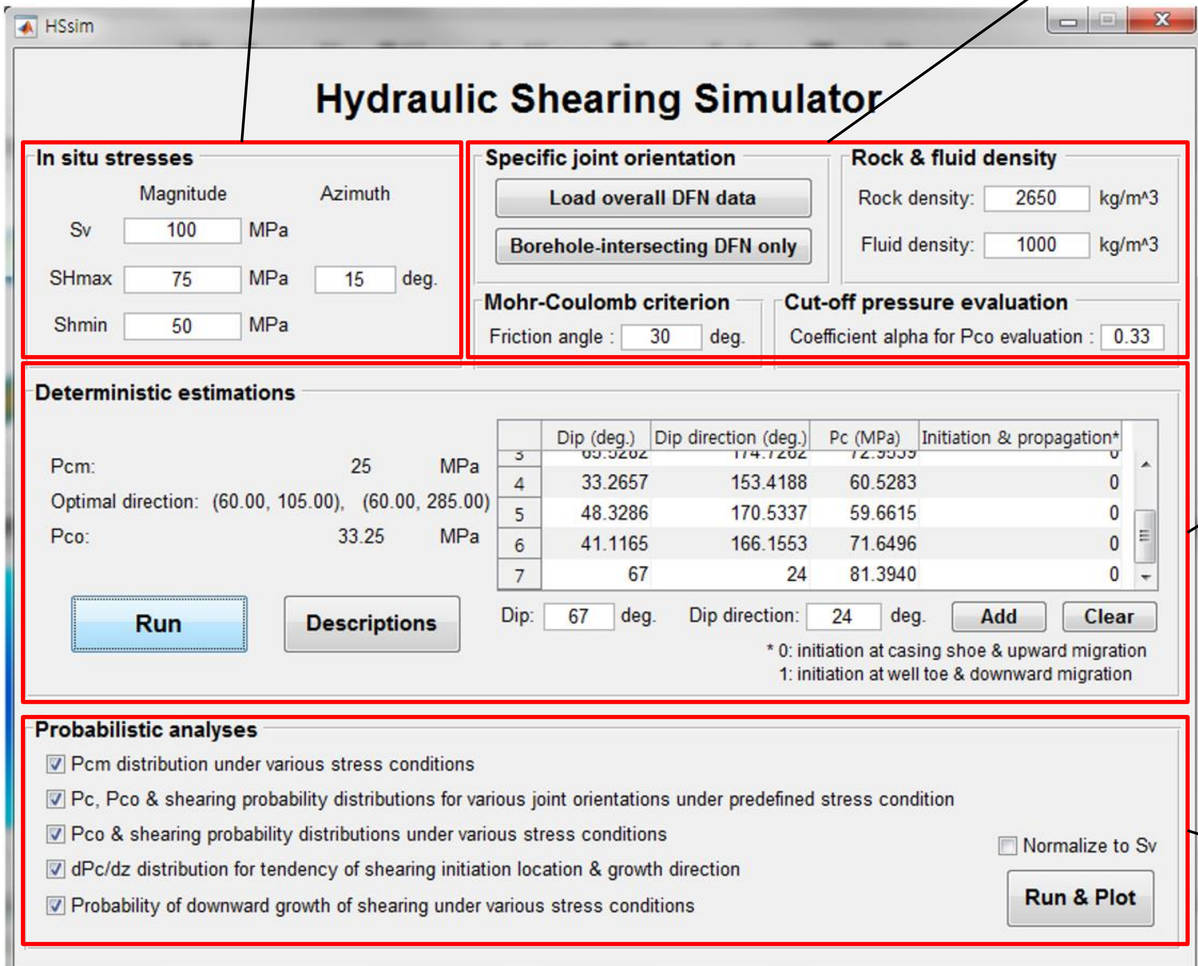

(3) Deterministic estimations:
Estimations under specific stress condition and joint orientations

(4) Probabilistic analyses:
Estimations under every possible stress conditions and joint orientations

Hydraulic Fracturing
Shear stimulation – SNU Geomechanics Toolbox

SEOUL NATIONAL UNIVERSITY

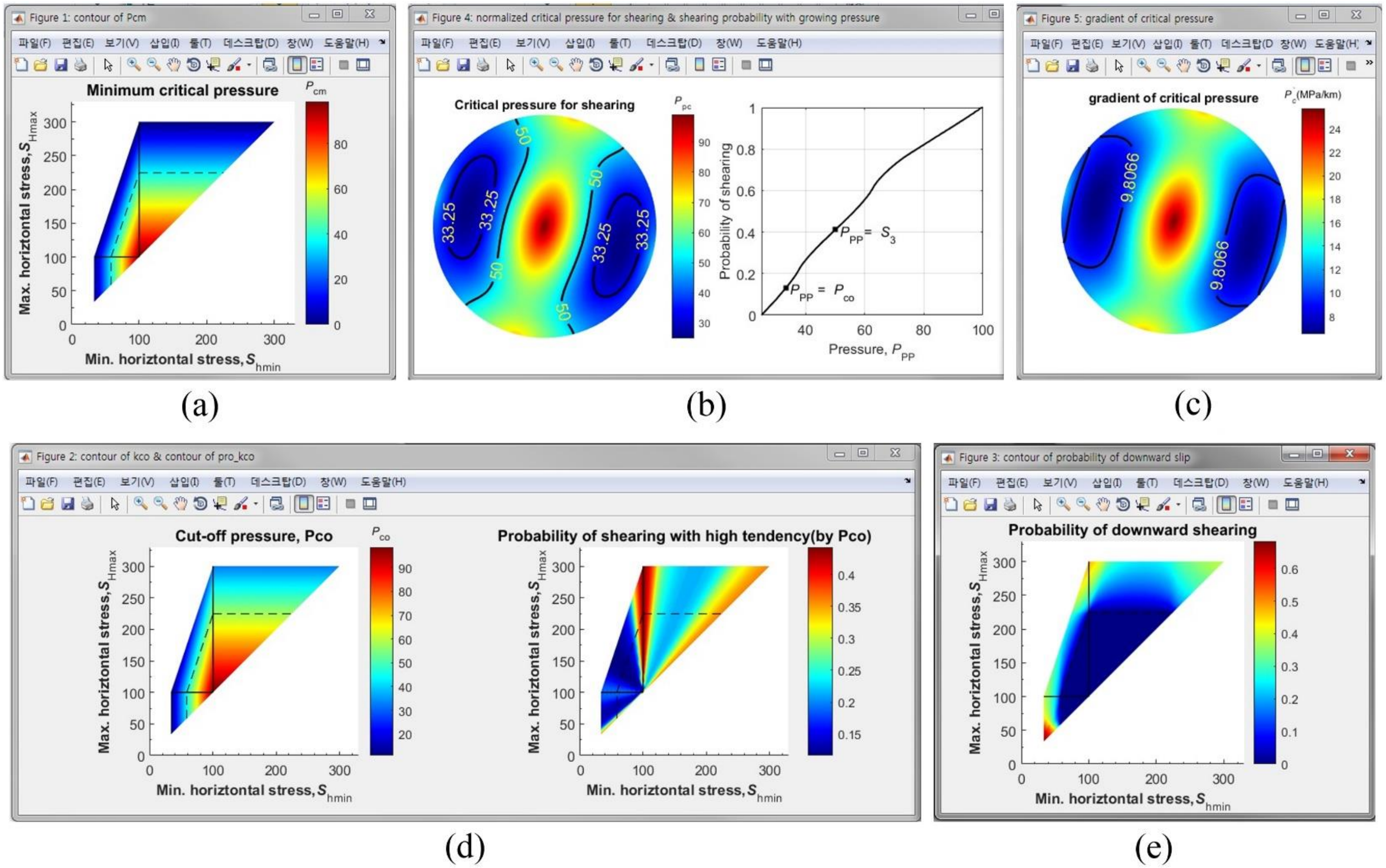

(a) Contour of minimum critical pressure (P_{cm}) for shearing on the in-situ stress polygon

(b) left – contour of critical pressure for shearing **(**P_c**)** , right – probability of shearing under given injection pressure

(c) Contour of critical pressure gradient(dPc/dz) on the equal-area stereonet of joint orientations

(d) left – contour of cut-off pressure **(**P_{co}**)**, right – probability of shearing judged by cut-off pressure

(e) Contour of downward shearing probability on the in-situ stress polygon

Hydraulic Fracturing

Shear stimulation – flow into matrix (permeable fracture)

SEOUL NATIONAL UNIVERSITY

- Linear flow into permeable fractures
  - Function of permeability, viscosity and length scale (and porosity, compressibility of fluid and rock)

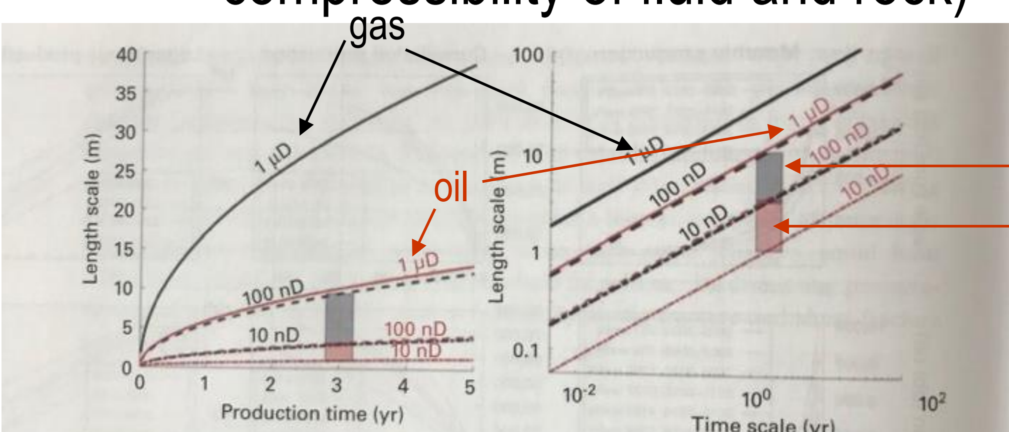

Typical range (gas): 10~100 nD

Typical range (oil): 10~100 nD

Figure 12.2 The time required for methane to diffuse through typical matrix permeabilities is given on a linear scale on the left and log–log scale on the right. The gray region indicates that approximately three years are required for gas to diffuse approximately 3–10 m through 10–100 nanodarcy matrix to a high permeability pathway. The corresponding time/distance relationship for oil is shown in red, with an approximately factor of 10 higher viscosity resulting in a corresponding decrease in diffusion distances. The gray and pink boxes reflect a representative range of matrix permeabilities for unconventional reservoirs. From Hakso & Zoback (2019).

$$\tau = \frac{l^2}{\kappa} = \frac{(\phi\beta_f + \beta_r)\eta l^2}{k} \quad (2.2)$$

η

where l is a characteristic length-scale of the process, $\boxed{\kappa \approx k/(\phi\beta_f + \beta_r)}$ is the hydraulic diffusivity, β_f and β_r are the fluid and rock compressibilities, respectively, ϕ is the rock porosity, k is the permeability in m^2 (10^{-12} m^2 = 1 Darcy), and η is the fluid viscosity.

Zoback MD, Kohli AH, 2019, Unconventional Geomechanics, Cambridge Univ

Mechanisms of overpressure generation
Disequilibrium compaction (undercompaction)

- Characteristic time for linear diffusion

Storativity

$$\frac{k}{\mu}\left(\frac{\partial^2 p}{\partial x^2}+\frac{\partial^2 p}{\partial y^2}+\frac{\partial^2 p}{\partial z^2}\right) = S\frac{\partial p}{\partial t}$$

$$\frac{\partial^2 p}{\partial x^2}+\frac{\partial^2 p}{\partial y^2}+\frac{\partial^2 p}{\partial z^2} = \frac{\mu S}{k}\cdot\frac{\partial p}{\partial t} = \frac{1}{c}\frac{\partial p}{\partial t}$$

$$S = \phi\beta_f + \beta_r \approx \phi\beta_f$$

$$\beta_f \approx 5\times10^{-4}/\mathrm{MPa} = 5\times10^{-10}/\mathrm{Pa}$$

$$\underset{(\eta)}{\mu} \approx 10^{-3}\ \mathrm{Pa\cdot s} = 1\ \mathrm{cp}$$

Diffusion equation
Dimensional Analysis

- Dimensionless group dictate the nature of diffusion process or demonstrate the competition between two rate process

$$\nabla^2 p = \frac{\mu S}{k}\frac{\partial p}{\partial t}$$

$$\nabla^{2+} p^+ = \frac{\mu S}{k}\frac{L^2}{t_0}\frac{\partial p^+}{\partial t^+} = \tau\cdot\frac{1}{t_0}\frac{\partial p^+}{\partial t^+}$$

$$\tau = \frac{l^2}{\kappa} = \frac{(\phi\beta_f + \beta_r)\eta l^2}{k} \qquad (2.2)$$

where l is a characteristic length-scale of the process, $\kappa \approx k/\eta(\phi\beta_f + \beta_r)$ is the hydraulic diffusivity, β_f and β_r are the fluid and rock compressibilities, respectively, ϕ is the rock porosity, k is the permeability in m^2 ($10^{-12}\ m^2 = 1$ Darcy), and η is the fluid viscosity.

1 D (darcy) = $0.987\times10^{-12}\ m^2 \sim 10^{-12}\ m^2$

Hydraulic Fracturing

Shear stimulation – flow into matrix (permeable fracture)

SEOUL NATIONAL UNIVERSITY

- Average production per wells
  - Production rapidly drops with production

mscf: thousand standard cubic feet
mmscf: million standard cubic feet

low matrix permeability to much more permeable planes. In linear flow, production rate is proportional to time$^{-1/2}$ as given by

$$q = \frac{1}{2}\frac{\alpha}{\sqrt{t}} \qquad (12.1)$$

1959). Cumulative production is obtaining by integrating Eqn. (12.1) and is thus given by

$$Q = \alpha\sqrt{t} \qquad (12.3)$$

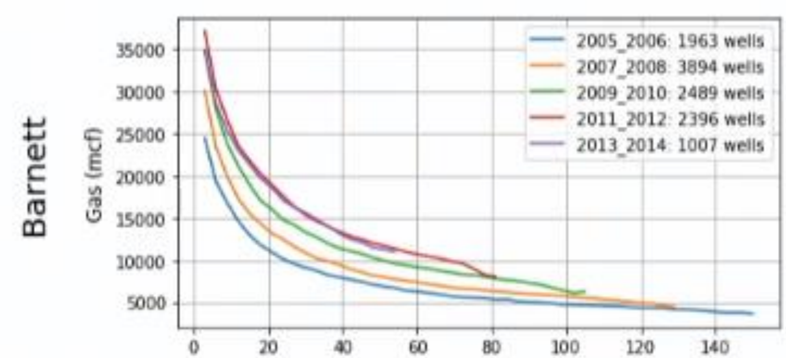

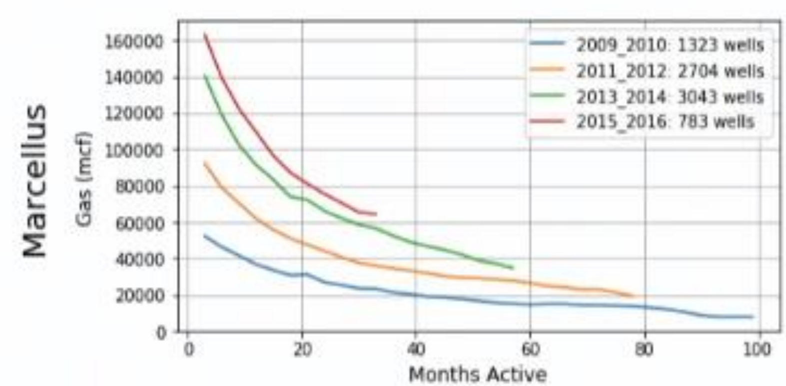

Zoback MD, Kohli AH, 2019, Unconventional Geomechanics, Cambridge Univ

Hydraulic Fracturing
Shear stimulation (Hydraulic shearing)

SEOUL NATIONAL UNIVERSITY

- Vertical growth
  - controlled with microseismicity monitoring and treatment volume

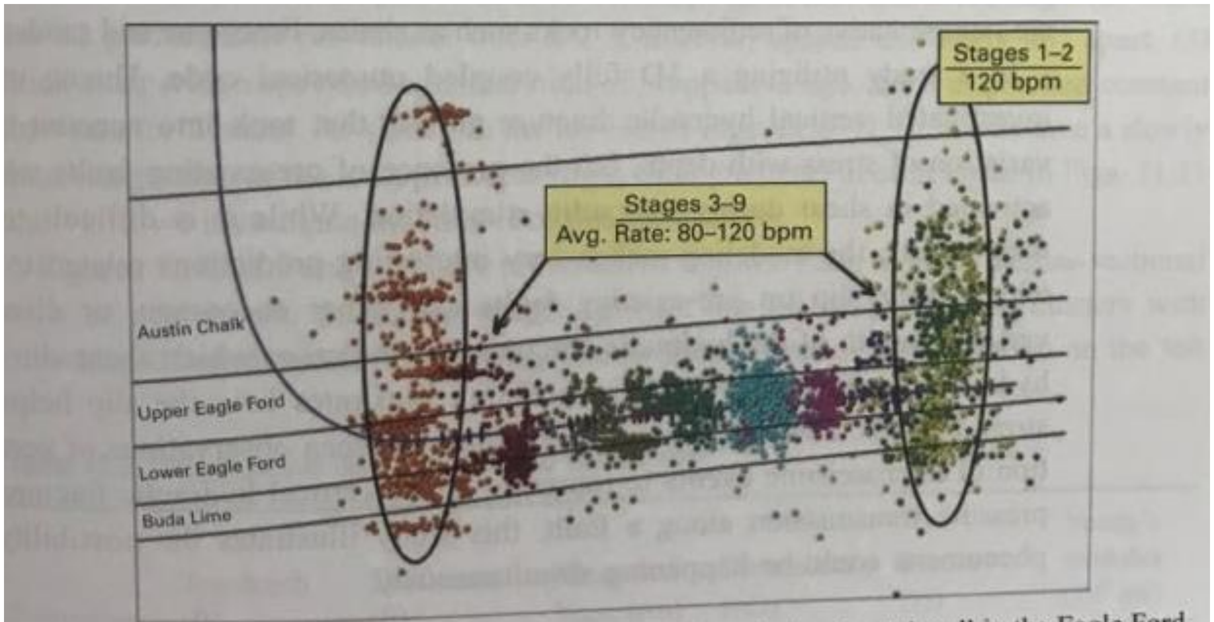

Figure 11.7 Cross-section view of multi-stage stimulation of a horizontal well in the Eagle Ford shale formation. Different colors represent different stages. The first two stages were carried out at 120 bpm which resulted in microseismicity well above the Austin chalk. In stage 3, the injection rate was decreased to 80 bpm and slowly increased for the remaining stages, resulting in microseismicity contained to the target lower Eagle Ford. Stage 9 was again at 120 bpm and again showed significant upward height growth. From Maxwell (2014).

Zoback MD, Kohli AH, 2019, Unconventional Geomechanics, Cambridge Univ

Hydraulic Fracturing
Shear stimulation – flow into matrix (permeable fracture)

- Reservoir simulation
  - Complex pore pressure and stress change in the reservoir need to be modeled numerically

Production and Depletion 355

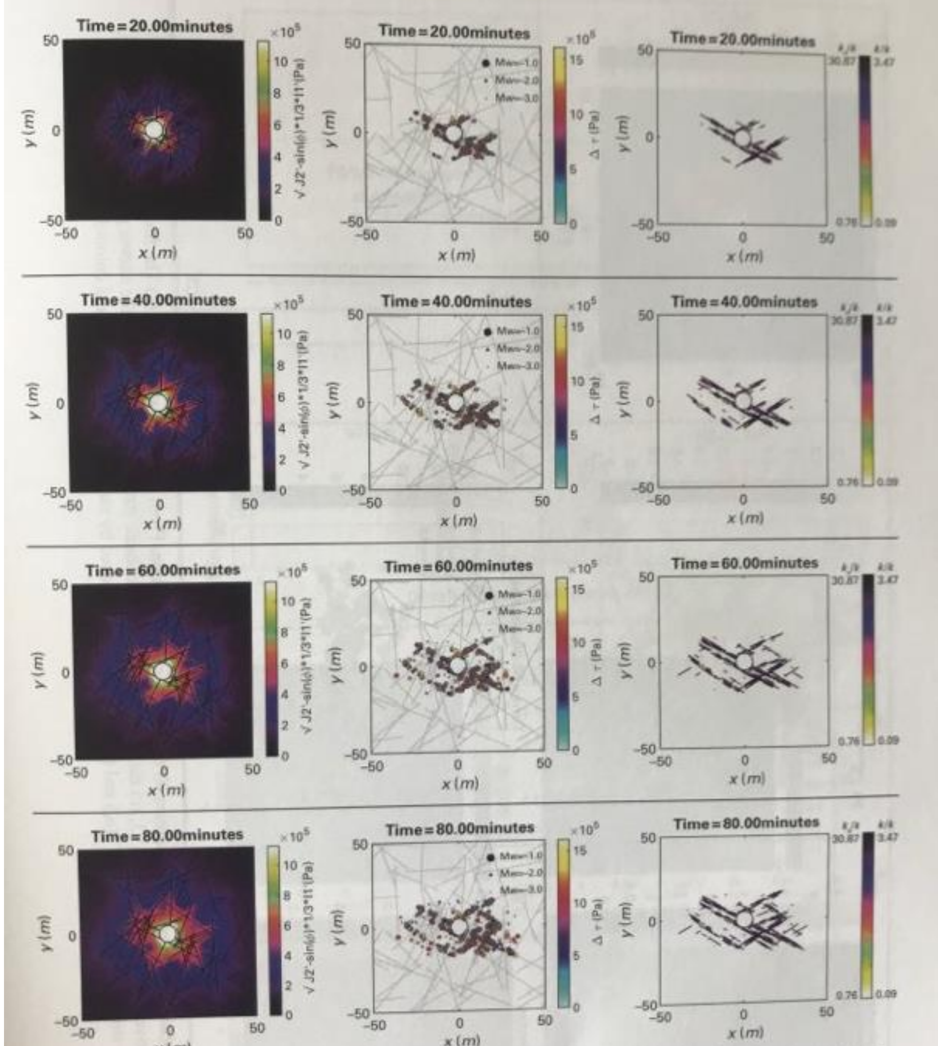

Figure 12.6 Simulation of the evolution of pore pressure (left), microseismic events (center) and permeability enhancement (right) during a modeled hydraulic fracturing operation. From Jin & Zoback (2018). Each row represents snapshots after 10, 20, 40 and 80 minutes (see text).

Zoback MD, Kohli AH, 2019, Unconventional Geomechanics, Cambridge Univ

Hydraulic Fracturing
Shear stimulation - Optimization

- Optimization of well spacing
  - < 200 ft ~2000 ft
  - Reservoir permeability, perforation cluster spacing, treatment volumes, time interval, etc.

Table 11.1 Estimates of optimal well spacing (modified from Liang et al., 2017).

Approach	Authors	Formation	Fluid type	Well spacing conclusions
Field pilot test and direct measurement of microseismic, pressure and tracer, and DNA sequencing to identify time-dependent drainage volume and inter-well communication	Friedrich & Milliken (2013)	Wolfcamp in Midland	Oil	400 ft
	Rucker et al. (2016)	Niobrara and Codell	Oil	Niobrara: < 200 ft Codell: < 700 ft
	Pettegrew & Qiu (2016)	Wolfcamp in Delaware	Oil	1,320 ft with 1,628 lb/ft
Operator data analytics	Sahai et al. (2012)	Marcellus	Gas	Variable for Marcellus
Numerical and analytical simulation. Fracture geometry or Stimulated Reservoir Volume (SRV) is directly assumed, i.e. planar and symmetric fracture with half length, conductivity and height are known or in a range	Sahai et al. (2012)	Haynesville	Gas	1,056 ft for Haynesville
	Lalehrokh & Bouma (2014)	Eagle Ford	Black oil; retrograde gas	330–400 ft for blackoil 440–450 ft for retrograde
	Yu & Sepehrnoori (2014)	Bakken	Black Oil	880 ft
	Siddiqui & Kumar (2016)	Eagle Ford	Retrograde gas	400 ft for single landing
Numerical and analytical simulation.	Belyadi et al. (2016)	Utica	Gas	1,200–1,300 ft
Fracture geometry or Stimulated Reservoir Volume (SRV) is derived from Rate Transient Analysis (RTA). Microseismic data and production log	Li et al. (2017)	Niobrara	Gas	2,000 ft
Numerical and analytical simulation.	Ramanathan et al. (2015)	Duvernay	Retrograde gas	200 m is not optimum

Optimal well spacing data

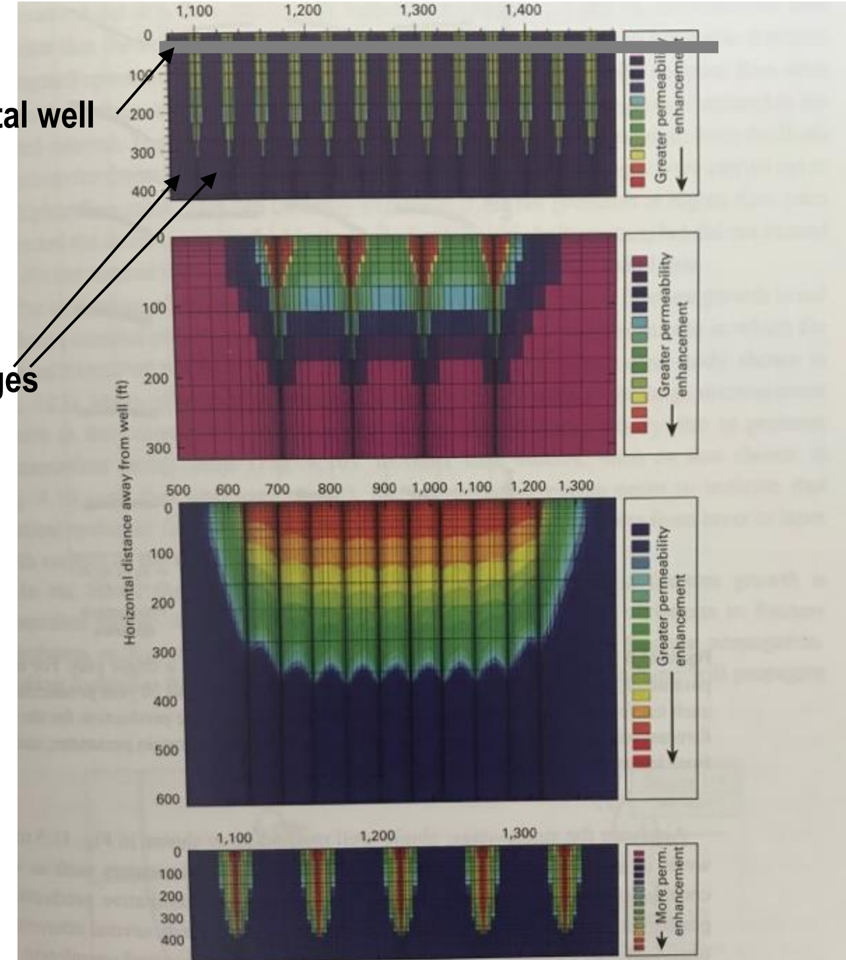

Figure 11.5 Plan views of models of permeability stimulation in four US onshore unconventional plays. Each panel represents a single stage. Note the strong variability in stimulated reservoir volumes surrounding a single hydraulic fracture propagating from a perforation cluster. The position of the well is along the top of edge of each figure. Because of symmetry, only half the hydraulic fractures are shown. The degree of permeability enhancement is indicated by the colors. Each panel represents a single stage, with variable numbers of clusters. From Sen et al. (2018).

Permeability enhancement with various stages in different cases

Zoback MD, Kohli AH, 2019, Unconventional Geomechanics, Cambridge Univ

Enhanced Geothermal Systems (EGS)
Definition

SEOUL NATIONAL UNIVERSITY

- EGS: Enhanced (or Engineered) Geothermal System
  - A system designed for primary energy recovery using heat-mining technology, which is designed to extract and utilize the Earth's stored thermal energy (Tester et al., 2006)
  - A geothermal system that requires hydraulic stimulation to improve the permeability.

Drill a deeper borehole (3~7 km) to reach a target temperature

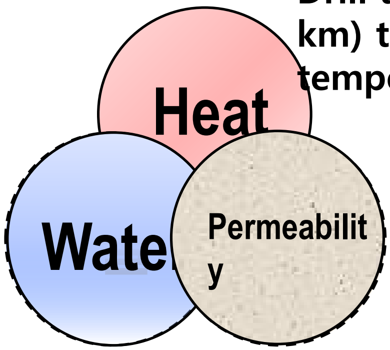

Artificially generate geothermal reservoir by hydraulic stimulation

- Provide water through injection

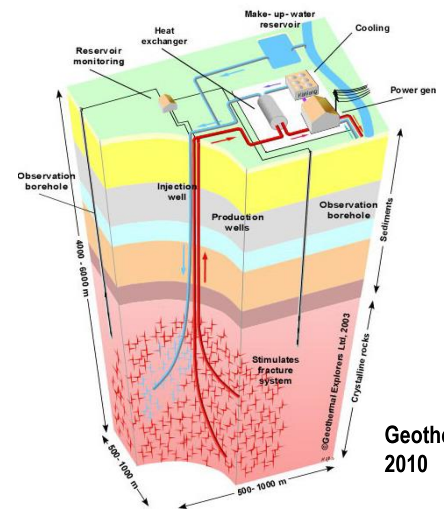

Geothermal Explorer, 2010

Enhanced Geothermal Systems
Hydraulic and thermal performance

- Temperature variation due to conduction-convection in a single fracture with unit width (e.g., Bodvarsson, 1969) (rectilinear model)

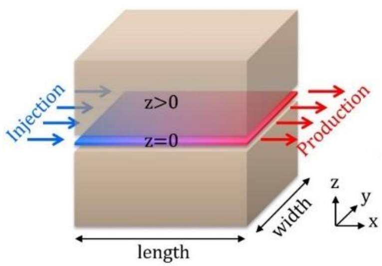

$$T_x = T_{rock} + \left(T_{inj} - T_{rock}\right) \cdot erfc\left[\left(\frac{k}{c_w m}\right) x / \sqrt{\alpha t}\right]$$

T_x : temperature at x

T_{rock} : temperature of rock

T_{inj} : injection temperature

k : thermal conductivity of rock

c_w : specific heat of water

m : mass flow rate per unit width (kg/sec/m)

α : thermal diffusivity of rock

t : time after injection(sec)

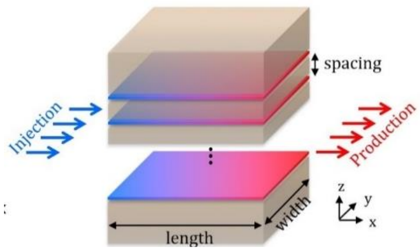

Multiple parallel fractures with thermal interference, rectilinear flow: Gringarten et al.(1975).

$$(x_D, z_D, s) = \frac{1}{s} exp[-x_D\sqrt{s} * tanh(\beta D_{ED}\sqrt{s})] * [cosh(\beta z_D\sqrt{s}) - tanh(\beta D_{ED}\sqrt{s}) sinh(\beta z_D\sqrt{s})]$$

Enhanced Geothermal Systems
Hydraulic and thermal performance

SEOUL NATIONAL UNIVERSITY

- Thermal performance: flowrates + fracture area

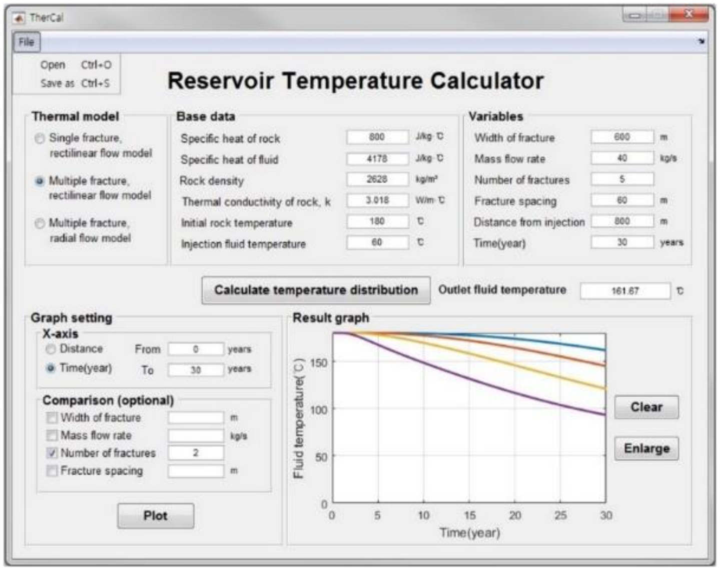

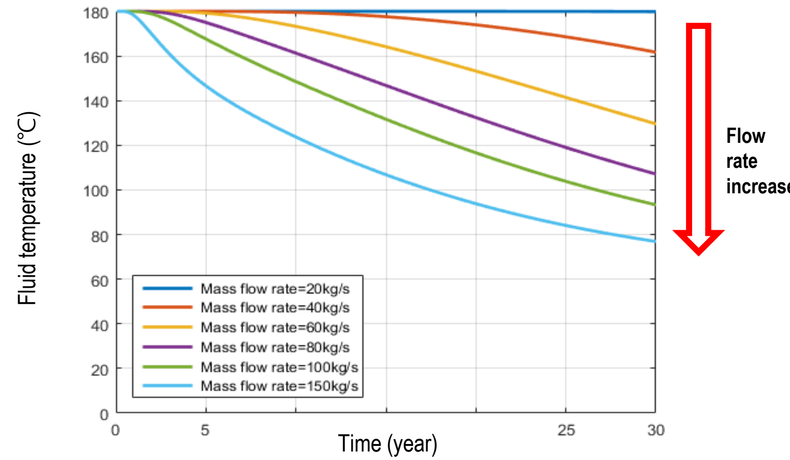

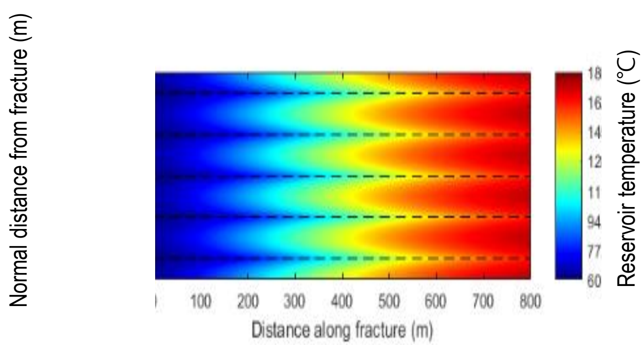

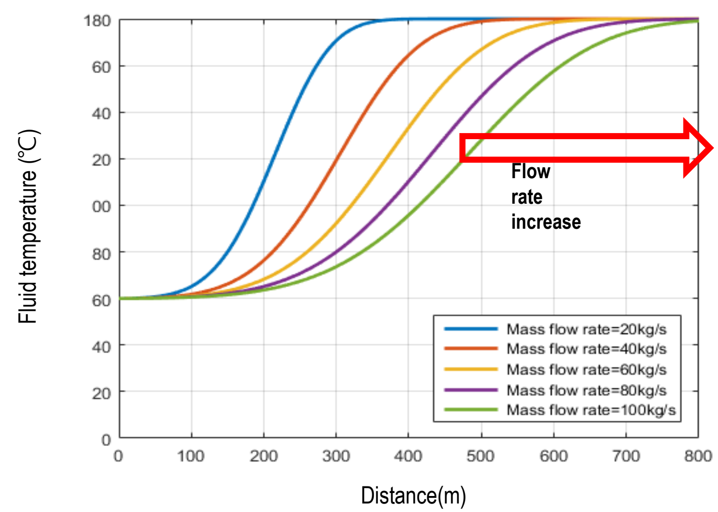

Park, Sehyeok, Kim, Kwang-Il, Kwon, Saeha, Yoo, Hwajung, Xie, Linmao, Min, Ki-Bok*, Kim, Kwang Yeom, Development of a hydraulic stimulation simulator toolbox for enhanced geothermal system design. Renewable Energy, 2018, 118C: 879-895.

Enhanced Geothermal Systems
Hydraulic and thermal performance

- 60 kg/sec for 30 years (with < 10 °C drawdown)
  → 6 fractures (1 km width), hole distance of 600 m

- Mass loading per unit area of the fracture $\dot{m}/R^2$ = 60 kg/sec/(6x10^{6}m^2)=1x10^{-5} kg/m^{2}s ~ tens of mD

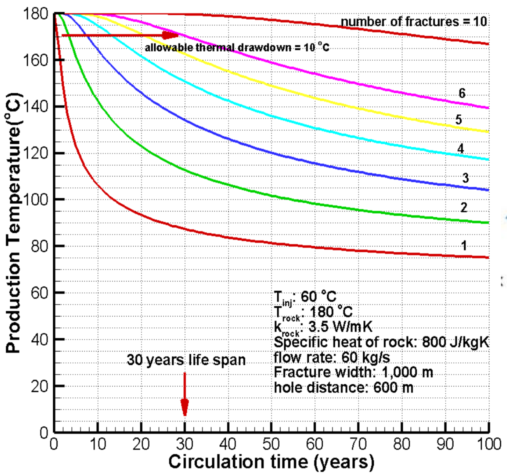

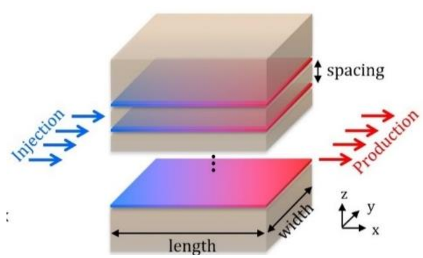

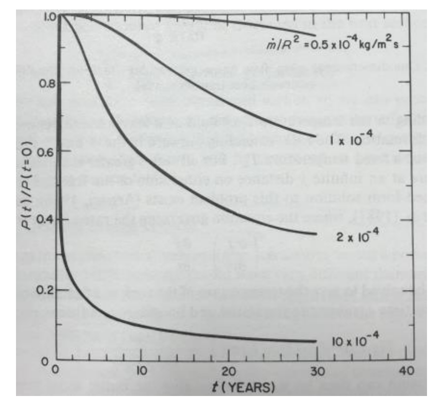

$$P(t)/P(t=0) = \mathrm{erf}\left[(\lambda_r \rho_r C_{pr}/t)^{1/2} A/\dot{m}C_p\right]$$

$\dot{m}$ = mass flow through the fracture = $\rho\dot{q}$ (kg/s)

Armstead HCH and Tester JW, 1987, Heat Mining – A new source of energy, E & FN SPON

Enhanced Geothermal Systems
History and status

Locations	Year	Depth	Max Temp	
Fenton Hill, New Mexico, USA	1972 - 1996	2.8 km/3.6 km/4.2 km	320 °C	
Rosemanowes, Cornwall, UK	1978 - 1991	2.0 km/ 2.2 km	85 °C	
Hijiori, Japan	1985 - 2002	1.8 km/2.2 km	270 °C	
Soultz, France	1987 ~Present	3.3 km/5.0 km	200 °C	success
Ogachi, Japan	1989 ~ 2001	0.7 km/1.0 km	250 °C	
Cooper Basin, Australia	2003 ~ 2015	4.2 km	240 °C	
Pohang, South Korea	2010~2017	4.3 km	142 °C(160 °C)	
Espoo, Finland	2018~	6.2 km	~120 °C	

The first EGS power generation at Fenton Hill, USA(Feb, 1980, fluid temperature: 150°C, R-114 binary cycle, electricity capacity: 60 kWe, Armstead and Tester, 1987)

Enhanced Geothermal Systems
Soultz Project, France – Rittershoffen, France

SEOUL NATIONAL UNIVERSITY

- Project at Rittershoffen: June 2016
  - 24 MWth, GRT-1@2580m, GRT-2@3196m
  - Flowrate: 70 l/s, T>165°C, Transportation: ΔT<5°C@15 km
  - Used in Starch industry (전분 공장)

Enhanced Geothermal Systems
Espoo EGS project (2018 - ongoing)

SEOUL NATIONAL UNIVERSITY

Site information of St1 EGS project in Finland

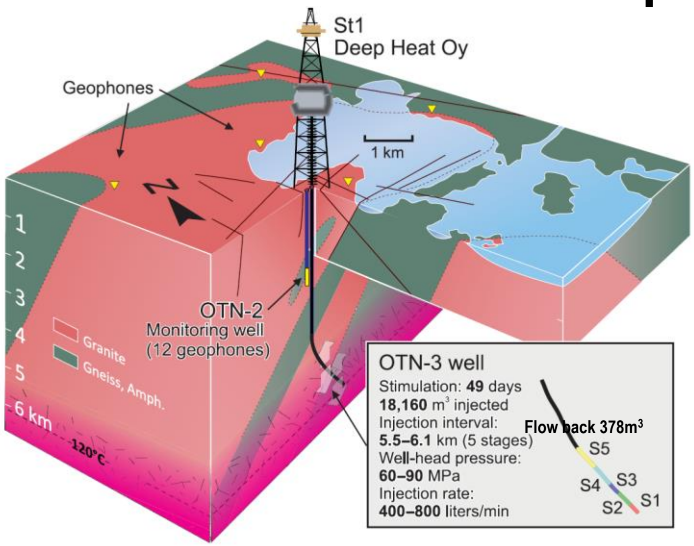

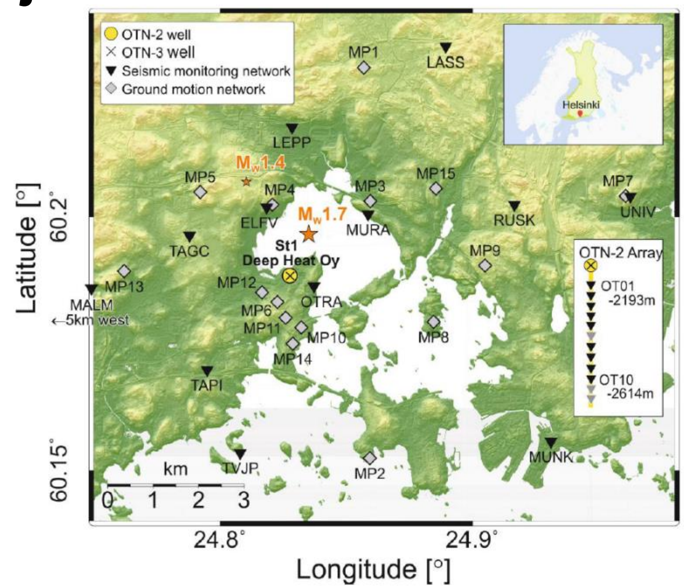

- OTN-2: 3.3 km MD, for earthquake monitoring
- OTN-3: 6.4 km MD, for stimulation
- Drilling: air and water hammer (vertical part) + rotary methods (deviated part)
- Multi-stage hydraulic stimulation (S1~S5). 1,000 m open-hole. Inclined at 42° to the NE
- 12-level vertical array of three-component seismometers: 2.20~2.65 km depth (OTN-2)
- 12 additional borehole sensors (0.3 ~ 1.15 km depth). 14 surface sensors.
- Background seismicity is very sparse: Mw 2.4 (2011, 50 km away), Mw 1.7, 1.4 (2011)

Kwiatek G., et al. 2019. Controlling fluid-induced seismicity during a 6.1-km-deep geothermal stimulation in Finland. Science Advances. 5:eaav7225. 1-11.

Enhanced Geothermal Systems
Outstanding technical issues

SEOUL NATIONAL UNIVERSITY

Outstanding technical issues

1) Drilling
2) Reservoir Creation
3) Characterization
4) Sustainable Production
5) Induced microseismicity

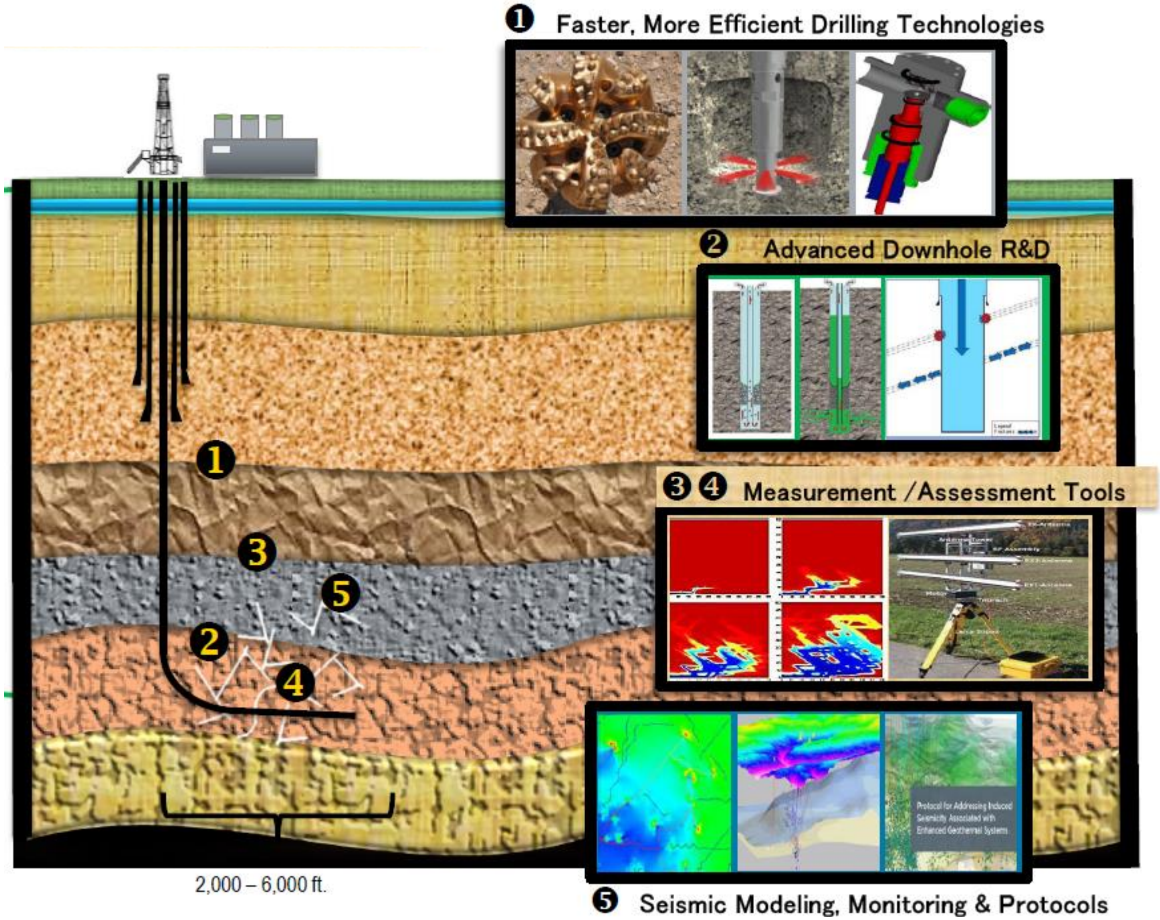

US DOE, 2013, Program overview

Enhanced Geothermal Systems
Outstanding technical issues

Outstanding technical issues

1) Drilling
2) Reservoir Creation
3) Characterization
4) Sustainable Production
5) Induced microseismicity

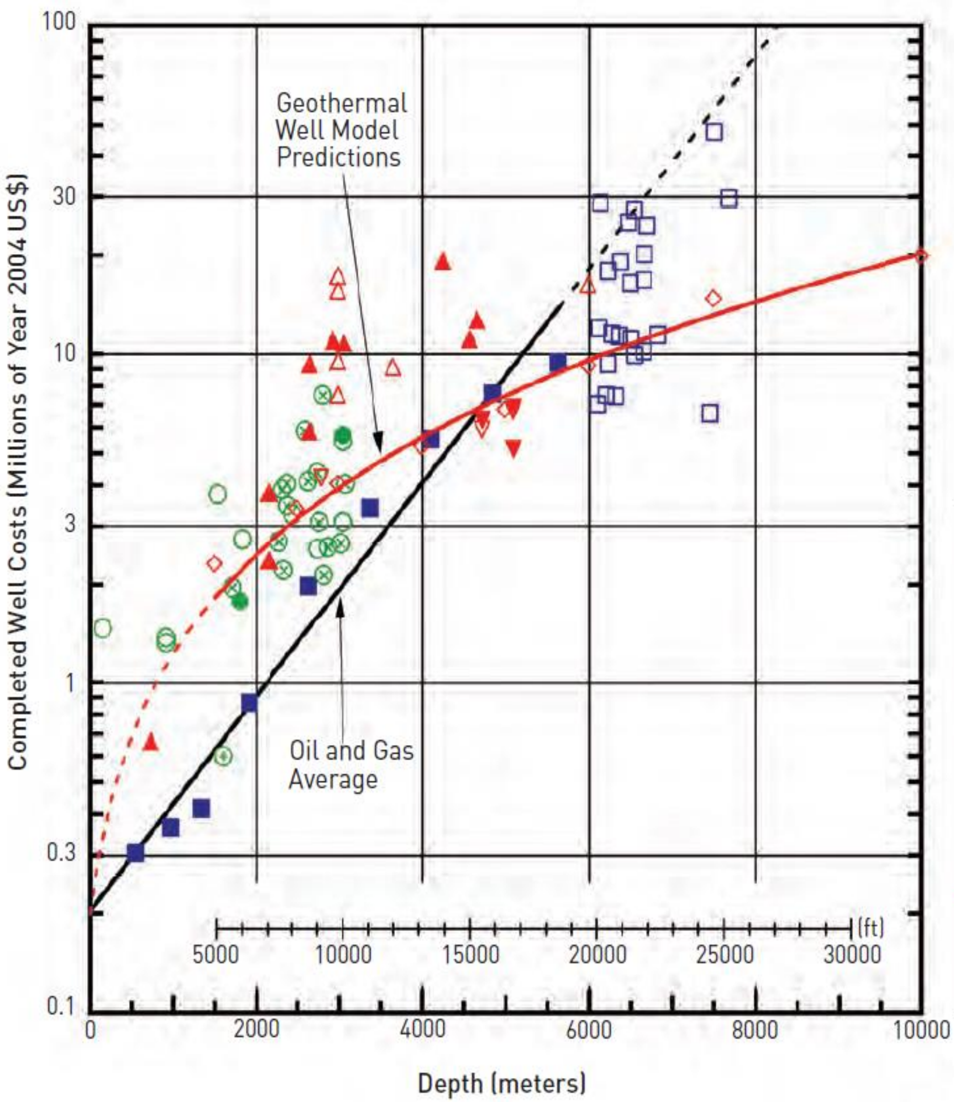

(MIT, 2006)

Enhanced Geothermal Systems
Outstanding technical issues

SEOUL NATIONAL UNIVERSITY

Outstanding technical issues

1) Drilling
2) Reservoir Creation
3) Characterization
4) Sustainable Production
5) Induced microseismicity

Cooper Basin – Jolokia #1 (2010)

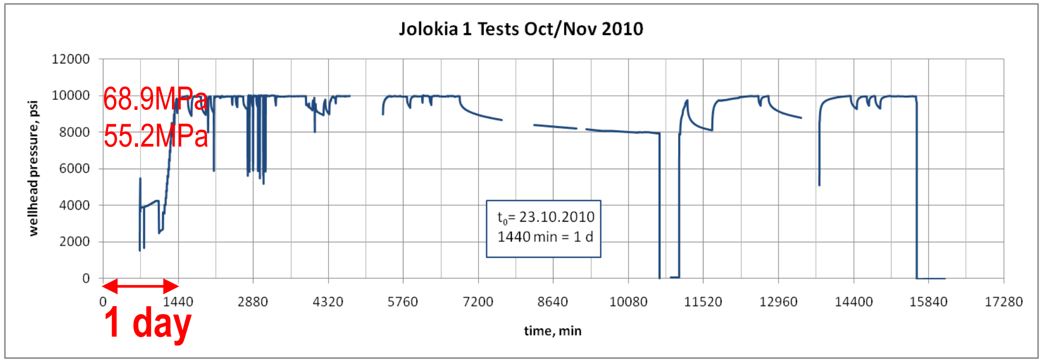

1 bpm = 2.65 L/s

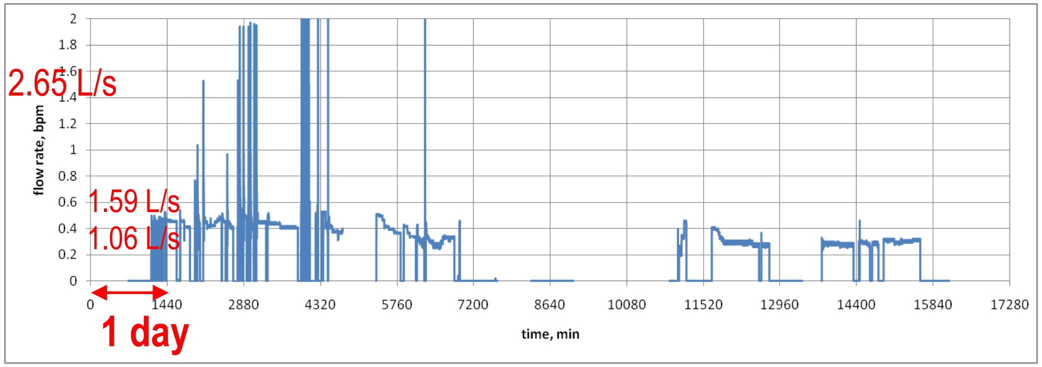

Well head Injection pressure ~ 70 MPa
Injection rate < 5 l/sec

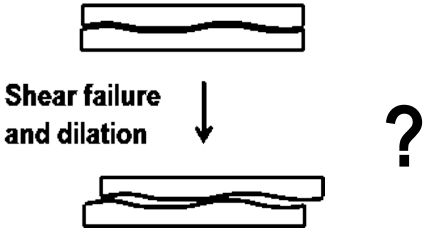

Enhanced Geothermal Systems
Outstanding technical issues

SEOUL NATIONAL UNIVERSITY

Outstanding technical issues

1) Drilling
2) Reservoir Creation
3) Characterization
4) Sustainable Production
5) Induced microseismicity

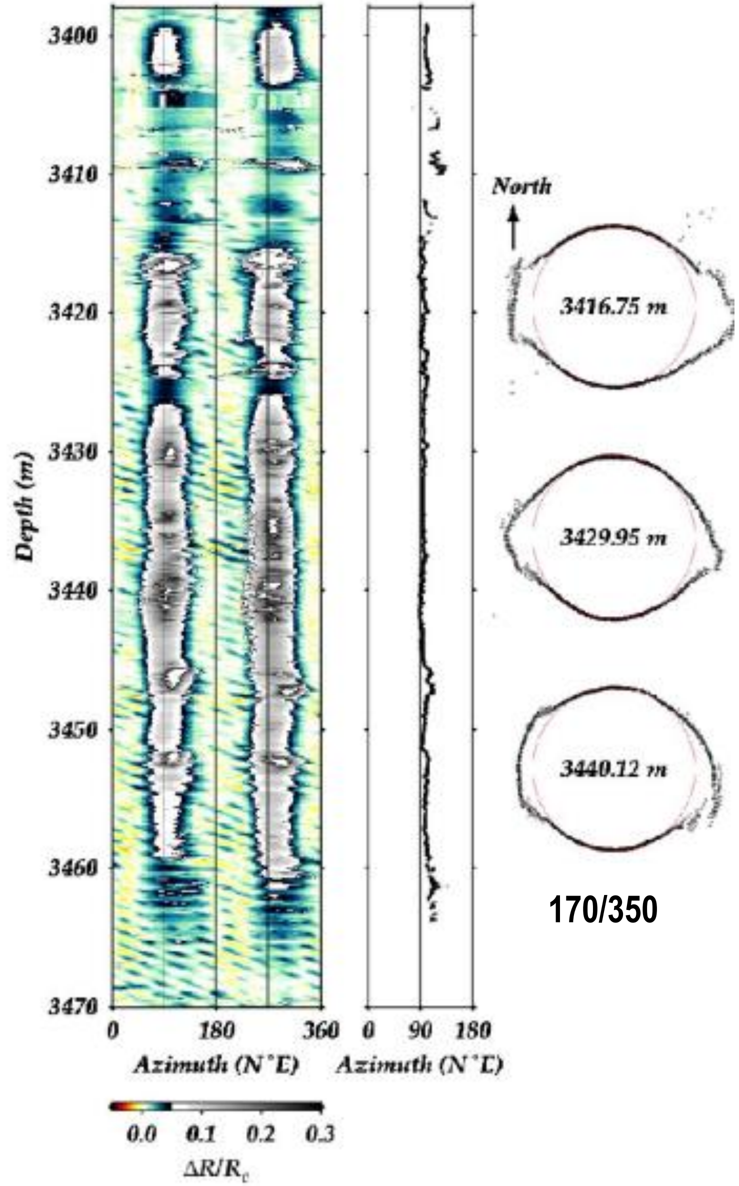

170/350

Borehole breakout at GPK1 @3450 m - Observed one year after drilling (Cornet et al., 2007)

Cornet, F. H., Th Bérard, and S. Bourouis. How Close to Failure Is a Granite Rock Mass at a 5 km Depth?. *Int J Rock Mech Min 44(1) (2007): 47-66.*

Enhanced Geothermal Systems
Outstanding technical issues

SEOUL NATIONAL UNIVERSITY

Outstanding technical issues

1) Drilling
2) Reservoir Creation
3) Characterization
4) **Sustainable Production**
5) Induced microseismicity

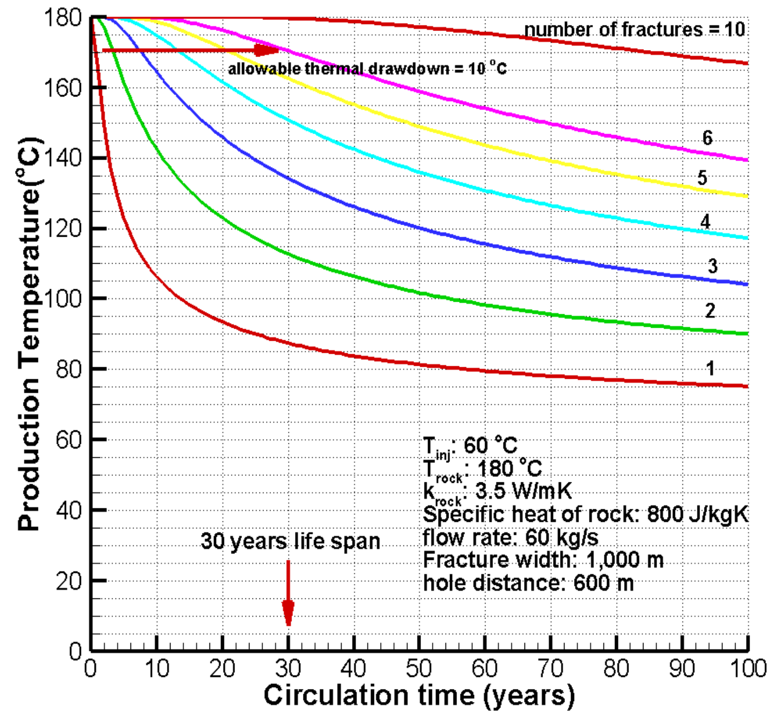

1 fracture

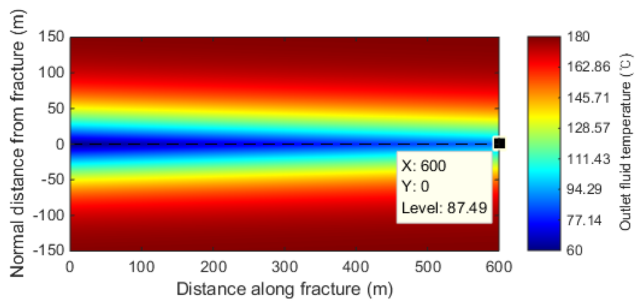

6 fractures

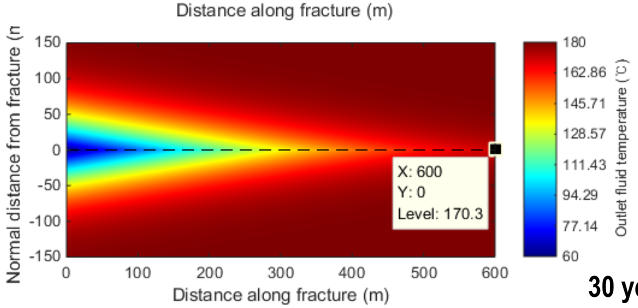

30 years, 60 kg/sec

- 60 kg/sec for 30 years (with < 10 °C drawdown)
  → 6 fractures (1 km width), hole distance of 600 m
- Mass flow rates per unit area matters

$$\dot{m}/R^2$$

Enhanced Geothermal Systems
Outstanding technical issues

SEOUL NATIONAL UNIVERSITY

Outstanding technical issues

1) Drilling
2) Reservoir Creation
3) Characterization
4) Sustainable Production
5) Induced microseismicity

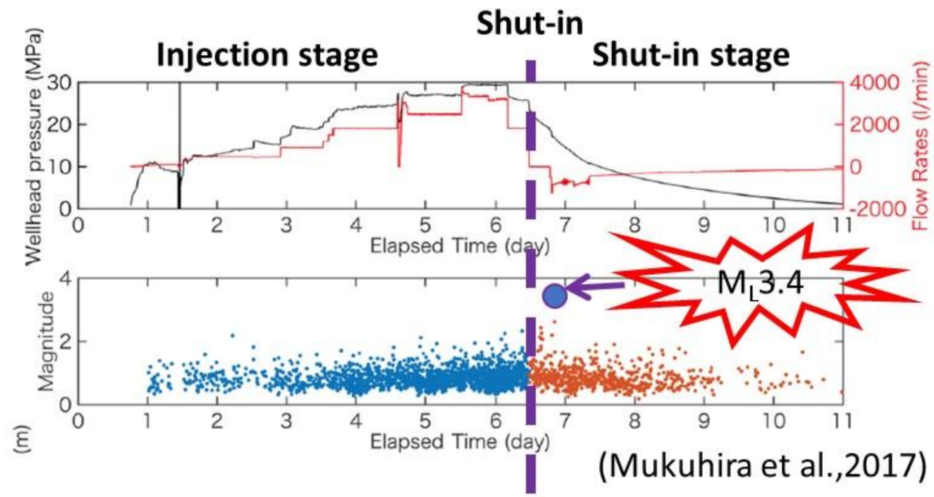

- Basel Deep Heat Mining project (2006)
  - Borehole at 5 km, Injection: 11,570m^3
  - Maximum seismicity: M_L 3.4 (5 hours after shut-in)
  - Property damage: 7 million swiss franc

Häring, M. O., et al. (2008). "Characterisation of the Basel 1 enhanced geothermal system." Geothermics 37(5): 469-495.

Enhanced Geothermal System
EGS and Shale gas production

- Shale Gas R&D spending and production*

EGS is arguably in the same techno-commercial space that shale gas was prior to validation. Challenges include the rate of advancement and innovation, and ability of the sector to run with game-changing technical advances. (D Hollett, US DOE Geothermal Program Manager, 2012).

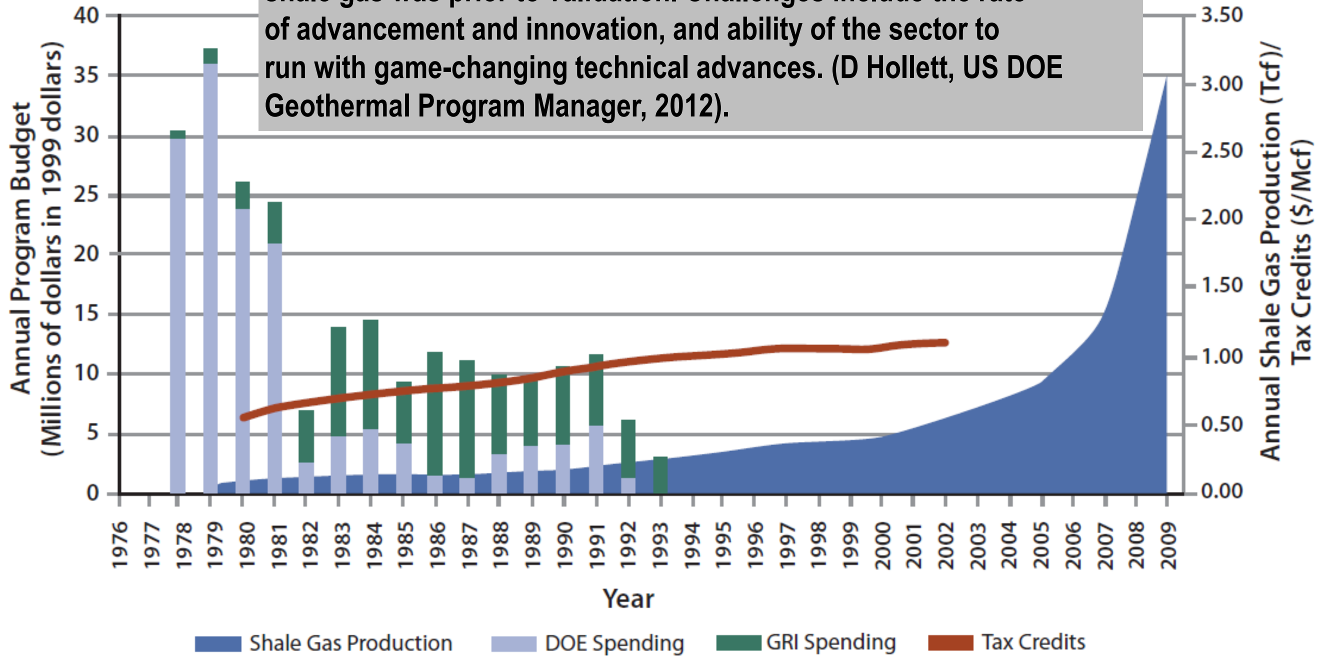

*Future of Natural Gas (MIT Report, 2009)

**GRI: Gas Research Institute